EVALUATION OF THE TOXICITY ASSOCIATED WITH COMPLEX ENGINEERED NANOMATERIALS UTILIZING *IN VIVO* AND *IN VITRO* MODELS

by

Sharlee Mahoney

Bachelor of Science, Chemical Engineering, University of Wyoming, 2012

Submitted to the Graduate Faculty of

Swanson School of Engineering in partial fulfillment

of the requirements for the degree of

Doctor of Philosophy

University of Pittsburgh

2016

UNIVERSITY OF PITTSBURGH

SWANSON SCHOOL OF ENGINEERING

This dissertation was presented

by

Sharlee Mahoney

It was defended on

November 8, 2016

and approved by

Ipsita Banerjee, Ph.D., Associate Professor, Departments of Chemical and Petroleum Engineering, Bioengineering

Edward A. Burton, M.D., Ph.D., Associate Professor, Department of Neurology

Aaron Barchowsky, Ph.D., Professor, Department of Environmental and Occupational Health

Joseph J. McCarthy, Ph.D., W.K. Whiteford Professor, Department of Chemical and Petroleum Engineering

Dissertation Director: Götz Veser, Ph.D., Nickolas A. DeCecco Professor, Department of Chemical and Petroleum Engineering

Copyright © by Sharlee Mahoney

2016

EVALUATION OF THE TOXICITY ASSOCIATED WITH COMPLEX ENGINEERED NANOMATERIALS UTILIZING *IN VIVO* AND *IN VITRO* MODELS

Sharlee Mahoney, PhD

University of Pittsburgh, 2016

Nanomaterials are about to fundamentally alter how we exploit the chemical and physical properties of materials. Due to their unique properties, they are being rapidly incorporated into products and industrial applications. However, there is growing concern that these materials will display unexpected nano-specific toxicity that will occur through mechanisms that cannot be extrapolated from the analogous bulk material. Consequently, there is a critical need to develop toxicity screening methods that are able to detect toxicity at the nano-scale. Furthermore, it is imperative to derive structure-toxicity correlations that can be used to design safer nanomaterials *a priori*.

Industry rarely uses individually structured nanoparticles (NPs) due to their instability. To overcome NP deactivation and promote stability, nano-enabled materials are often designed as multi-component materials which embed active NPs within a protective matrix, referred to as complex engineered nanomaterials (CENs). However, most nanotoxicity studies to-date focus on individually structured NPs, rather than CEN structures. Moreover, these structures offer a unique opportunity to systematically study how nano-structuring influences the NPs physicochemical properties, which in turn, affects toxicity. By correlating the physicochemical properties of these complex structures with the toxicity of the CENs, it is possible to derive structure-toxicity correlations. These correlations can help identify structures that minimize properties that cause toxicity, while still providing NP functionality.

In this work, we systematically study the toxicity associated with CENs. We investigate three structures that allow us to systematically study the effect nano-embedding has on toxicity: i.) metal NPs deposited on a silica support ii.) metal NPs embedded throughout a porous silica NP and iii.) metal NPs encapsulated in a hollow core surrounded by a silica shell. These CENs underwent rigorous characterization including analyzing the CENs' size, surface area, ion dissolution, aggregation and settling. Both *in vitro* (3T3 fibroblasts) and *in vivo* (zebrafish; *Danio rerio*) toxicity tests were conducted. The physicochemical characterization was correlated with toxicity studies to determine structure-toxicity correlations. Overall, we showed that embedding the NP, and reducing ion dissolution, led to a reduction in toxicity. Our results suggest that CENs offer a relatively straightforward stepping stone towards the rational design of safer nanomaterials.

TABLE OF CONTENTS

LIST OF TABLES

LIST OF FIGURES

PREFACE

First I would like to thank my research advisors Dr. Veser and Dr. Banerjee for their guidance, patience and support through the last five years. It has been an exciting, inspiring journey in learning how to conduct, and present, thought-provoking research. I am thankful for them teaching me the “ropes” on how to excel in research; from discussing results, designing experiments, to editing papers. I also would like to thank Dr. Burton, a research collaborator and committee member, for his expertise and knowledge on zebrafish. I have thoroughly enjoyed passing on the knowledge you have instilled in me about zebrafish to unsuspecting friends and family members. I also would like to thank my committee members Dr. Barchowsky and Dr. McCarthy for their expertise, advice and insights into my research.

I would like to thank the undergraduates and graduate students who have helped on this project. Their dedication, hard work, and smiling faces made it possible to complete these studies. I would like to express my gratitude to my fellow lab-mates for their inspiration and patience. Having to explain my research to a catalysis group helped me better understand my research. Furthermore, the lab’ out-of-the-box questions led to intriguing discussions that influenced the creativity in my project.

I could have not completed this PhD without the friends I made in Pittsburgh. After leaving Wyoming, I was still able to find friendly faces and make life-long friends in the big city of Pittsburgh (what I consider big at least). Their friendship in the forms of climbing nights, hikes, pot lucks, and small group has made this a life-changing adventure. Lastly, but not least, I want to thank my family who supported me through my PhD. From my family sneaking into

conferences to watch me give my talk, to my siblings/parents listening to me complain about my zebrafish and cells controlling my life, they have supported me throughout this process and continue to love me. I am not sure how much they enjoyed all my tidbits and random facts about nanotechnology and zebrafish, but I appreciate their love and support to pursue my passion in research.

1.0 INTRODUCTION

1.1 NANOMATERIALS

Nanomaterials are defined as materials with at least one dimension smaller than 100 nm. At this size, nanomaterials have enhanced properties compared to their correlating bulk counterparts. This is due to an increased surface area:volume ratio (Figure 1)[1]. A significant portion of the atoms, contributing to the makeup of nanomaterials, lay near or at the surface[1,2]. This dominance of surface atoms leads to more reactive properties. The correlating micro-size structure, is dominated by atoms present in the bulk state. For example, the commonly known bulk gold is yellow and inert. However, at the nano scale, gold nanoparticles (NPs) range in color from purple to pink, depending on the NP size. Furthermore, gold NPs have found use in multiple industries and products including biomedical, catalytic, sensors, solar cell, and fuel cell applications[3-13]. Overall, these unique properties associated with nanosize materials have led to an use in over 1,300 consumer products and industrial processes[14]. This includes applications in the semiconductor, catalysis, and pharmaceutical industries and is projected to be a $1 trillion market in the US alone by 2020[14].

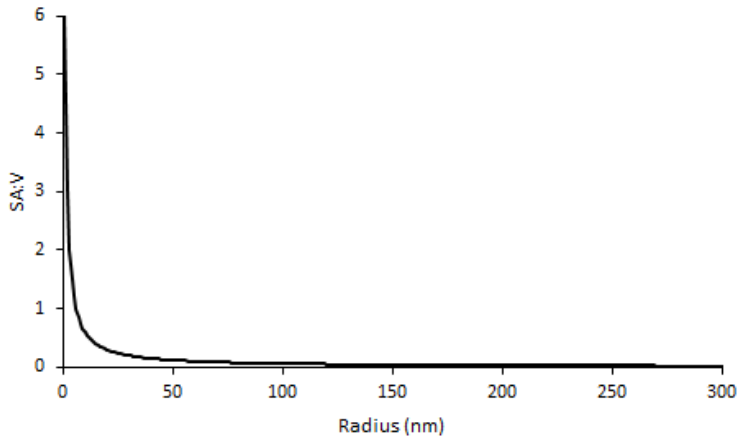

Figure 1. Surface area : Volume ratio for radius from 0.5 -300 nm. As radius decreases, the SA:V ratio increases.

1.2 NANOTOXICITY

Due to these unique properties, nanomaterials toxicities are expected to differ from their corresponding bulk structure[1,15]. This toxicity differences is related to either 1. the different properties that emerge due to the small size or 2. the ability of these materials to be transported in a way that the micro size material cannot be e.g. crossing the blood-brain barrier or blood-placenta barrier[16]. For example, previous studies showed that TiO_2 NPs crossed the blood-brain barrier in mice studies[17-19]. Also, inhaled CeO_2 NPs by mice were transported from the lungs, to the blood stream, and to other organs including the liver and kidneys[20,21]. Despite growing evidence that nanomaterials exhibit different toxicities compared to the bulk structure, there are no specific guidelines from the EPA on handling the disposal of these nanomaterials. However, EPA has realized the potential risk and hazard these nanomaterials pose and are currently

working with many universities and companies to understand the risk of these materials and establish proper guidelines for the use and disposal of nanomaterials[22,23].

Many nanotoxicity studies focus on studying the toxicity of a specific NP. This will often including studying the effect properties, like size or surface chemistry, affects toxicity. In addition, these studies may test the toxicity associated with 1-3 *in vivo* or *in vitro* models. While these studies are crucial with providing us with important information on the toxicity of specific nanomaterials, the results are limited and rely on extrapolating the studied toxicity to different NP materials, doping, sizes, coatings and environments. At the rapid rate that nanomaterials are being incorporated into products, it is insurmountable to be expected to study the toxicity of every nanomaterial, in every product, on all possible avenues of toxicity. Hence, a viable solution is needed to aid in ensuring safety when these NPs are incorporated into products and industrial applications.

Following the current protocols for screening the toxicity of new chemicals, it is crucial to determine appropriate test models and standards. There are protocols in place by the Organisation for Economic Co-operation and Development (OECD), National Institute of Standards and Technology (NIST) and ASTM to examine the toxicity of chemicals. These protocols are not necessary suitable for nanomaterial toxicity screening. However, there is current work on re-designing these standards to be suitable for nanotoxicity screenings[24-26]. One example of this, Hanna et al., at NIST determined that positively charged polystyrene NPs impacted the growth of Caenorhabditis elegans. This was linked to interactions between the NPs and the food source (E. coli). They found that other positively charged NPs (independent of material) caused similar toxicity. However, when an alternate C. elegans study was conducted, that did not require E. coli as a food source, there was no toxicity determined (as was the

expected outcome)[27]. Thus, it was concluded that this assay, as currently designed for chemicals, is unreliable for positively charged NPs. Thus, adaptations must be made to ensure reliable toxicity results.

Since nanomaterials offer many advantages compared to the micro-size materials, they will continue to be incorporated into products. Thus, a possible avenue to aid in reducing toxicity is to provide structure-toxicity correlations that can be used *a priori* to ensure design of safer nanomaterials. These correlations can be determined by utilizing model nanomaterials that systematically study the influence physicochemical properties, like surface area, size, dissolution, aggregation, settling and NP coatings, have on toxicity[28]. These correlations can give rise to insights into toxicity mechanisms, and can be used to design safer nanomaterials that minimize these properties[29-34].

1.3 METAL OXIDE NANOPARTICLE TOXICITY

Metal NPs are finding widespread use in a range of consumer products and industrial applications. Silica NPs are the most highly produced NP in terms of volume. In contrast, Ag NPs are used in the most consumer application due to their antimicrobial properties[35,36]. They are found in a range of applications from clothing[37,38] to coatings for surgical implants[39]. TiO_2 and ZnO NPs are used in sunscreen to increase opaqueness of the sunscreen while still providing protection from the harmful sun rays[40-44]. CuO NPs are used in many applications including pesticides[45-47], pressurized lumber[48-50], and drug delivery[51-56]. Ni NPs find use in synthesizing carbon nanotubes[57-59], as industrial catalysts[60-63] and use in electronics[64,65]. In turn, this wide spread use of nanomaterials has led to extensive toxicity screening of metal NPs.

Metal NPs have been rapidly screened for toxicity, including studying how NP size, shape, and surface coatings influence toxicity[66-69]. In addition, toxicity mechanisms have been identified, including shedding of ions into the media which passively diffuse into the cell and cause toxicity or a Trojan horse mechanism (Figure 2). Passive diffusion of dissolved ions into the cells/organisms tend to be present for toxicity studies utilizing bacteria. The bacteria have limited capability of engulfing the NPs and thus the toxicity associated with these materials are often associated with the dissolved ions in the media[70,71]. In contrast, Trojan horse mechanisms are nano-specific toxicity mechanism. They rely on the NP acting as vehicle for delivery into the cell/organism. The subsequent ion dissolution into the cell causes toxicity. Thus, the toxicity is not from interaction with the NP itself, but from the metal ions (which have a known toxicity). This Trojan horse mechanism relies on the NPs' small size which leads to 1. Rapid dissolution due to the increased surface areas and 2. Ability for the NP to cross barriers and enter cells/organisms that the micro-structure cannot[29,30,33,34]. Overall, there is strong evidence that the ions dissolved from metal NPs greatly influence toxicity. It is important to take into consideration the metal ion dissolution when studying the toxicity associated with metal NPs.

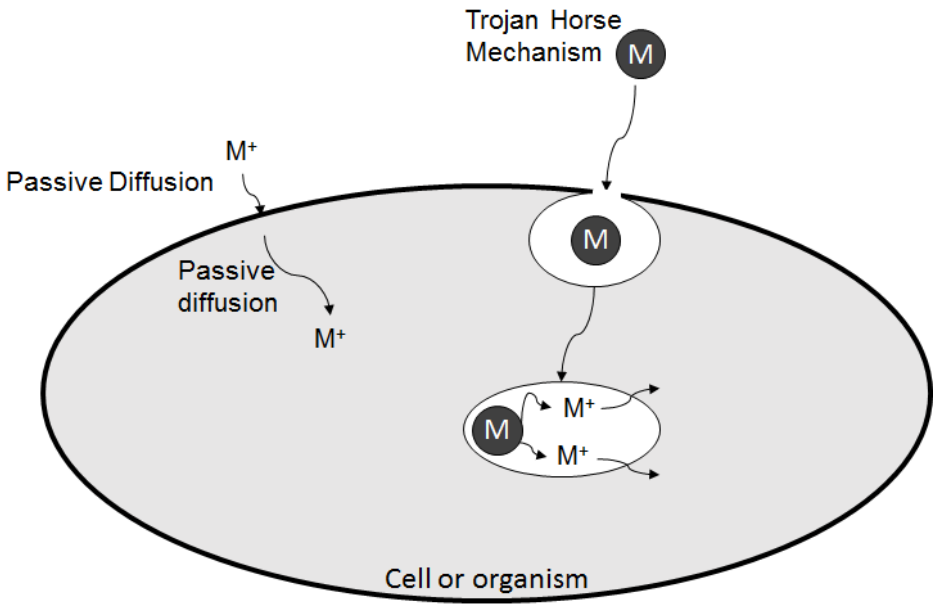

Figure 2. Passive diffusion of metal ions vs Trojan horse mechanism. While metal ions are limited to areas that they can passively diffuse in, nanomaterials may enter through different mechanisms and these areas then can facilitate dissolution and hence release of metal ions within a different area.

1.4 COMPLEX ENGINEERED NANOMATERIAL TOXICITY

Complex engineered nanomaterials (CENs) are a rapidly increasing class of nanomaterials that are used to overcome aggregation and sintering that is observed with individually structured NPs. These CENs are designed as multi-component materials designed in hierarchal nanostructures. They usually are made up of an active NP with an inert stable support NP[72-75]. These CENs are excellent model structures to determine structure-toxicity correlations that can be used to design safer nanomaterials. By systematically altering the hierarchal structure or composition, it is possible to determine how physicochemical properties are altered and, hence, toxicity.

While complex engineered nanomaterials are not widely studied, there are some important studies that have occurred. ZnO NPs have been shown to be toxic via a Trojan horse mechanism[33,76,77]. To eliminate this toxicity, Sotiriou et al., surrounded the photo chemical active NP with a nonporous silica shell. This shell reduced Zn^{2+} dissolution and direct exposure to the NP, while still maintaining the ZnO NP functionality[78]. As another example, nickel manganese colbalt (NMC) nanomaterials have emerged as a class of battery materials with the potential to be used in electric cars due to their high performance at a reduced cost[79-81]. These materials offer the advantage of redesigning the chemical composition to optimize functionality, while reducing toxicity. However, based on the model used, different optimal NMC compositions were determined to reduce toxicity. When the toxicity was studied with *Shewanella oneidensis*, it was determined that the Ni and Co materials contributed the most to toxicity[70]. In contrast, the Mn contributed the greatest to toxicity associated with zebrafish[82]. Thus, when determining the safest composition, care and thought must be taken into the expected exposure routes to determine the highest at risk species. Overall, these initial studies suggest that by redesigning the active metal NP with another material, it could provide a possible pathway to mitigating toxicity. These CEN structures maintain functionality while minimizing properties associated with toxicity (like ion dissolution).

2.0 TROJAN HORSE MECHANISM AND LOCALIZATION EXPLAIN TOXICITY OF NI/SiO_2 COMPLEX ENGINEERED NANOMATERIALS

2.1 INTRODUCTION

Nanotechnology is leading to revolutionary advances in consumer products, medicine, and engineering. It is projected to become a $1 trillion market in the US alone by 2020[14]. However, there is evidence that these nanomaterials pose potential health risks due to their unique properties as a consequence of their small size[1,15]. Yet, the drastic improvements that they promise to make to our quality of life are too significant to eliminate nanomaterials from industrial and consumer products in order to prevent potential health concerns. Thus, there is an urgent need to understand these materials' toxicities and provide structure-toxicity correlations that can be used *a priori* to design safer nanomaterials.

In order to evaluate the toxicity of nanomaterials, *in vivo* toxicity models, as opposed to *in vitro* models, may provide more physiology-relevant insight. However, the cost, time, and effort required, make it impractical to run animal toxicity studies on the vast number of nanomaterials being developed[83]. As a result, *in vitro* models are being used more frequently to quickly and economically screen nanomaterials for potential toxicity[84,85].

While the toxicity of (bare) metal nanoparticles (NPs) are being widely studied, very few studies to-date have focused on an emerging class of nanomaterials, so-called "complex

engineered nanomaterials" (CENs)[86,87]. These multicomponent materials consist of at least two constituent materials, usually with a hierarchal structure (e.g. core@shell nanomaterials[74,75,88]). CENs are used in a wide range of technologies, such as in catalysis, medical treatments and advanced electronics[89].

Importantly, the toxicity of embedded metal NPs is expected to differ from that of bare metal NPs due to the CEN structure and altered interactions of the metal NPs with the support matrix. For example, Sotiriou *et al.* demonstrated that by surrounding a ZnO NP with a nonporous silica shell (ZnO@SiO_2 CENs), the toxicity of the ZnO NP was eliminated[78]. The dense silica shell removed any interaction of the ZnO NP with the environment, while still maintaining their optoelectronic properties. However, complete encapsulation of NPs will result in a loss of functionality in many other applications, such as catalysis, where it is necessary for the NP to interact with the surroundings. For CENs, this can be achieved via *porous* encapsulations, which may still be advantageous in mitigating toxicity by modifying the interactions between the embedded NPs and their surroundings. Specifically, one could expect that a porous shell with sufficiently small pore size might mitigate direct interactions of the embedded NP with the cell. Furthermore, as the properties of embedded NP can change based on the nature of the embedding matrix, due to NP-matrix interactions, it can be expected that toxicity will vary with the CEN structure as well.

By systematically varying the nanoconfiguration of CENs with a defined composition, it has become possible to study how structural properties affect toxicity, and hence, to develop structure-toxicity correlations that offer insight into the design of safer nanomaterials[90,91]. However, in order to derive these structure-toxicity correlations, it is crucial to study the CEN's

physicochemical properties that influence toxicity, including size, shape, surface area, surface chemistry, aggregation, settling, and dissolution[28].

The present Chapter aims to establish the toxicity of Ni/SiO_2 CENs. These CENs are finding widespread applications in industrial catalysis, where embedding the nickel nanoparticles (Ni NPs) enhances reactivity while simultaneously stabilizing the Ni NPs within the SiO_2 support matrix[60-63,92-94], and hence pose a risk for occupational exposure in the chemical and fuel processing industry[95,96]. Previous *in vitro* studies of (bare) Ni NP agree qualitatively on their toxicity; however, the toxic concentration range varies strongly with NP size and tested cell and organ phenotype[97-102]. Furthermore, Pietruska *et al*. and Ke *et al*., both suggest that the toxicity of Ni NPs is mediated through a Trojan horse mechanism, i.e. that toxicity is based on Ni^{2+} dissolved from the Ni NPs engulfed by the cell rather than direct interaction with the NP surface[103,104].

In this Chapter, we will examine the toxicity of Ni/SiO_2 CENs using an *in vitro* NIH 3T3 fibroblast model. This model was chosen to reduce complexity associated with *in vivo* models and determine the influence of other properties on toxicity (including Ni^{2+} dissolution from the Ni NPs). Three CEN morphologies were studied that represent prototypical complex engineered nanomaterials: (i) Ni NPs deposited on the external surface of a porous amorphous silica NP (Ni-SiO_2), (ii) Ni NPs embedded within a porous silica shell (nhNi@SiO_2), and (iii) Ni NPs encapsulated in a hollow core within a porous silica shell (hNi@SiO_2). The three CENs were subjected to thorough physicochemical characterization, including dissolution and settling properties. These properties were then correlated with 24 hour cytotoxicity assays to determine structure-toxicity correlations.

2.2 METHODS

2.2.1 Nanomaterial synthesis and characterization

Ni/SiO_2 CENs were made using a one-pot, multi-step reverse microemulsion synthesis previously developed in our laboratory. The three nanomaterials utilized variations of the same synthesis protocol, assuring close structure similarity. Hollow $Ni@SiO_2$ ($hNi@SiO_2$) materials were synthesized using a one-pot reverse microemulsion synthesis previously developed in our laboratory. First, 50 mL of cyclohexane (≥99%) and 10.5 g surfactant Brij 58 (≥99% polyethylene glycol hexadecyl ether, Mn ~1124, Sigma-Aldrich) were refluxed at 50°C until the surfactant was fully dissolved. 1.5 mL of 1 M $Ni(NO_3)_2{\cdot}6H_2O$ (99.999%) was then added drop-wise, followed by 1.5 mL hydrazine hydrate (Sigma-Aldrich) to form a nickel hydrazine complex. Next, 5 g of tetraethylorthosilicate (TEOS, ≥99%) was added, followed by 3 mL of ammonium hydroxide (30%). After 2 hours of aging for silica growth, particles were precipitated with 2-propanol, collected via centrifugation, washed three times with 2-propanol, and dried in air. The crushed powder was then calcined in a Thermolyne 79300 tube furnace for 2 hours at 500°C in air.

Non-hollow $Ni@SiO_2$ ($nhNi@SiO_2$) CENs were made by a simple modification of the $hNi@SiO_2$ synthesis method, omitting the hydrazine addition step. Absence of the micelle-stabilizing Ni-hydrazine complex results in the formation of a solid (but porous) silica particle with embedded Ni NPs throughout the silica matrix. The precipitated material was dried and calcined as described above. To remove external nickel from the materials, calcined particles were reduced and etched in nitric acid by dispersing 0.20 g of material in aqueous nitric acid (35

vol%) for 30 min. The etched materials were washed twice in water to neutral pH, dried, and calcined.

For surface-deposited Ni-SiO_2, nickel-free spherical silica spheres were first synthesized using the microemulsion nhNi@SiO_2 procedure above but replacing aqueous Ni salt with 1.5 mL deionized (DI) water. Following calcination of the Ni-free silica, a deposition-precipitation method, modified from Deng et al.[105], was used to deposit very small and near-monodisperse nickel NPs on the surface of the calcined silica spheres. 0.6 g of silica NPs were dispersed in 15 mL of DI water by sonication, Ni salt solution was added (0.55 g $NiCl_2$ in 10 mL DI water), and the mixture was again sonicated for 20 min. Ammonium hydroxide (30%) was then added drop-wise (~5 mL, 52 drops, slowly over 20 min) until the pH of the solution was ~9.5. The resulting material was mixed for 20 min, centrifuged, dried, calcined at 300^{o}C in air, rinsed twice in DI water, dried, and calcined again at 300^{o}C in air.

CEN size and morphology were characterized with transition electron microscopy (TEM, JEOL-2000FX electron microscope). Particle measurements of TEM images were done using ImageJ software (http://rsb.info.nih.gov/ij/). Scanning Electron Microscopy (SEM) equipped with EDX was used at beam voltage of 15kV to determine elemental composition. Surface area and porosity were determined by Brunauer Emmett Teller (BET) analysis using a Micromeritics ASAP 2020 surface area and porosity analyzer. Pre-treatment consisted of 2-3 hour degassing at 200^{o}C under vacuum. Typically, a 6-point BET analysis was used for total surface area measurement and an 84-point N_2 Barrett-Joyner-Halenda (BJH) analysis with Halsey thickness curve correction and Kruk-Jaroniec-Sayari correction for pore size and volume determination.

2.2.2 Dissolved trace metal ion concentration

Ni^{2+} dissolution from the CENs was measured under radial detection by inductively coupled plasma atomic emission spectroscopy (ICP-AES, Thermo Electron Corporation iCAP6500 Duo Series ICP-OES Spectrometer). Standards were formulated from a stock standard solution (Fischer Scientific) with 3 wt% HNO_3 in deionized water to generate a standard curve. The degree of nickel ion dissolution from the CENs in 3T3 media was determined at specific time points. 10 mL dispersions (200 mg Ni/L) were prepared in 3T3 media. CENs were removed from the dispersions by centrifugation followed by filtration (Amicon 10,000 molecular weight cut-off filters, ~3.1 nm). HNO_3 (Sigma, 70%) was added dropwise to the filtrate to a concentration of 3 wt%.

2.2.3 CEN settling

Ni/SiO_2 CEN settling in 3T3 media was measured by UV-Visible spectroscopy (Beckman Coulter DU720). Path length was 1 cm and wavelength was 287 nm. CENs were dispersed in 3T3 media and deposited in a cuvette to a liquid height of 1.27 cm.

2.2.4 3T3 fibroblast cell culture

NIH 3T3 fibroblasts were used to evaluate the toxicity associated with the Ni materials. Cells were cultured in Dulbecco's Modified Eagle Medium (DMEM, Life Technologies) supplemented with 10% fetal bovine serum (FBS, Atlanta Biologicals) and 1% penicillin streptomycin (P/S, Life technologies), referred to as 3T3 media. The cells were cultured at 37^oC in 5% CO_2

environment. Cells were passaged at 70% confluency (every 2-4 days). For LIVE/DEAD analysis, the cells were plated in 6-well plates at 500,000 cells/well. For all other assays, cells were plated at 100,000 cells/well in 24-well plates.

2.2.5 CEN media preparation

CEN media solutions were made by exposing the dry CENs to a UV environment for one hour for sterilization. Initial 300 mg Ni/L concentration was made by adding CENs to 3T3 media supplemented with 20 mM HEPES buffer and sonicated for 15 minutes. Next, the CENs were serially diluted to the necessary concentrations and added immediately to the wells.

2.2.6 MTS cell metabolism

CellTiter 96® AQueous One Solution Cell Proliferation Assay MTS assay (Promega) was used to assess the cell metabolism, according to manufactures instructions. Briefly, 24 hours after seeding the cells, 0-300 mg Ni/L $NiCl_2$ or CEN media was added to the wells. The cells were exposed for 24 hours, after which the media was aspirated and 3T3 media (without CENs or $NiCl_2$) with 20% (v/v) MTS was added. The cells were incubated for 1 hour, and the absorbance at 490 nm was measured with a Synergy 2 multimode Microplate Reader.

2.2.7 Cell number quantification

Li-Cor IRDye Cell Tag 700 dye was used to stain and quantify cell number. After a 24 hour propagation time, cells were exposed to 0-300 mg Ni/L $NiCl_2$ or Ni/SiO_2 CENs for 24 hours.

Next, the cells were fixed with 4% formaldehyde (Thermo Scientific) in for 25 minutes. The cells were permeabilized with 0.5% Triton-X in phosphate-buffer saline (PBS) for five minutes and then blocked with 10% donkey serum in 1% bovine serum albumin/PBS for 45 minutes at room temperature (RT). The cells were then rinsed with PBS and incubated with IRDye cell tag 700 dye (Li-Cor) for one hour at RT. The cells were rinsed with PBS twice, then with DI water once, prior to imaging the cells with the LI-COR Odyssey CLx.

2.2.8 Cell viability

Cell viability after CEN exposure was analyzed by the LIVE/DEAD assay (Life Technologies), according to the manufacturer's instructions. Briefly, cells were exposed to 0-200 mg Ni/L $NiCl_2$ or Ni/SiO_2 CENs for 24 hours. Next, cells were incubated with 2 μM ethidium homodimer-1 and 1 μM calcein-AM in 3T3 media for 25 minutes at RT. Cells were washed three times with PBS before fluorescent imaging.

2.2.9 Newport green and side scatter

Newport Green™ DCF indicator (NPG, Life Technologies) was used to analyze the intracellular Ni^{2+} concentration [106]. After a 24 hour propagation period, the cells were exposed to 0-300 mg Ni/L $NiCl_2$ or Ni/SiO_2 CEN for 24 hours. Next, 10 μM NPG was incubated with the cells for 20 minutes at RT. Immediately following incubation, the cells were dissociated using trypsin, centrifuged, rinsed, and resuspended in PBS. Finally, an Accuri C6 flow cytometer was used to quantify the fluorescent intensity (488 nm). At least 10,000 events were collected per sample to

obtain a viable histogram. In parallel, the side scatter was also quantified using the Accuri C6 flow cytometer.

2.2.10 BCA protein assay

Pierce BCA protein assay kit (Thermo Scientific) was performed according to the manufacturer's instructions. Briefly, 300 mg Ni/L CENs were dispersed in 3T3 media and incubated for 2 or 24 hours. After the incubation period, the CENs were separated and re-dispersed in PBS. A 10 µL sample was mixed with 200 µL working reagent and incubated at 37^{o}C for 30 minutes. Next, the samples were cooled to RT and the absorbance was read at 562 nm.

2.2.11 Confocal microscopy

50,000 cells/well were plated in a 24-well MatTek dish with glass bottom (No. 1.5 coverslip; 13 mm glass diameter). After 24 hour exposure to 0-200 mg Ni/L $NiCl_2$ or Ni/SiO_2 CEN, the toxic media was aspirated and replaced with 3T3 media supplemented with 100 nM Lysotracker Red (Thermo Fisher Scientific) and 10 µM NPG. The cells were then incubated for one hour. Finally the cells were rinsed multiple times and observed with Nikon A1 Spectral Confocal microscope.

2.2.12 Statistics

All experiments were carried out in triplicate replicates, and three independent trials were completed for each assay. Error bars indicate standard deviation. *indicates $p>0.05$ for

significance compared to the unexposed control after one-way ANOVA followed by Dunnett's test[107].

2.3 RESULTS

2.3.1 CEN physicochemical characterization

Three Ni/SiO_2 complex engineered nanomaterials (CENs) were synthesized: Ni NPs deposited on the external surface of SiO_2 NPs (Ni-SiO_2), Ni NPs embedded throughout a porous SiO_2 NP (nhNi@SiO_2), and Ni NP embedded in a hollow core surrounded by a porous SiO_2 shell (hNi@SiO_2). Figure 3 shows the transmission electron microscopy (TEM) images of the three Ni/SiO_2 CENs, and Table 1 shows the CENs size, weight loading and surface area. Overall, all three CENs had near-identical chemical compositions and dimensions, and differ in nanostructure configuration only. The Ni NPs were ~2 nm in diameter, while the composite CENs were ~40-50 nm. The silica matrix was amorphous in all three cases. All three CENs had similar silica pore structures with average silica pore diameters of ~0.7 nm and surface areas of ~200±20 m^2/g (0Figure 52).

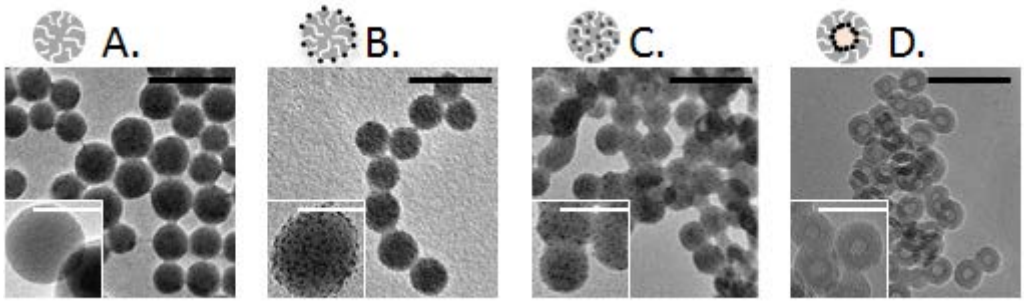

Figure 3. TEM images of Ni/SiO_2 CENs. A. Ni-free SiO_2 NPs B. Ni-SiO_2 C. nhNi@SiO_2 and D. hNi@SiO_2. Black scale bars are 100 nm and white inset scale bars are 50 nm.

Table 1. Ni loading, Ni particle size, CEN particle size and surface area for all three CENs.

CEN	Ni loading (wt% Ni)	Ni particle size (nm)	Primary particle size (nm)	Surface area (m^2/g)
Ni-SiO_2	12.0 ± 2.4	2.0 ± 0.2	50.8 ± 5.3	212
nhNi@SiO_2	7.3 ± 1.0	2.1 ± 0.3	43.2 ± 3.6	186
hNi@SiO_2	8.0 ± 0.6	< 2	41.0 ± 4.1	216

2.3.2 Ni^{2+} dissolution depends on CEN structure

Ion dissolution from the NP has been shown to be an important toxicity mechanism for metal NPs[30,108-110], including nickel[66,103,104,111]. It is hence critical to characterize the metal dissolution from the CENs. The Ni/SiO_2 CENs were dispersed in 3T3 media (DMEM supplemented with 1% P/S and 10% FBS) and removed at specific time points using centrifugal ultrafiltration. The

dissolved Ni^{2+} concentration in the solution was then determined via ICP-AES. Figure 4 shows the Ni^{2+} dissolution at three time points over 24 hours: Ni-SiO_2 showed the lowest dissolution (~4 mg Ni^{2+}/L) of all three CENs. Interestingly, the dissolution occurred during the first hour with no additional dissolution over the next 24-hour period. In contrast, nhNi@SiO_2 showed the highest dissolution (~20 mg Ni^{2+}/L) with continuous dissolution over the 24 hour period. hNi@SiO_2 exhibited a similar dissolution trend to nhNiSiO_2, albeit at a lower rate and hence a lower final Ni^{2+} concentration of ~15 mg Ni^{2+}/L.

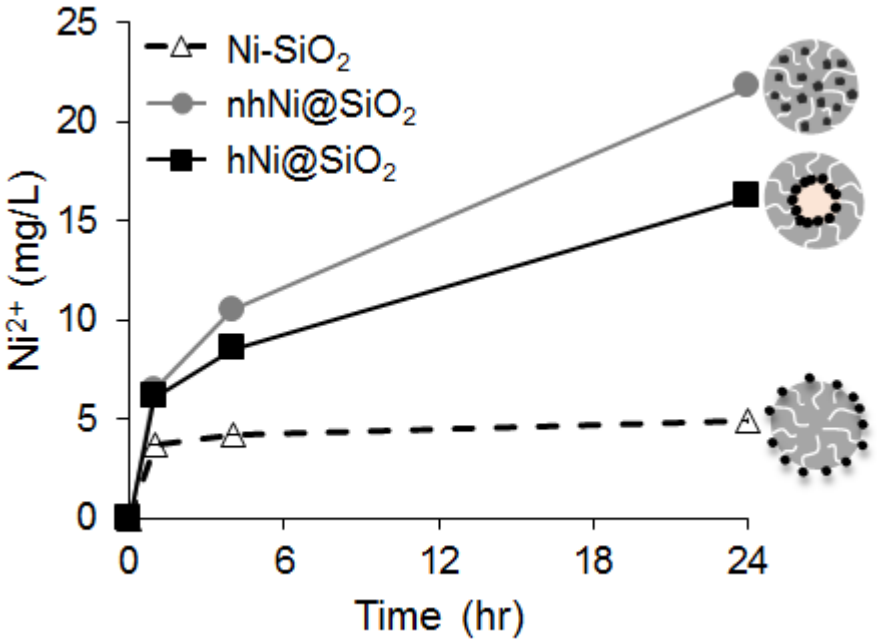

Figure 4. Ni^{2+} dissolution for 200 mg Ni/L CEN in 3T3 media over 24 hours.

2.3.3 CENs settling behavior is independent of structure

Settling of NPs can modify the effective cell exposure and is hence of critical importance for nanotoxicity studies in aqueous media [112,113]. UV-visible spectroscopy was used to measure settling for 200 mg Ni/L CEN dispersed in 3T3 media, Figure 5. While Ni-SiO_2 initially seems to settle slightly faster than the other CENs, all three CENs exhibited similar settling rates after one hour. Hence, significant differences in effective exposure due to settling behavior of the three materials can be excluded for the present study.

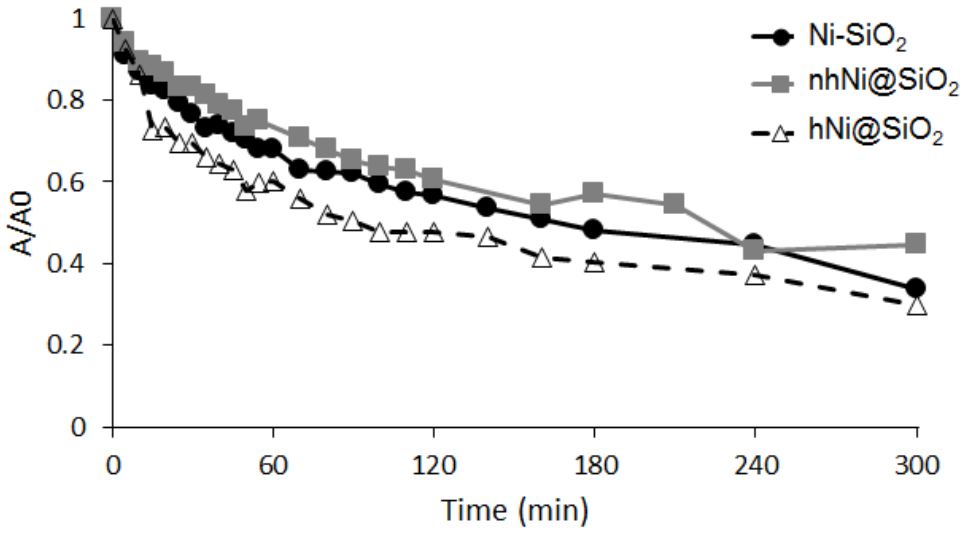

Figure 5. 200 mg Ni/L CEN settling behavior in 3T3 media over five hours. The absorbance at each time point was normalized by the initial absorbance at time zero.

2.3.4 Toxicity testing

3T3 fibroblasts are used as an FDA standard test model for evaluating biomaterials[114,115]. They are furthermore a robust, inexpensive cell line that is finding increasing use in nanotoxicity studies[69,116,117]. A 24 hour exposure time was selected to study toxic effects associated with an acute exposure, in addition to reducing complications associated with multiple cell-division cycles. Seven concentrations between 0-300 mg Ni/L were chosen to thoroughly study the Ni materials' effects on cell viability. $NiCl_2$ was used as a control to mimic the toxicity associated with ionic Ni^{2+} dissolved from the CENs.

2.3.5 Cell metabolism decreased after exposure to Ni materials

After 24 h exposure, the metabolism of the cell population was analyzed using MTS, which monitors the bioreduction of a tetrazolium compound into a red formazan product. As further reference, cell metabolism was also analyzed after exposure to (Ni-free) amorphous silica which showed no change in metabolism for concentrations from 0-2700 mg SiO_2/L, corresponding to the highest SiO_2 exposure in the CEN tests (Figure 54). Figure 6 presents the cell metabolism normalized to the control cell metabolism (with no CEN or $NiCl_2$ exposure), after 24 hour exposure. Exposure to $NiCl_2$ and hNi@SiO_2 resulted in a continuous decrease of the cell metabolism with increasing concentration. In contrast, exposure to Ni-SiO_2 and nhNi@SiO_2 showed a similar initial decrease in metabolism which, however, was followed by a plateau for concentrations above ~150 mg Ni/L. A 50% reduction in metabolism of the cell population was caused by ~200 mg Ni/L $NiCl_2$, ~85 mg Ni/L Ni-SiO_2, 200 mg Ni/L nhNi@SiO_2, and 125 mg Ni/L hNi@SiO_2, i.e. the CEN's toxicity ranked Ni-SiO_2 > hNi@SiO_2 > nhNi@SiO_2 = $NiCl_2$.

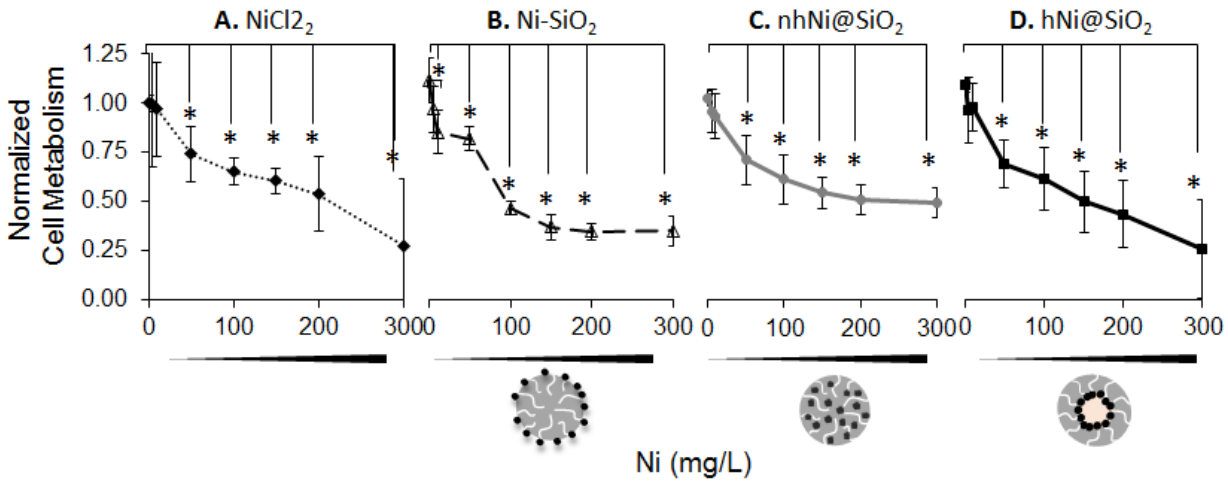

Figure 6. Cell metabolism by MTS, normalized to the control cells, after 24 hour exposure to 0-300 mg Ni/L A. $NiCl_2$ B. Ni-SiO_2 C. nhNi@SiO_2 and D. hNi@SiO_2. *$p \geq 0.05$ Dunnett's test, compared to control.

2.3.6 3T3 fibroblast viability depends on CEN structure

The reduction in metabolism observed above can be due to either a reduction in cell viability/number (while maintaining the cell metabolism of surviving cells), or a reduction in the metabolic activity (while maintaining the number of live cells). Hence, to explain the observed reduction in metabolism, we next determined cell viability by quantifying the cell number using a Li-Cor IRDye Cell Tag 700, imaged on the Li-Cor platform. Figure 7 presents the cell number after exposure to Ni/SiO_2 CENs, with $NiCl_2$ again serving as reference point for pure ionic Ni^{2+} exposure. The fluorescent intensity of exposed cells was normalized to the fluorescent intensity of control cells (without any exposure to $NiCl_2$ or CENs). Again the toxic effect of (Ni-free) SiO_2 NPs were first evaluated to determine if any observed toxicity could result from the silica shells of the CENs. In agreement with the MTS data discussed above, the amorphous SiO_2 NPs

showed no toxicity (Figure 55). After exposure to $NiCl_2$, the cell fluorescent intensity, and hence cell viability, continuously decreased with increasing Ni^{2+} concentration (50-300 mg Ni/L). Interestingly, after exposure to all three CENs, the cell viability initially decreased for low exposure dose (~10 – 50 mg Ni/L), but then plateaued as Ni concentrations further increased. The cell viability stabilized at ~27% after exposure to Ni-SiO_2, ~88% after exposure to nhNi@SiO_2 and ~68% after exposure to hNi@SiO_2. This trend was further corroborated qualitatively by LIVE/DEAD staining (, Figure 56).

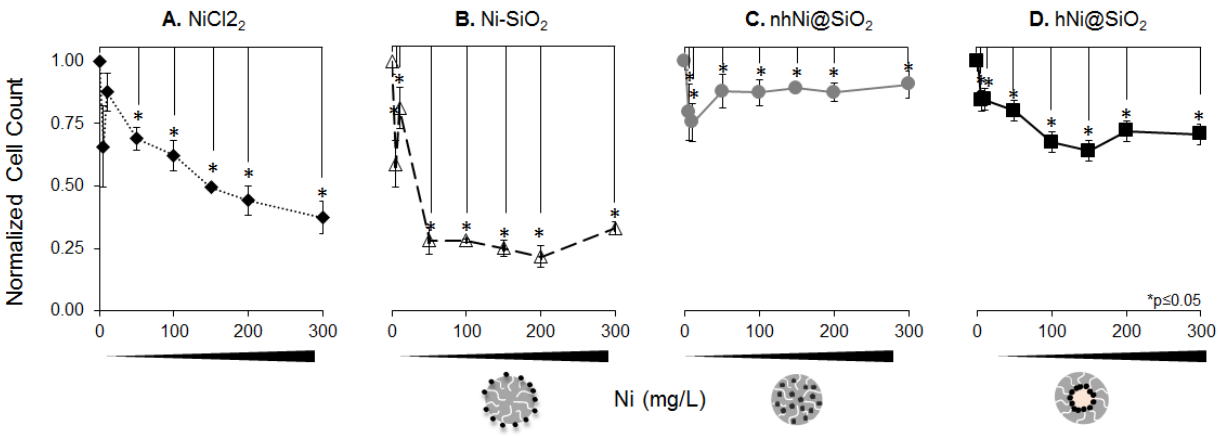

Figure 7. Cell count after 24 hour exposure to 0-300 mg Ni/L A. $NiCl_2$ B. Ni-SiO_2 C. nhNi@SiO_2 and D. hNi@SiO_2. *indicates p≤0.05 for Dunnett's test.

The close correspondence between metabolism and cell viability for $NiCl_2$ and Ni-SiO_2 indicates that the reduction in metabolism can be attributed primarily to cell death. However, such correspondence was lacking for nhNi@SiO_2 and hNi@SiO_2 CENs, where cell metabolism was lowered considerably by CEN exposure, even though cell viability was not strongly

affected. This suggests that the two CENs with nanoconfined Ni NP, hNi@SiO_2 and nhNi@SiO_2, decreased cell metabolism while not causing cell death.

2.3.7 Toxicity mechanism

Thus far, the toxicity tests show a clear correlation between structure and toxicity: The Ni-SiO_2 CEN caused significant cell death while the nhNi@SiO_2 and hNi@SiO_2 CENs decreased cell metabolism while maintaining cell viability. Previous studies have suggested that bare Ni NPs are toxic via a Trojan horse mechanism in which the Ni NP acts as a delivery vehicle, i.e. NP is taken up by the cell and subsequent Ni^{2+} dissolution inside the cell causes toxicity[103,104]. To determine if the toxicity of the present CENs is also mediated via a Trojan horse mechanism, the NP uptake was quantified, followed by evaluation of intracellular Ni^{2+} concentration.

2.3.8 CEN uptake depends on the CEN surface

To evaluate if the CEN toxicity can be directly attributed to CEN uptake into the cells, we determined the CEN uptake by analyzing the side scatter (SSC) with flow cytometry[118,119]. SSC is correlated with cell density and will hence increase with increasing CEN concentration in the cell. Figure 8 shows changes in SSC after exposure to the CEN materials by normalizing the SSC to that of unexposed control cells. As expected, cells exposed to $NiCl_2$ showed minimal increase in SSC. Cells exposed to all three CENs experienced a rapid increase in uptake (at low concentrations 5-50 mg Ni/L), followed by a plateau. However, uptake of nhNi@SiO_2 and hNi@SiO_2 CENs occurred at similar rates, while Ni-SiO_2 was taken up at a significantly higher rate. Since settling of CENs occurred at similar rates and effective exposure is hence equal, these

uptake difference must be associated with differences in CEN morphology. Both core@shell materials (hNi@SiO_2 and nhNi@SiO_2) have a silica terminated external surface, while the external surface of Ni-SiO_2 is largely covered by Ni NP. This suggests that the surface chemistry (i.e. surface termination) has significant impact on the CEN's interactions with the cell membrane and thus affects the uptake rate. To further study this, we determined the protein concentration on each CEN after being dispersed in 3T3 media for two or 24 hours by BCA, Table 2. As hypothesized, the Ni-terminated surfaces had a much higher concentration of protein, per CEN, compared to the silica-terminated surfaces. There were minimal differences in protein concentration between the 2 and 24 hour time points. Overall, this suggests that the surfaces play a crucial role in formation of a protein corona which influences the CEN uptake into the cell. The uptake rates correlate closely with the toxicity ranking of the CENs: nhNi@SiO_2 and hNi@SiO_2 CENs, which do not elicit high cell death, are taken up at a slower rate than the more toxic Ni-SiO_2 CEN (which caused cell death).

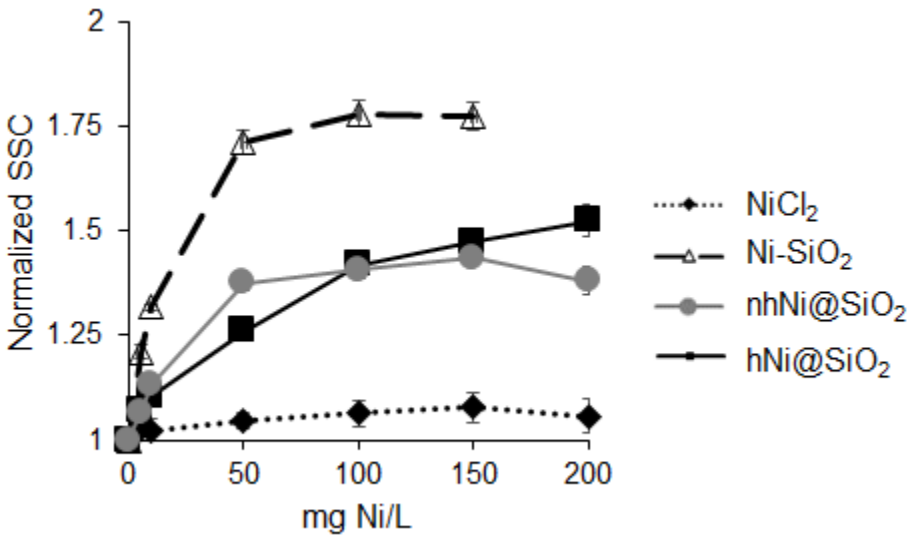

Figure 8. Side scatter (SSC), normalized to control, after exposure to 0-200 mg Ni/L $NiCl_2$ and Ni/SiO_2 CENs for 24 hours.

Table 2. Protein concentration normalized by CEN number to determine ng protein/CEN.

	ng protein/CEN		
	Ni-SiO_2	**nhNi@SiO_2**	**hNi@SiO_2**
2 hour	3.21E-04	9.11E-04	8.36E-05
24 hour	3.00E-04	1.02E-04	8.28E-05

2.3.9 Intracellular Ni^{2+} concentration depends on structure

While the above observed differences in CENs uptake correlate well with the toxicity of the CENs, they do not confirm a Trojan horse mechanism as being responsible for this toxicity. We therefore evaluated the intracellular Ni^{2+} concentration using Newport Green, a fluorescent dye

whose fluorescence is enhanced in the presence of Ni^{2+} but not bulk Ni[104,106]. Newport Green can be used to determine the presence of high concentrations of zinc ions. However, the dye is not as sensitive to change in zinc concentration as to Ni^{2+}. Zhao et al., showed that when 20 μM of Zn was added to cells exposed to 100 μM Ni^{2+}, the NPG fluorescent intensity was changed by less than 10% compared to the cells exposed to just Ni^{2+}. Hence, the changes in NPG fluorescent intensity is dominated by changes in Ni^{2+} concentration and not changes in zinc ion concentration that may result from the Ni toxicity[106]. Cells were exposed to 0-200 mg Ni/L CEN or $NiCl_2$ for 24 hours, followed by addition of the Newport Green dye. The cells were then collected and the intracellular Ni^{2+} concentration was analyzed using flow cytometry. The 200 mg Ni/L Ni-SiO_2 could not be analyzed due to its high toxicity, making it impossible to collect enough cells to obtain a viable histogram in flow cytometry.

Figure 9 presents the fluorescent intensity measured by flow cytometry, normalized to the control cells, thus yielding a measurement of relative signal enhancement that quantifies the intracellular Ni^{2+} concentration. Cells exposed to Ni-SiO_2 showed the highest intracellular Ni^{2+} concentration, followed by hNi@SiO_2, nhNi@SiO_2, and lastly $NiCl_2$. The intracellular Ni^{2+} concentration increased in a dose-dependent near-linear manner for cells exposed to $NiCl_2$. Cells exposed to low concentrations (5-50 mg Ni/L) of all three Ni/SiO_2 CENs experienced a rapid dose-dependent increase in intracellular Ni^{2+}. However, at higher concentrations (>50 mg Ni/L), the intracellular Ni^{2+} concentration stabilized for exposure to Ni-SiO_2 and nhNi@SiO_2 CEN. The intracellular Ni^{2+} concentration for cells exposed to hNi@SiO_2 slightly increased from 50-150 mg Ni/L, though much more gradually than for the lower concentration range. The intracellular Ni^{2+} concentration agree well with the CEN uptake and toxicity rankings: The most toxic CEN,

Ni-SiO_2, showed the highest uptake into the cell and, consistent with this, also shows the highest intracellular Ni^{2+} concentration.

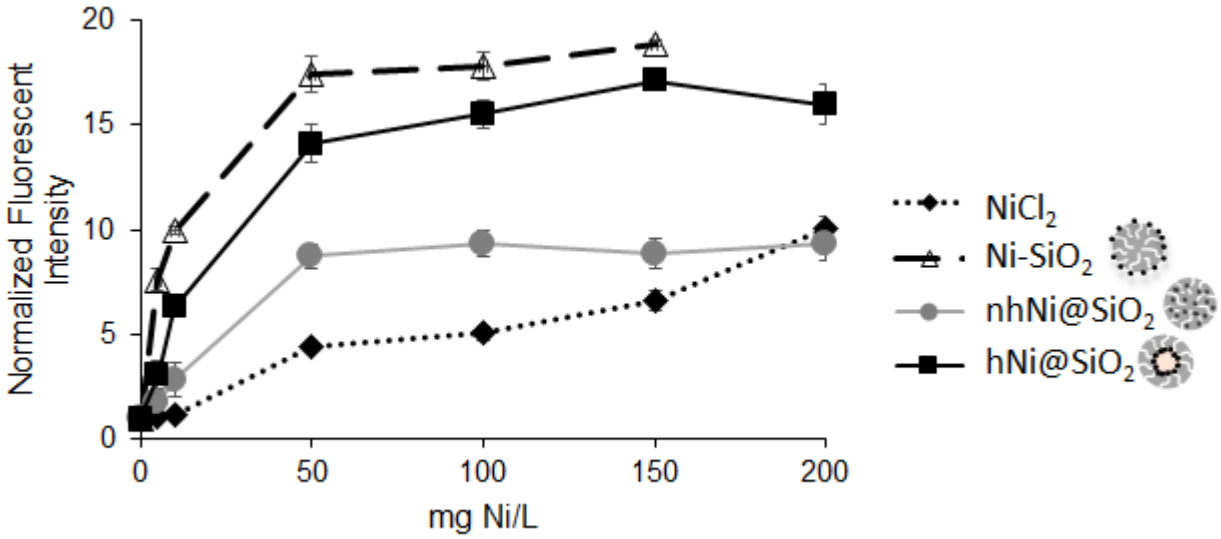

Figure 9. NPG fluorescent intensity, normalized to control cells, after 24 hour exposure to 0-200 mg Ni/L $NiCl_2$ and Ni/SiO_2 CENs.

2.3.10 Ni^{2+} dissolved from CENs localizes in lysosomes

Interestingly, unlike for the CENs, where toxicity, uptake, and intracellular concentrations showed a clear correlation, $NiCl_2$ was more toxic than nhNi@SiO_2 and hNi@SiO_2, yet showed the lowest intracellular Ni^{2+} concentration. However, toxicity is not necessarily just a result of intracellular concentrations, but can also be affected by intracellular localization of the toxin. Hence, we determined the intracellular localization of Ni^{2+} using confocal microscopy. Cells were exposed to 50 mg Ni/L concentrations of $NiCl_2$ and Ni/SiO_2 CENs, respectively, for 24

hours. After exposure, Lysotracker Red was used to stain the lysosomes, and NPG was added to determine the Ni^{2+} location, allowing determination of localization of Ni^{2+} in the lysosomes. Confocal images, Figure 10, showed strong co-localization, which differed significantly between the four samples. In order to quantify the degree of co-localization, the fraction of free Ni^{2+} vs co-localized in the lysosome was determined via the pixel count and intensity for green (free Ni^{2+}) and yellow (colocalization of Ni^{2+} and lysosome) pixels, Figure 11.

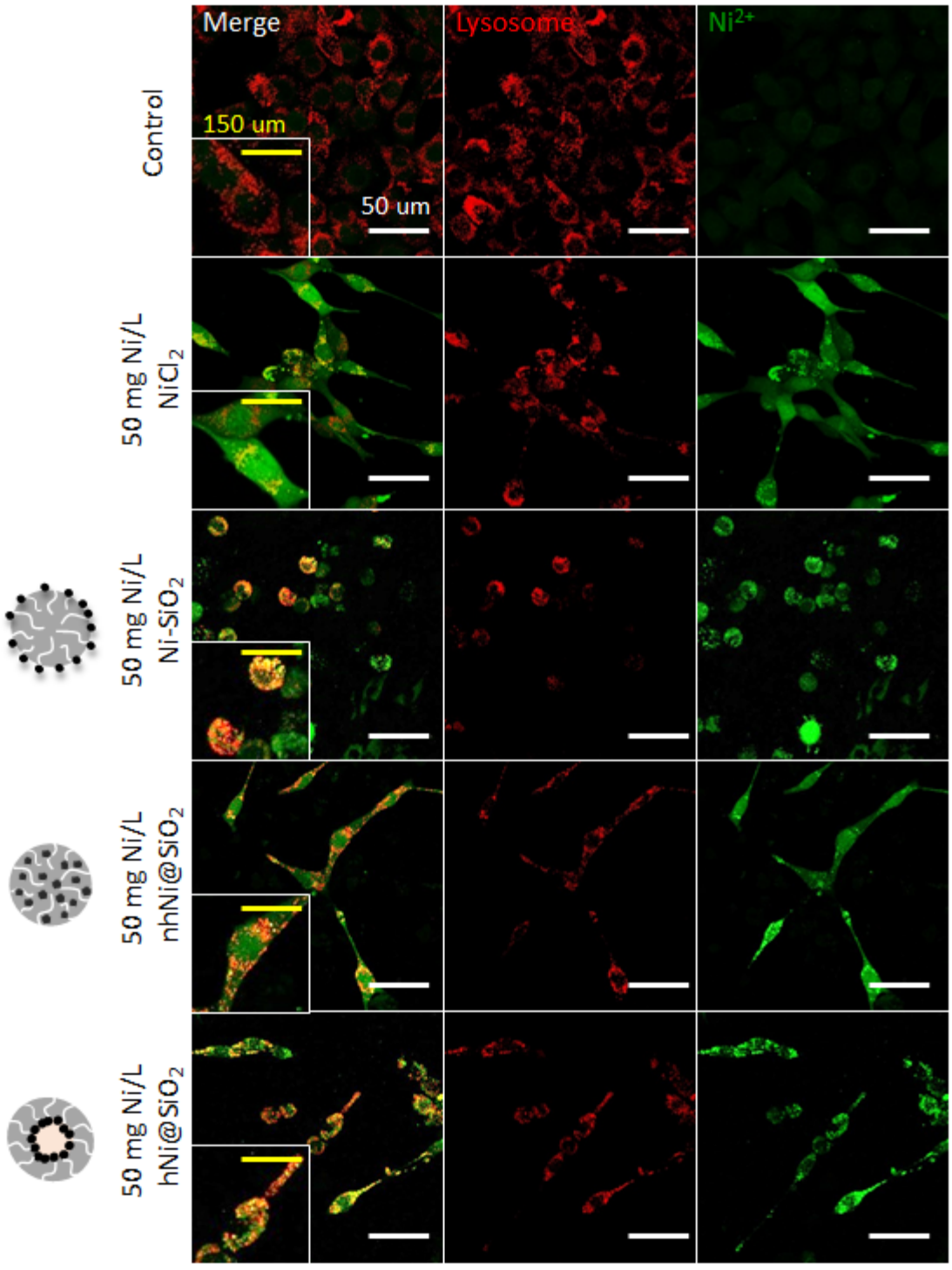

Figure 10. Maximum projected confocal images of 3T3 fibroblasts after exposure to 50 mg Ni/L $NiCl_2$ or Ni/SiO_2 CENs for 24 hours. Cells are stained with Lysotracker Red (second column) and Newport Green (third column). White scale bars are 50 µm and yellow inset scale bars are 150 µm.

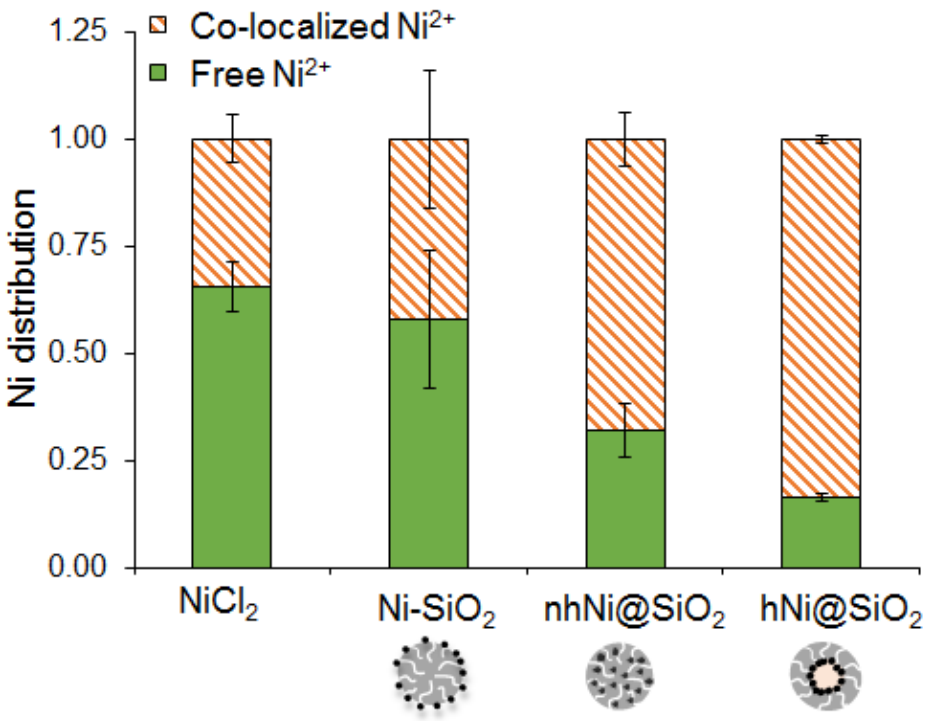

Figure 11. % of Ni^{2+} presented as free Ni^{2+} throughout the cell and Ni^{2+} colocalized with lysosomes in the cell after 24 hour exposure to 50 mg Ni/L $NiCl_2$ or Ni/SiO_2 CENs.

From the confocal images it was evident that Ni^{2+} from $NiCl_2$ exposure was present throughout the cell, including the nucleus, and ~35% of the intracellular Ni^{2+} was co-localized with the lysosomes. Cells exposed to Ni-SiO_2 showed unhealthy morphology and were rounding up, reflecting the high toxicity associated with the CEN. 42% of intracellular Ni^{2+} after exposure to Ni-SiO_2 was contained in the lysosome. On the other hand, 68% of the intracellular Ni^{2+} after exposure to nhNi@SiO_2 and 84% of the intracellular Ni^{2+} after exposure to hNi@SiO_2 was located within the lysosomes. Both core@shell CENs showed a very high co-localization of Ni^{2+} with lysosomes, while the Ni-SiO_2 and $NiCl_2$ showed a wider distribution of Ni^{2+} throughout the cell. As additional internal consistency check, the pixel intensity was measured and agreed with

the rankings in the above discussed NPG analysis using flow cytometry. Ni-SiO_2 showed the highest integral intensity, i.e. highest total intracellular Ni^{2+} concentration, followed by hNi@SiO_2 which was closely followed by nhNi@SiO_2, with $NiCl_2$ finally showing the lowest integral pixel intensity.

2.4 DISCUSSION

Complex engineered nanomaterials (CENs) are expected to dominate the next generation of nano-enabled products. It is hence imperative to assess and understand the toxicity associated with these nanomaterials in order to inform "safe-by-design" materials design. The present set of carefully designed CENs represent common CEN morphologies that differ only in their nanostructure (i.e. embedding of Ni NPs) without altering NP size and surface area. Thus we are provided with the unique opportunity to derive structure-toxicity correlations that can be utilized to design safer nanomaterials for future applications.

2.4.1 Structure influences toxicity

Overall, our results reveal clear and strong correlations between structure and toxicity of the studied CENs. 3T3 fibroblasts exposed to the core@shell nanomaterials (nhNi@SiO_2 and hNi@SiO_2) exhibited a decrease in individual cell metabolism without significant cell death, while cells exposed to $NiCl_2$ and Ni-SiO_2 caused widespread cell death. This observation is noteworthy from at least two vantage points: First, it indicates that surface termination (silica vs Ni) has strong impact on toxicity of the CENs, i.e. size and composition (which are virtually

identical among all three materials) alone do not suffice to characterize or predict toxicity. We observe that the surface termination results in differences in protein concentrations, suggesting the Ni surface is likely to adsorb different proteins than a silica surface and form different protein coronas (Table 2). This is also in agreement with the reduced Ni dissolution from the Ni-SiO_2 compared to the core@shell materials (Figure 4), again likely due to a "protein protection" of the Ni clusters on the external surface of Ni-SiO_2.

Second, the observed difference in CEN toxicity highlights the need to combine multiple complementary toxicity assays in order to capture structure-toxicity correlations in a robust and reliable way. Based on cell metabolism alone (Figure 6), one would deduce that all three CENs have similar toxicity which in turn is similar to the toxicity of $NiCl_2$. In contrast to that, while the cell viability results agree better with the toxicity rankings, based on those assays alone the nhNi@SiO_2 CEN would appear to be virtually non-toxic (Figure 7). The combination of multiple assays not only allows deeper understanding of the cells response to a toxin, but also helps to avoid spurious conclusions.

2.4.2 Ni/SiO_2 CENs toxicity is induced through a Trojan horse mechanism

The Ni-SiO_2 CENs emerged as the most toxic CEN in the present study by causing considerable cell death, followed by hNi@SiO_2, and lastly nhNi@SiO_2 which inhibit cell metabolism without inducing cell death. This toxicity ranking is in close agreement with the intracellular Ni^{2+} concentration: Ni-SiO_2 resulted in the highest intracellular Ni^{2+} concentrations, followed by hNi@SiO_2, and lastly nhNi@SiO_2. This close correlation hence suggests that the observed toxicity results from Ni^{2+} dissolved from the CENs rather than from direct interactions of cellular functions with the Ni NPs themselves. This indicates the presence of a Trojan horse mechanism,

as previously suggested by Pietruska *et al*. and Ke *et al*. for (bare) Ni NPs[30,103,104,120], in which the main role of the CEN is to facilitate transport of the Ni NPs into the cells, while the observed toxicity then results from intracellular dissolution of the NP. This is further supported by the observation that exposure to Ni-SiO_2 resulted in the highest intracellular Ni^{2+} concentration despite showing the lowest Ni^{2+} dissolution in the extra-cellular media. This suggests that the intracellular Ni^{2+} concentration results predominantly from dissolution inside the cell (due to the acidic pH in the lysosomes) rather than from transportation of dissolved Ni^{2+} from the media into the cell. Hence, the relative stability of Ni-SiO_2 against dissolution in the media, leads to increased Ni uptake (in NP form) as compared to the other two CENs, resulting in more Ni to be dissolved and kill the cell. In contrast, the other two CENs show faster extracellular dissolution and hence "lose" some of their Ni in the media before uptake into the cell and thus have less available to dissolve in the cell (see Figure 4).

The Trojan horse mechanism is further corroborated by comparing the intracellular Ni^{2+} concentrations after exposure of the cells to CENs, and to an equivalent dose of $NiCl_2$. For example, 200 mg Ni/L nhNi@SiO_2 dissolved in the 3T3 media to a concentration of ~25 mg Ni^{2+}/L and resulted in a NPG signal enhanced 8-fold. However, the cell exposed to 25 mg Ni^{2+}/L from $NiCl_2$, resulted in a 2.5-fold increase in NPG signal. Thus, one can conclude from this observation that at least 68% of the intracellular Ni^{2+} is from CEN dissolution inside the cell. A similar increase in signal, compared to the corresponding dissolved Ni^{2+} exposure from $NiCl_2$, is present after exposure to all three CENs. Thus, we conclude that the intracellular Ni^{2+} concentration is dominated by CEN dissolution inside the cell rather than by diffusion of Ni^{2+} from the media into the cells.

2.4.3 Localization of Ni^{2+} explains toxicity difference between $NiCl_2$ and CENs

Interestingly, exposure to $NiCl_2$ resulted in the lowest intracellular Ni^{2+} concentrations, despite showing among the highest toxicity in this study. This can be traced back to the location of the Ni^{2+} ions. While Ni^{2+} ions are able to passively diffuse from the media into the cell and interact with many cell organelles, including the nucleus[121], nanomaterials are taken up via endocytosis-mediated pathways and are hence contained in lysosomes[122-128]. This containment in the lysosomes results in a decrease in toxicity over the tested period, despite the higher intracellular Ni^{2+} concentration. However, it is possible that the Ni^{2+} inside the lysosome could eventually be released into the cellular environment, causing a delayed toxic response (such a long term exposure was beyond in the scope of the present study). Finally, it seems noteworthy that uptake of the CENs through a lysosome-mediated pathway, which has an acidic pH, will cause the Ni NPs to dissolve rapidly[122-128]. This suggests that for the characterization or design of nanomaterials, characterizing the dissolution in the cell media, while necessary, may not be sufficient. It is equally critical to take into consideration the intracellular dissolution upon CEN uptake.

2.4.4 CEN properties are dependent on test environment

Finally, it is instructive to compare the results from the present study with those in which we evaluated the same set of CENs using zebrafish models (Chapter 4.0). Remarkably, we found quite different dissolution and settling behavior for the three nanomaterials, and hence also different toxicity rankings. Surprisingly, the present Ni^{2+} dissolution studies (Figure 4) showed Ni-SiO_2 to be the most resistant to dissolution. Intuitively, one might expect Ni-SiO_2 to show the

highest dissolution, since the Ni NPs in this configuration have direct exposure to the media solution. This is in fact what we had observed when investigating the toxicity of the same three CENs using zebrafish models (Figure 19). In those studies, Ni-SiO_2 CENs indeed showed higher Ni^{2+} dissolution in E3 zebrafish media than the other two CENs. The primary difference between the zebrafish media and the current media is the absence of proteins (specifically FBS) in the former. Hence, we speculate that these CENs form a protein corona that caps the surface of the Ni NPs on the Ni-SiO_2 CEN, thus stabilizing the NPs and limiting dissolution[129]. In contrast, the Ni NPs in the other two CENs are embedded within the silica matrix in which the silica pores are sufficiently small (<1 nm) to block proteins from penetrating and accessing the Ni NPs. Thus, the Ni NPs are shielded by the silica support against protein capping, leaving the Ni NPs exposed to the media and hence prone to dissolution. This suggests that the presence of proteins in the media greatly impacts the extracellular dissolution and can influence the toxic response elicited by the CENs. Hence, media composition needs to be considered as a critical parameter in evaluating nanomaterial toxicity in laboratory studies.

2.5 CONCLUSION

Complex engineered nanomaterials constitute a rapidly emerging group of nanomaterials that has to-date found relatively little attention in nanotoxicity studies. Our Chapter aimed at contributing towards closing this gap by investigating the toxicity associated with three Ni/SiO_2 CENs. The materials were chosen to combine a non-toxic matrix (SiO_2) with a metal with well-known high toxicity, and then carefully designed to utilize the nanostructure to control the exposure of the biological cell environment to the supported or embedded metal NP. Our results confirm that

such nanostructuring can indeed strongly affect the toxicity of the resulting CEN and may hence offer a promising path towards rational design of nanomaterials with lowered toxicity.

Interestingly, our results do not indicate that the altered toxicity can be correlated with changes in the (direct) interactions of the metal NPs with the cellular environment, such as the spatial barrier between the Ni NPs that are embedded into the silica matrix and hence have no path of direct interaction with the cell. Instead, the differences between the CEN toxicities could be traced back to differences in both cellular uptake and dissolution, presumably due to formation of different protein coronas between those CEN that showed a silica-terminated external surface vs those that were decorated with Ni NPs.

Remarkably, all three CENs were less toxic than a corresponding dose of $NiCl_2$ salt (i.e. purely ionic Ni^{2+}), despite the fact that cell exposure to the CENs resulted in higher intracellular Ni^{2+} concentrations. This strongly suggests that the CEN serve as a "Trojan horse" that facilitates uptake of Ni into the cell: While ionic Ni^{2+} in solution (from the Ni salt) passively diffuse into the cell and interacts with many cell organelles including the nucleus, Ni^{2+} from the CENs is highly localized in the lysosomes, suggesting dissolution from the CEN in the acidic environment. This shelters the cell at least temporarily from a higher dose of toxic exposure.

Overall, we were hence able to correlate the CEN structure with toxicity and propose as key conclusion from the present study that the safest Ni/SiO_2 CEN configuration is one that limits dissolution inside the cell. Since this conclusions is largely based on the physicochemical properties of the CEN (i.e. dissolution and uptake, rather than the specific, complex interactions and toxic pathways of the metal ions inside the cell), we propose that these conclusions are likely to hold for a wide range of similar core@shell CENs in which metal NPs are embedded in a non-toxic oxide shell.

3.0 MITIGATING TOXICITY BY SLOWING DISSOLUTION OF Ni^{2+} WITH THICKER SILICA SHELL

3.1 INTRODUCTION

Complex engineered nanomaterials (CENs) are a rapidly emerging class of nanomaterials. They combine two or more materials, usually within a hierarchal structure, to prevent NP deactivation or sintering. These materials are not as readily studied for toxicity compared to individual (bare) NPs. However, these CENs offer many advantages in systematically varying the structure (altering NP embedding, composition, or shell thickness) to allow structure-toxicity correlations to be determined. In Chapter 2.0 , we studied the toxicity on 3T3 fibroblasts associated with three Ni/SiO_2 CENs that systematically varied the embedding of Ni NPs in a SiO_2 support. By embedding the Ni NPs in the SiO_2 support (compared to deposited externally on the support), we were able to reduce the toxicity. These CENs were toxic via a Trojan horse mechanism: the CENs were taken up into the cells and the Ni^{2+} dissolution inside the cell led to the observed toxicity. By embedding the Ni NP embedding we reduced the intracellular Ni^{2+} dissolution. Therefore, we hypothesize that by altering the silica shell thickness, we will be able to slow the Ni^{2+} dissolution even more. This slowed dissolution will cause a decrease in toxicity.

In this current Chapter we synthesized Ni NPs embedded in a hollow core surrounded by a porous silica shell. We systematically varied the silica shell thickness from 8-15 nm. These

CENs were characterized for physicochemical properties including settling and Ni^{2+} dissolution. The CENs toxicity was determined by evaluating their effect on cell metabolism. We also determined intracellular Ni^{2+} concentration and the CEN uptake into the cell using fluorescently tagged CENs. This provided insight into the changes in intracellular Ni^{2+} dissolution.

3.2 METHODS

3.2.1 hNi@SiO_2 CEN with varying shell thickness synthesis

The hNi@SiO_2 CENs were synthesized using a one pot reverse microemsulsion sol-gel procedure. First, 50 mL of cyclohexane (≥99%) and 10.5 g surfactant Brij 58 (≥99% polyethylene glycol hexadecyl ether, M_n ~1124, Sigma-Aldrich) were refluxed at 50ºC until the surfactant was fully dissolved. 1.5 mL of 1 M $NiCl_2$ in water was then added drop-wise. After 15 minutes, 1.5 mL of hydrazine hydrate (Sigma Aldrich) was added and allowed to stir for one hour. Next, tetraethylorthosilicate (TEOS, ≥99%) was added, followed by ammonium hydroxide (30%). After aging for silica growth, particles were precipitated with 2-propanol, collected via centrifugation, washed three times with 2-propanol, and dried in air. The crushed powder was then calcined in a Thermolyne 79300 tube furnace for 2 hrs at 500ºC in air. To obtain the different shell thicknesses, different amounts of TEOS and ammonium hydroxide were added and the aging time was altered. For the 8 nm shell, 10 g of TEOS and 3 mL of ammonium hydroxide were added. The solution was aged for 2 hours before the CENs were separated. For the 11.5 nm shell 20 g of TEOS and 3 mL of ammonium hydroxide were added. The solution was aged for 24 hours before the CENs were separated. For the 15 nm shell, 40 g of TEOS was

added and 3 mL of ammonium hydroxide was added. After 2 hours of aging, an extra 4.5 mL ammonium hydroxide was added. The solution was aged for 48 hours before the CENs were separated.

The CENs were fluorescently tagged with an Alexa Fluor 488 NHS ester dye (Thermo Fisher Scientific). 0.2 g CEN was dispersed in 1:1 H_2O:HCl. 50 µL (3-Aminopropyl)trimethoxysilane, and 50 µL 0.0155 M Alexa Fluor 488 NHS Ester were added and the mixture was allowed to stir for 2 hours. The CENs were separated using centrifugation and washed three times in DI water.

3.2.2 CEN size, morphology and surface area characterization

Particle measurements of TEM images were done using ImageJ software (http://rsb.info.nih.gov/ij/). Scanning Electron Microscopy (SEM) equipped with EDX was used at beam voltage of 15kV to determine elemental composition. Surface area and porosity were determined by Brunauer Emmett Teller (BET) analysis using a Micromeritics ASAP 2020 surface area and porosity analyzer. Pre-treatment consisted of 2-3 hour degassing at 200^{o}C under vacuum. Typically, a 6-point BET analysis was used for total surface area measurement and an 84-point N_2 Barrett-Joyner-Halenda (BJH) analysis with Halsey thickness curve correction and Kruk-Jaroniec-Sayari correction for pore size and volume determination.

3.2.3 Ni^{2+} dissolution

The degree of Ni^{2+} dissolution from the CENs in E3 medium was determined at specific time points. Six mL dispersions (100 mg Ni/L) were prepared in 3T3 media. CENs were removed

from the dispersions by centrifugation followed by filtration (Amicon 10,000 molecular weight cut-off filters, ~3.1 nm). HNO_3 (Sigma, 70%) was added dropwise to the filtrate to a concentration of 3 wt%. Dissolved Ni^{2+} was measured under radial detection by inductively coupled plasma atomic emission spectroscopy (ICP-AES, Thermo Electron Corporation iCAP6500 Duo Series ICP-OES Spectrometer). Standards were formulated from a stock standard solution (Fischer Scientific) with 3 wt% HNO_3 in deionized water to generate a standard curve.

3.2.4 Nanomaterial suspension preparation

CEN media solutions were made by exposing the dry CENs to an UV environment for one hour to sterilize the materials. Initial 300 mg Ni/L concentration was made by adding CENs to 3T3 media supplemented with 20 mM HEPES buffer and sonicated for 15 minutes. Next, the CENs were serially diluted to the necessary concentrations and added immediately to the wells.

3.2.5 Cell culture

Mouse-derived NIH 3T3 fibroblasts were used to evaluate the toxicity associated with the Ni materials. Cells were cultured in Dulbecco's Modified Eagle Medium (DMEM, Life Technologies) supplemented with 10% fetal bovine serum (FBS, Atlanta Biologicals) and 1% penicillin streptomycin (P/S, Life technologies), referred to as 3T3 media. The cells were cultured at 37^{o}C in 5% CO_2 environment. Cells were passaged at 70% confluency (every 2-4 days). For LIVE/DEAD analysis, the cells were plated in 6-well plates at 500,000 cells/well. For all other assays, cells were plated at 100,000 cells/well in 24-well plates.

3.2.6 MTS metabolism

CellTiter 96® AQueous One Solution Cell Proliferation Assay MTS assay (Promega) was used to assess the cell metabolism, according to manufactures instructions. Briefly, twenty-four hours after seeding the cells, 0-300 mg Ni/L $NiCl_2$ or CEN media was added to the wells. The cells were exposed for 24 hours, after which the media was aspirated out and 3T3 media (without CENs or $NiCl_2$) with 20% MTS was added. The cells were incubated for 1 hour, and the absorbance at 490 nm was measured with a Synergy 2 multimode Microplate Reader.

3.2.7 Newport green

Newport Green™ DCF indicator (NPG, Life Technologies) was used to analyze the intracellular Ni^{2+} concentration [106]. After a 24 hour propagation, the cells were exposed to 0-300 mg Ni/L $NiCl_2$ or Ni/SiO_2 CEN for 24 hours. Next, 10 μM NPG was incubated with the cells for 20 minutes at RT. Immediately following incubation, the cells were dissociated using trypsin, centrifuged, rinsed, and resuspended in PBS. Finally, an Accuri C6 flow cytometer was used to quantify the fluorescent intensity (488 nm). At least 10,000 events were collected per sample to obtain a viable histogram.

3.2.8 CEN uptake

CEN uptake was determined using fluorescently tagged CENs. After a 24 hour propagation, the cells were exposed to 0-300 mg Ni/L Ni/SiO_2 CENs for 24 hours. After exposure, the cells were dissociated using trypsin, centrifuged, rinsed, and resuspended in PBS. An Accuri C6 flow

cytometer was used to quantify the FL1 fluorescent intensity. At least 10,000 events were collected per sample to obtain a viable histogram.

3.2.9 Statistics

Data for each of the assays were parametrically distributed. To compare the effects of multiple different concentrations of each nanomaterial with embryo buffer in the same experiment, we employed one-way ANOVA followed by Dunnett's test[107]. * indicates $p \leq 0.05$. Three independent experiments were conducted for each endpoint with three replicates per condition.

3.3 RESULTS AND DISCUSSION

3.3.1 Characterization of Ni/SiO_2 CENs

Ni NPs embedded in a hollow core with a porous silica shell (hNi@SiO2) were synthesized with multiple shell thicknesses (8 nm, 11nm, 15 nm; hNi@SiO_2^{8nm}, hNi@SiO_2^{11nm}, hNi@SiO_2^{15nm}, respectively) using a reverse microemulsion sol-gel synthesis. Transition electron microscopy (TEM) images of the Ni/SiO_2 CENs are shown in Figure 12, and material characteristics are summarized in Table 3. The Ni NPs are similar in size (<2 nm). As the shell thickness increased, the Ni weight loading decreased. Additionally, as the shell thickened, the surface area increased.

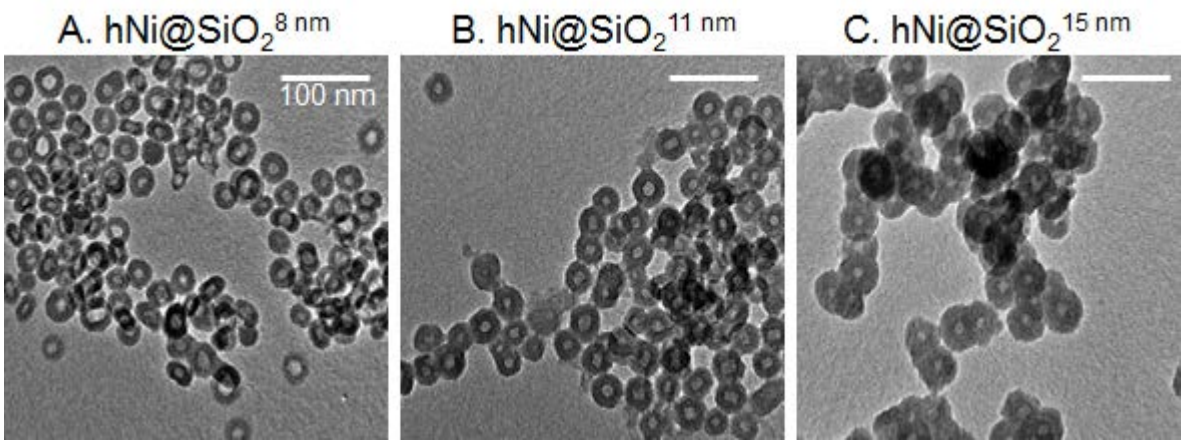

Figure 12. TEM images of typical (a.) hNi@SiO_2^{8nm}, (b.) hNi@SiO_2^{11nm} and C. hNi@SiO_2^{15nm}. Scale bar is 100 nm.

Table 3. Ni loading (from EDX), CEN particle size (from TEM), SiO_2 shell thickness (from TEM), and surface area for hNi@SiO_2 with shell thickness from 8-15 nm, shown in Figure 12.

CEN	Ni loading (wt% Ni)	D_p, primary particle (nm)	SiO_2 shell thickness (nm)	Surface area (m^2/g)
hNi@SiO_2^{8nm}	8.1	28.3 ± 3.5	8 ± 0.8	114
hNi@SiO_2^{11nm}	6.5	32.7 ± 5.1	11.5 ± 1.1	175
hNi@SiO_2^{15nm}	4.3	41.3 ± 7.7	15 ± 2.1	229

3.3.2 Ni^{2+} dissolution slows as shell thickness increases

Ion dissolution from the NP has been shown to be an important toxicity mechanism for metal NPs[30,108-110], including nickel[66,103,104,111]. Additionally, our previous study indicated that the intracellular Ni^{2+} dissolution from the Ni NP was responsible for the observed toxicity (Chapter

2.0). Thus, we hypothesize that by thickening the silica shell, we will slow the dissolution of the Ni NP by elongating the diffusion pathway. The metal dissolution from the CENs was characterized by dispersing the CENs in 3T3 media (DMEM supplemented with 1% P/S and 10% FBS) and removed at specific time points using centrifugal ultrafiltration. The dissolved Ni^{2+} concentration in the solution was then determined via ICP-AES. Figure 13 shows the Ni^{2+} dissolution at three time points over 24 hours. As we hypothesized, as the shell thickness increased, the dissolved Ni^{2+} concentration reduced ($hNi@SiO_2^{15nm}$ dissolved 2.3 mg Ni/L; $hNi@SiO_2^{11nm}$ dissolved 3.6 mg Ni/L; $hNi@SiO_2^{8nm}$ dissolved 7.7 mg Ni/L).

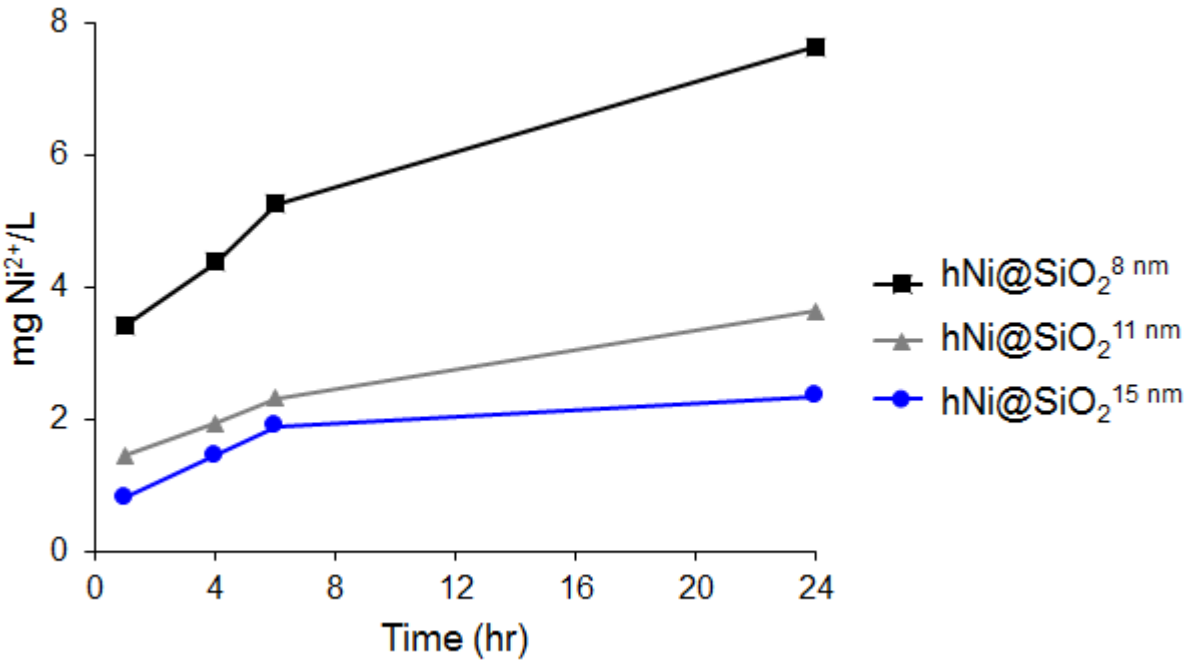

Figure 13. Dissolved Ni^{2+} concentration from $hNi@SiO_2$ CENs with different SiO_2 shell thicknesses in 3T3 media at room temperature for 24 hours with a starting concentration of 100 mg Ni/L.

This reduction in dissolved Ni^{2+} concentration is likely due to a slowing of the Ni^{2+} dissolution. Using Einstein's equation for diffusion, Equation 1, we were able to find the time necessary for the Ni^{2+} to diffuse through the pores[130]. However, this equation assumes that only inter-particle collisions are relevant and does not account for interactions between the pore and the molecule. Since the size of the pore (8 Å) and the size of the Ni^{2+} (6 Å) are similar, we would expect interactions between the pore wall and the Ni^{2+}. As an initial step to account for this, the diffusion coefficient was corrected using the Renkin equation which corrects for the hydrodynamic hindrance factor[131].

$$D = \frac{L^2}{t}$$

Equation 1. D is diffusion coefficient[132]. L is pore length. t is time.

We are interested in the relative acceleration/slow-down caused by the pore elongation. To achieve this ratio, the calculated time for each shell thickness was normalized to the calculated time for the Ni^{2+} to diffuse through the $hNi@SiO_2^{8nm}$. As expected, as the pore shell thickness increases, the relative time to diffuse throughout the pore increases. Ni^{2+} diffusing through the 11 nm pore would be expected to take 1.89X as long as the 8 nm. This would result in a 52% reduction in Ni^{2+} media concentration. The Ni^{2+} diffusing through the 15 nm pore would be expected to take 3.5X as long. This would reduce the Ni^{2+} concentration in the solution by 28%. This calculated reduction in Ni^{2+} concentration agrees with the observed experimental reduction in Ni^{2+} concentration (47% for the $hNi@SiO_2^{11nm}$ and 30% for the $hNi@SiO_2^{15nm}$).

This suggests that the reduction in the Ni^{2+} concentration in the media indeed might be due to the elongated pathway for Ni^{2+} diffusion through the silica shell.

3.3.3 CEN settling increases as shell thickness increases

CEN settling can modify the effective cell exposure and is hence of critical importance for nanotoxicity studies in aqueous media[112,113]. UV-visible spectroscopy was used to measure settling for 200 mg Ni/L CEN dispersed in 3T3 media, Figure 14. As the shell thickness increased, the settling rate increased. This could lead to a higher dosing of $hNi@SiO_2$ with thicker shells and must be considered when comparing toxicity results and rankings.

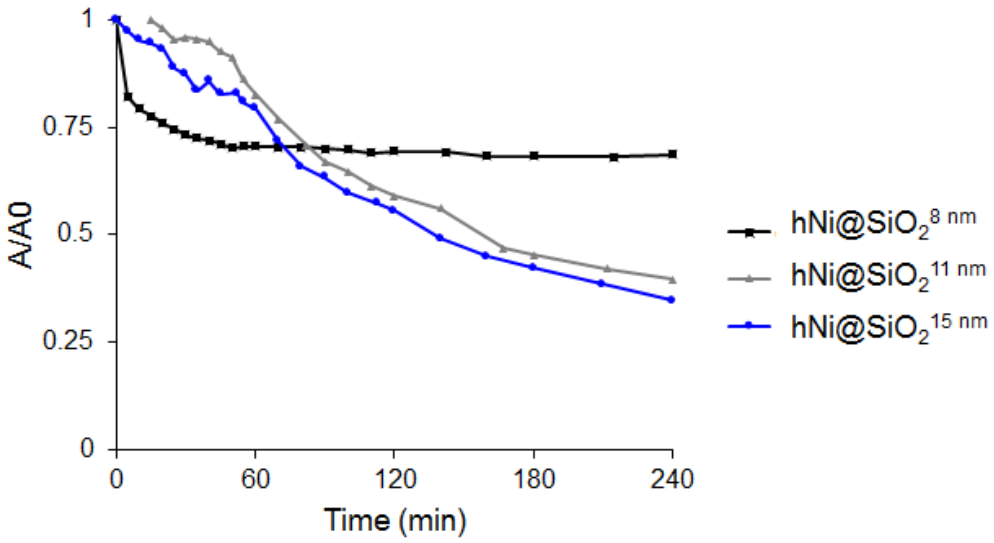

Figure 14. 200 mg Ni/L CEN settling behavior in 3T3 media over four hours. The absorbance at each time point was normalized by the initial absorbance at time zero.

3.3.4 Toxicity of hNi@SiO_2 CENs

3T3 fibroblasts are used as an FDA standard test model for evaluating biomaterials[114,115]. They are a robust, inexpensive cell line that is finding increasing use in nanotoxicity studies[69,116,117]. A 24 hour exposure time was selected to study toxic effects associated with an acute exposure, in addition to reducing complications associated with multiple cell-division cycles. Seven concentrations between 0-300 mg Ni/L were chosen to thoroughly study the Ni materials' effects on cell viability. $NiCl_2$ was previously studied and reported as a control to mimic the toxicity associated with ionic Ni^{2+} dissolved from the CENs (Chapter 2.0).

3.3.5 Cell metabolism decreased as shell thickness decreased

After 24 hour exposure, the metabolism of the cell population was analyzed using MTS, which monitors the bioreduction of a tetrazolium compound into a red formazan product. Figure 15 presents the cell metabolism normalized to the control cell metabolism (with no CEN exposure), after a 24 hour exposure. The hNi@SiO_2^{8nm} was the most toxic material in which ~75 mg Ni/L caused a 50% reduction in cell population metabolism. Interestingly, the hNi@SiO_2^{11nm} and hNi@SiO_2^{15nm} caused no significant change in metabolism compared to the control cells. Additionally, there was no distinguishable difference in toxicity between these two materials, suggesting the presence of a critical shell thickness.

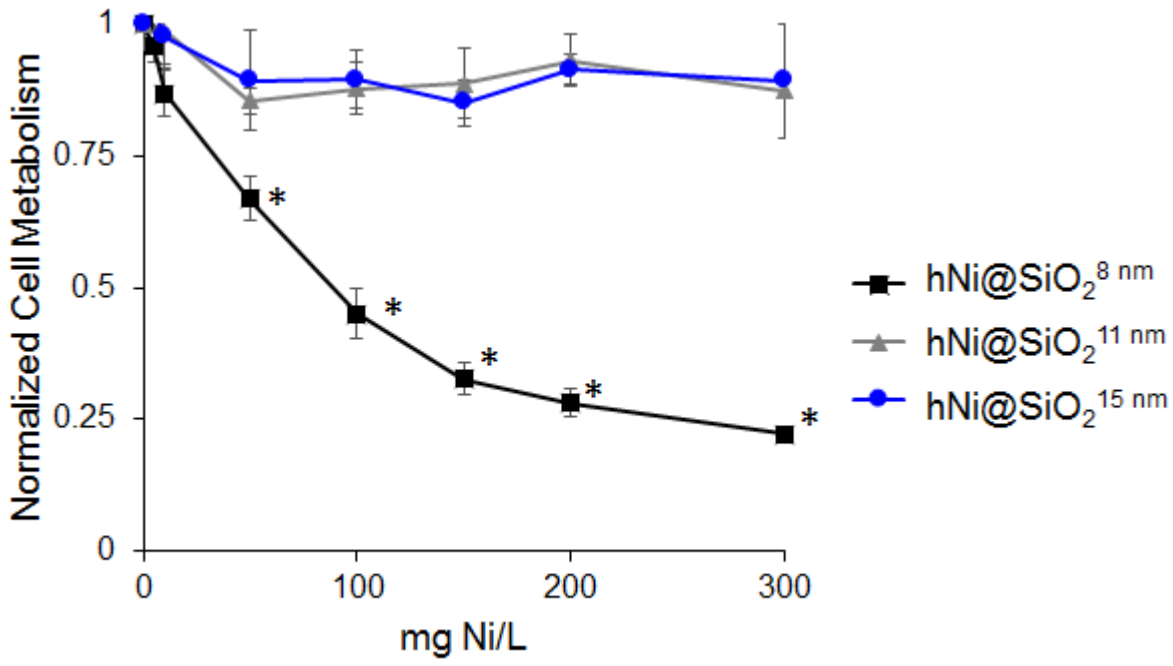

Figure 15. Cell metabolism, normalized to the control cells, after 24 hour exposure to 0-300 mg Ni/L $hNi@SiO_2^{8nm}$ or $hNi@SiO_2^{11nm}$ or $hNi@SiO_2^{15nm}$. *indicates $p \geq 0.05$ Dunnett's test, compared to control[107].

3.3.6 Toxicity mechanism

Thus far, there is a clear correlation between the shell thickness and the corresponding toxicity: As the SiO_2 shell thickness increased, the toxicity initially decreased but reached a plateau for thicker shells. Our previous studies indicate that our Ni/SiO_2 CENs are toxic via a Trojan horse mechanism. Thus, the Ni NP acts as a delivery vehicle and are taken up by the cell. The subsequent Ni^{2+} dissolution inside the cell causes toxicity (Chapter 2.0)[103,104]. Thus, we hypothesize the thickening of the silica shell is slowing the intracellular dissolution (as well as the extracellular media dissolution). This would reduce the Ni^{2+} concentration in the cell, and

thus cause the observed reduced toxicity. To determine if this hypothesis holds, the intracellular Ni^{2+} concentration was evaluated and followed by the quantification of the CEN uptake.

3.3.7 Intracellular Ni^{2+} concentration decreases as shell thickness increases

Since Ni^{2+} (and not the Ni NP itself) are expected to be the toxic source, we evaluated the intracellular Ni^{2+} concentration using Newport Green, a fluorescent dye whose fluorescence is enhanced in the presence of Ni^{2+} but not bulk Ni[104,106]. Cells were exposed to 0-200 mg Ni/L CEN for 24 hours, followed by addition of the Newport Green dye. The cells were then collected and the intracellular Ni^{2+} concentration was analyzed using flow cytometry. The fluorescent intensity was normalized to the control cells, Figure 16. The intracellular Ni^{2+} concentration decreased with increasing shell thickness. There was a large decrease in intracellular Ni^{2+} concentration from 8 to 11 nm. As the shell thickened from 11 to 15 nm, there was a slight decrease in intracellular Ni^{2+} concentration. However the decrease in intracellular Ni^{2+} concentration was not as large as the drop from 8-11nm.

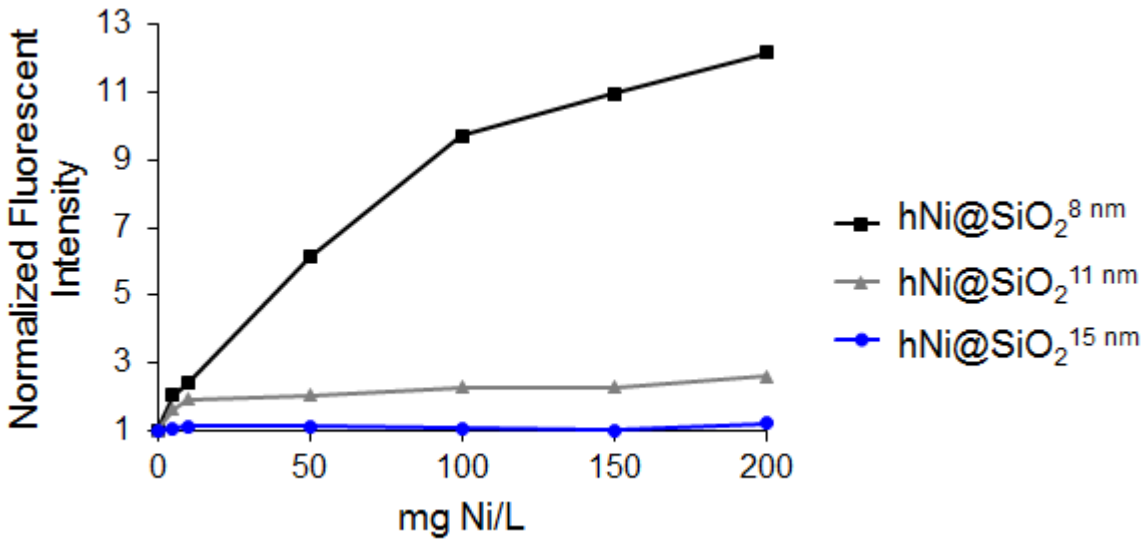

Figure 16. NPG fluorescent intensity, normalized to control cells, after 24 hour exposure to 0-200 mg Ni/L hNi@SiO_2 CENs with different shell thicknesses.

Further, we wanted to determine if the intracellular Ni^{2+} concertation was solely from the Ni^{2+} that was dissolved in the media. To do this, we compared the fluorescent enhancement observed after exposure to the CENs with the correlating fluorescent enhancement from the $NiCl_2$ salt concentration (i.e. the Ni^{2+} concentration expected from the dissolution experiment) (Figure 13). For example, 100 mg Ni/L hNi@SiO_2^{11nm} dissolved 3.65 mg Ni/L over 24 hours. This correlating $NiCl_2$ concentration had no presence of fluorescent enhancement. However, the cells exposed to 100 mg Ni/L hNi@SiO_2^{11nm} indicated a 2.3X increase in NPG fluorescent enhancement. Therefore, this suggests that the intracellular Ni^{2+} concentration is dominated by the intracellular dissolution. However the dissolution in the media which passively diffuses into the cell does play a slight role. This trend was evident for all the tested materials. Therefore,

there was evidence for a nano-specific effect that requires the uptake of the CEN to cause toxicity (a Trojan horse mechanism).

The intracellular Ni^{2+} concentration agrees well with the toxicity ranking and supports a Trojan horse mechanism. However, it still needs to be determined if the reduction in intracellular Ni^{2+} concentration was due to the reduction in CEN dissolution, or due to a reduction in CEN uptake due to changes in the materials size. Next, we determined the uptake of the CEN using fluorescently tagged CENs.

3.3.8 hNi@SiO_2 with different shell thickness is taken up similarly

There is clear correlation between the reduction in cell metabolism and the intracellular Ni^{2+} concentration. However, this reduction in intracellular Ni^{2+} concentration can be due to either a reduction in CEN uptake or a reduction in dissolution. Hence, we determined the CEN uptake into the cell. CENs were tagged with an Alexa Fluor dye and the fluorescently tagged CENs were exposed to the cells for 24 hours. After the exposure, the cells were collected and analyzed for fluorescent intensity using flow cytometry. The fluorescent intensity was normalized to the control cells natural fluorescent, Figure 17. Due to the change in CEN size (from the thicker silica shell), the surface area increased. This led to an increase in Alexa Fluor dye concentration per CEN. Hence, the hNi@SiO_2^{15nm} CEN would seem to have a higher uptake than the other CENs due to the increase in fluorescence per CEN. To correct for this, the average fluorescent intensity per CEN was determined by analyzing the fluorescently tagged CENs in flow cytometry (no cells present). The fluorescent intensity of each CEN was then normalized to the fluorescent intensity of the hNi@SiO_2^{8nm}. Thus, the changes in fluorescence intensity was weighted based on the CEN fluorescence intensity. hNi@SiO_2^{8nm} was taken up at a slightly

faster rate (~7-10% increase) than the hNi@SiO_2^{11nm} and hNi@SiO_2^{15nm}. This suggests that even though the CEN size increased (from 28 to 41 nm) and there was an increase in settling, and hence possible dosing, for the thicker shell CENs (Figure 14) there was no drastic changes in CEN uptake. The cell was able to efficiently take up all three CENs at similar rates. Moreover, the hNi@SiO_2^{11nm} and hNi@SiO_2^{15nm} were shown to be non-toxic due to the reduction in intracellular Ni^{2+} concentration. Thus, as hypothesized, the thicker shell caused the Ni^{2+} dissolution from the embedded Ni NP to be slowed, which led to a reduction in toxicity.

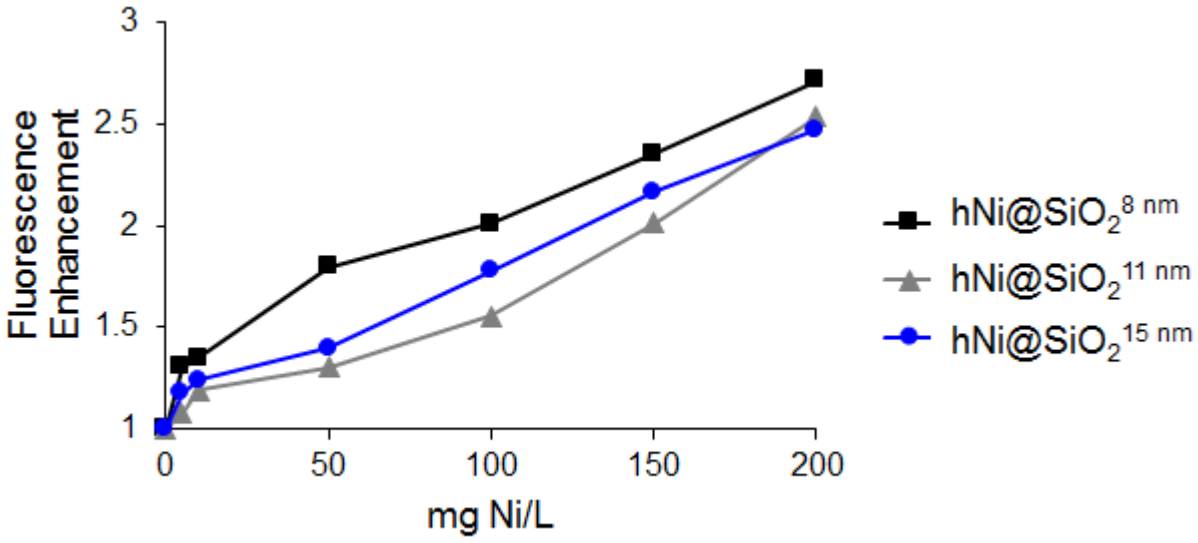

Figure 17. Cell fluorescent intensity, normalized to control, after exposure to 0-200 mg Ni/L fluorescently tagged hNi@SiO_2 CENs with different shell thickness for 24 hours.

3.4 CONCLUSION

Based on our previous work, we determined that our Ni/SiO_2 CENs were toxic due to a Trojan horse mechanism and the degree of toxicity was reliant on the intracellular Ni^{2+} dissolution. Hence, we took this observation and designed a safer nanomaterial by thickening the SiO_2 shell and slowing the Ni^{2+} dissolution while maintaining Ni NP accessibility and functionality. We systematically studied the effect the silica shell thickness had on toxicity and determined that as the shell thickness increased, there was a decrease in toxicity. This change in toxicity was linked to the reduction in dissolution, both in 3T3 media and intracellular Ni^{2+} dissolution. Interestingly, there was a rapid decrease in toxicity, and Ni^{2+} dissolution, as the shell increased from 8 to 11 nm. However, there was no benefits to increasing the shell thickness past 11 nm in terms of reducing toxicity. The cell is capable of protecting itself from a certain Ni^{2+} concertation. By continuing to increase the shell, and hence decreasing the ion dissolution, the cells were not relieved from a stress it cannot handle itself. However, it is important to note that this critical Ni^{2+} concentration is dependent on the model used. Therefore, it may be crucial to use a materials with a 15 nm silica shell (or even thicker) to eliminate the toxicity.

Our results demonstrate that safer nanomaterials can be designed utilizing a thicker silica shell and is likely applicable to other metals. By increasing the shell thickness, the ionic dissolution can be designed to be below the no observed effect level (NOEL) while still providing accessibility and functionality of the embedded NPs.

While the 3T3 fibroblasts are a well-suited model for determining the toxicity mechanisms associated with CENs, it lacks physiological relevancy. Therefore, the next Chapters investigate the CENs toxicity using an *in vivo* zebrafish (*Danio rerio*) model.

4.0 THE DEVELOPMENTAL TOXICITY OF COMPLEX SILICA-EMBEDDED NICKEL NANOPARTICLES IS DETERMINED BY THEIR PHYSICOCHEMICAL PROPERTIES

4.1 INTRODUCTION

Nanomaterials are about to fundamentally alter how we exploit the chemical and physical properties of materials. This raises the possibility that unexpected nano-specific toxicity will occur through mechanisms that cannot be extrapolated from the analogous bulk material properties[109,133-135]. The size range over which reported nanotoxicity is greatest ($d < 20$ nm)[90] correlates with the range in which most of the unique and desirable properties of nanomaterials appear[136], and development and production of materials in this size range is rapidly accelerating[14]. Consequently, there is an urgent need to develop methods that allow for sensitive and high-throughput evaluation of nanomaterial toxicity.

In practice, nanoparticles (NPs) are rarely used as independent structures because they tend to aggregate and/or sinter, resulting in deactivation and loss of their desired nano-specific properties. To overcome deactivation, nano-enabled materials are often designed as multi-component materials which embed active NPs within a protective matrix[72,73]. When these multicomponent nanomaterials are rationally designed in hierarchical nanostructures, they are

often referred to as complex engineered nanomaterials (CENs). CENs are expected to dominate future nanomaterials. However, to date, few studies have been conducted on CENs, despite the observations that, compared to single component nanostructures, the toxicity of CENs can be enhanced[137,138] or attenuated[139].

In order to guide the design of safer nanomaterials, a thorough characterization of the materials' physicochemical properties is critical in order to identify robust structure-toxicity correlations. Size, shape, surface area, surface chemistry, aggregation, agglomeration, settling, and dissolution have all been identified as key material properties that can be indicators for nanotoxicity[28]. These material attributes are often difficult to characterize for CENs due to their increased structural and compositional complexity compared to single-component materials. A systematic variation of the nanoconfiguration of a CEN with defined composition, combined with a thorough physicochemical characterization, allows to break down this complexity and can hence offer a novel approach towards studying how structural properties affect toxicity. This can offer insights into the design of safer nanomaterials through specific nano-configurations that minimize toxic properties, and allows prioritizing high risk materials for further evaluation[90,91].

Zebrafish (*Danio rerio*) provide a rapid, inexpensive, and well-characterized model to evaluate the toxicity of chemical structures in a vertebrate organism *in vivo*[110,139,140]. They are prolific breeders, producing between 50-100 offspring with each mating. Zebrafish embryos and larvae are small and can be housed in 96-well plates[141]. This provides a convenient and powerful format for high-throughput assays to evaluate the toxicity of different compounds rapidly and over a range of concentrations[83]. As a vertebrate, the zebrafish shares a common basic body plan with other vertebrates, including mammals, and many molecular mechanisms governing early embryogenesis are also shared[142-144]. Consequently, zebrafish assays may provide insights into

the teratogenic potential of test compounds in humans[145,146]. Furthermore, zebrafish develop rapidly and externally, allowing direct observation of survival and morphology, which can be employed as simple assay end-points in parallel with sensitive physiological measurements such as assays of neurological function[141,145]. Zebrafish are also uniquely placed as a model to provide insights into the harmful effects of industrial discharges on aquatic life. In view of these advantages, zebrafish are already used to test the toxicity of chemicals and drugs[141,147-149], including early life stage toxicity tests of ToxCast Phase I chemicals using high throughput assays such as survival and malformations[150]. More recently, zebrafish embryos and larvae have been used for nanotoxicological research, using simple and robust end points, such as mortality[66,111,151-153], hatching[34,110,140,154-159], malformation[160,161]. Significantly, zebrafish larval motility has now been employed as an endpoint in several developmental nanotoxicity studies, and validated as a separate index of neurodevelopmental outcome[68,162-164]. In comparison with other vertebrate models, zebrafish studies are characterized by low cost[165], and high throughput, due to the prolific breeding potential of adult zebrafish and the ability to study a large number of animals in parallel with limited space requirements. Additionally, automated assays measuring neurobehavioral parameters can be carried out in samples of 96 animals simultaneously, substantially increasing the throughput in comparison with mammalian models. Zebrafish studies typically focus on the first five days post fertilization, during which there is rapid development from the single-cell stage to a free-swimming vertebrate with all major organogenesis complete and a repertoire of simple and complex behaviors. Together, these properties of the zebrafish model allow multiple concentrations of different toxicants to be evaluated quickly and in parallel, with functional and morphological end points relevant to vertebrate embryogenesis and physiology.

In the present study, we investigated the toxicity of well-defined nanostructured nickel-silica CENs. Nickel NPs are finding widespread applications in industrial catalysis[60-63] and are often supported on silica[92-94] to enhance reactivity and stability. However, nickel NPs have been shown to be toxic[66,100] in both *in vivo* and *in vitro* models, while amorphous silica is generally reported to be non-toxic[166,167]. Workers in chemical plants and the fuel processing industry are at risk for occupational exposure to nickel and silica CENs. It is therefore important to fully understand the toxicity associated with these materials[95,96].

We selected three morphologies representing prototypical complex engineered nanomaterials: (i) materials in which nickel NPs are deposited on the external surface of a silica particle (Ni-SiO_2), and (ii) hollow and (iii) non-hollow core-shell materials (hNi@SiO_2 and nhNi@SiO_2, respectively), which consist of nickel NPs embedded into (porous) silica shells. These materials are thus compositionally complex and rationally designed to have a well-controlled hierarchical structure and hence constitute prototypical CENs. We hypothesize that the structure and embedding of the nickel NPs in the amorphous silica will alter the CENs physicochemical properties and thus affect their toxicity. In order to test this hypothesis, these CENs were subjected to thorough physicochemical characterization, including the determination of dissolution, settling and aggregation properties. The toxicity of these materials was then evaluated in zebrafish larvae, using three complementary endpoints: survival, developmental morphology and motor function. The first two are considered robust, established assays in nanotoxicology, whereas motor function is a novel and recently emerging assay for evaluating nanotoxicity.

4.2 METHODS

4.2.1 Ni/SiO_2 CEN synthesis

Ni/SiO_2 CENs were made using a one-pot, multi-step reverse microemulsion synthesis previously developed in our laboratory. The three nanomaterials utilized variations of the same synthesis protocol, assuring close structure similarity. Hollow $Ni@SiO_2$ ($hNi@SiO_2$) materials were synthesized using a one-pot reverse microemulsion synthesis previously developed in our laboratory. First, 50 mL of cyclohexane (≥99%) and 10.5 g surfactant Brij 58 (≥99% polyethylene glycol hexadecyl ether, Mn ~1124, Sigma-Aldrich) were refluxed at 50°C until the surfactant was fully dissolved. 1.5 mL of 1 M $Ni(NO_3)_2 \cdot 6H_2O$ (99.999%) was then added drop-wise, followed by 1.5 mL hydrazine hydrate (Sigma-Aldrich) to form a nickel hydrazine complex. Next, 5 g of tetraethylorthosilicate (TEOS, ≥99%) was added, followed by 3 mL of ammonium hydroxide (30%). After 2 hours of aging for silica growth, particles were precipitated with 2-propanol, collected via centrifugation, washed three times with 2-propanol, and dried in air. The crushed powder was then calcined in a Thermolyne 79300 tube furnace for 2 hours at 500°C in air.

Non-hollow $Ni@SiO_2$ ($nhNi@SiO_2$) CENs were made by a simple modification of the $hNi@SiO_2$ synthesis method, omitting the hydrazine addition step. Absence of the micelle-stabilizing Ni-hydrazine complex results in the formation of a solid (but porous) silica particle with embedded Ni NPs throughout the silica matrix. The precipitated material was dried and calcined as described above. To remove external nickel from the materials, calcined particles were reduced and etched in nitric acid by dispersing 0.20 g of material in aqueous nitric acid (35

vol%) for 30 min. The etched materials were washed twice in water to neutral pH, dried, and calcined.

For surface-deposited Ni-SiO_2, nickel-free spherical silica spheres were first synthesized using the microemulsion nhNi@SiO_2 procedure above but replacing aqueous Ni salt with 1.5 mL deionized (DI) water. Following calcination of the Ni-free silica, a deposition-precipitation method, modified from Deng et al.[105], was used to deposit very small and near-monodisperse nickel NPs on the surface of the calcined silica spheres. 0.6 g of silica NPs were dispersed in 15 mL of DI water by sonication, Ni salt solution was added (0.55 g $NiCl_2$ in 10 mL DI water), and the mixture was again sonicated for 20 min. Ammonium hydroxide (30%) was then added drop-wise (~5 mL, 52 drops, slowly over 20 min) until the pH of the solution was ~9.5. The resulting material was mixed for 20 min, centrifuged, dried, calcined at 300^{o}C in air, rinsed twice in DI water, dried, and calcined again at 300^{o}C in air.

4.2.2 CEN size and surface area characterization

CEN size and morphology were characterized with transition electron microscopy (TEM, JEOL-2000FX electron microscope). Particle measurements of TEM images were done using ImageJ software (http://rsb.info.nih.gov/ij/). Scanning Electron Microscopy (SEM) equipped with EDX was used at beam voltage of 15kV to determine elemental composition. Surface area and porosity were determined by Brunauer Emmett Teller (BET) analysis using a Micromeritics ASAP 2020 surface area and porosity analyzer. Pre-treatment consisted of 2-3 hr degassing at 200^{o}C under vacuum. Typically, a 6-point BET analysis was used for total surface area measurement and an 84-point N_2 Barrett-Joyner-Halenda (BJH) analysis with Halsey thickness curve correction and Kruk-Jaroniec-Sayari correction for pore size and volume determination.

4.2.3 CEN aggregation size characterization

CEN dispersions were tested by dynamic light scattering (DLS, Zetasizer Series Nano-ZS) to estimate the hydrodynamic diameter of the CEN in E3 medium (49 mM NaCl, 1.6 mM KCl, 3.3 mM $CaCl_2$, 3.3 mM $MgSO_4$, pH 7.4). E3 medium was chosen as it is the zebrafish medium used for the toxicity studies. The samples were first dispersed by sonication and then ~1 mL of dispersed solution was added to a cuvette. The refractive index of silica was used for all measurements.

4.2.4 CEN settling

CEN Settling was measured by UV-Visible spectroscopy (Beckman Coulter DU720). Path length was 1 cm and wavelength was 287 nm. CENs were dispersed in E3 medium and deposited in a cuvette to a liquid height of 1.27 cm.

4.2.5 CEN Ni^{2+} dissolution

Dissolved trace metal ion concentration was measured under radial detection by inductively coupled plasma atomic emission spectroscopy (ICP-AES, Thermo Electron Corporation iCAP6500 Duo Series ICP-OES Spectrometer). Standards were formulated from a stock standard solution (Fischer Scientific) with 3 wt% HNO_3 in deionized water to generate a standard curve. The degree of nickel ion dissolution from the CENs in E3 medium was determined at specific time points. 10 mL dispersions (200 mg Ni/L) were prepared in E3 media. CENs were removed from the dispersions by centrifugation followed by filtration (Amicon 10,000 molecular weight

cut-off filters, ~3.1 nm). HNO_3 (Sigma, 70%) was added dropwise to the filtrate to a concentration of 3 wt%.

4.2.6 CEN SiO_2 dissolution

Dissolved silica concentration was measured using the ASTM D859-00 standard test method for silica in water[168]. Briefly, 10 mL dispersions (200 mg Ni/L) were prepared in E3 media. At specific time points the CENs were removed by centrifugation followed by filtration. 0.2 mL of HCl (1:1 water:acid) and 0.4 mL of ammonium molybdate (75 g/L, Sigma-Aldrich) was added in succession to the collected sample. After five minutes, 0.3 mL of oxalic acid (100 g/L, Sigma-Aldrich) was added. 0.4 mL of amino-naphthol-sulfonic acid (0.5 g 1-amino-2-naphthol-4-sulfonic acid + 150mL DI water + 1 g Na_2SO_3 + 30 g $NaHSO_3$) was added after 1 minute. After ten minutes the absorbance was read at 815 nm using UV-Visible spectroscopy. A blank was prepared using E3 medium without CENs.

4.2.7 Zebrafish studies

Zebrafish studies were carried out in compliance with all federal and local regulations, in accordance with NIH guidelines for animal care and use and with full approval from the University of Pittsburgh Institutional Animal Care and Use Committee. Embryos for experiments were generated by crossing healthy adult WT strain AB zebrafish of 4 – 12 months of age. The afternoon before mating, zebrafish were placed in breeding tanks with false bottoms, and dividers to separate males and females. On the morning of mating the divider was removed at 08:00 when the zebrafish facility lights are illuminated to allow breeding. Timed embryos were

collected within the first hour of breeding. The embryos were washed in system water and then E3 buffer and transferred to 10cm plates containing E3 buffer with methylene blue (0.0001% w/v). A maximum of 30 embryos were housed in each dish. Plates were kept at 28.5°C in an incubator with white light illumination (color temperature 4900K; brightness 200 Lux) on a light-dark cycle (14 hours light:10 hours dark, light starts at 08:00). At 24 hours post-fertilization (hpf) embryos that showed developmentally appropriate morphology, Prim-5 as defined by Kimmel et. al.[144], and a visible heart beat were mechanically dechorionated and transferred to fresh E3 without methylene blue at 28.5°C. After two further rinses in E3 without methylene blue, animals were randomly split into separate experimental groups and one healthy embryo was transferred to each well of a 24-well plate. Dried CEN powder was weighed, added to E3 media, and sonicated 20 min. Serial dilutions were then prepared volumetrically. The solutions were re-dispersed by sonication for 1-2 minutes immediately prior to addition to the well. The bulk of the E3 buffer was removed from the well prior to adding the nanoparticle suspension, so that any dilution of the nanoparticle from E3 carryover was minimal quantitatively insignificant. In accordance with standard zebrafish rearing procedure no external source of nutrients was added during the 4 days exposure while zebrafish naturally depleted their yolk[169]. Zebrafish embryos were mechanically dechorionated and incubated for four days at 28.5ºC and analyzed visually each day for survival and developmental malformations. Solutions were not changed over the course of the experiment to eliminate a buildup of NP concentration during the multi-day exposures. The excess volume of buffer in each well was adequate to ensure that the control groups developed normal morphology and motor function. 12-18 embryos were tested at each concentration of toxicant per experiment.

4.2.8 Zebrafish larval motility behavior

Zebrafish embryos were exposed to CENs at 24hpf as detailed above; surviving larvae were collected on day 4, zebrafish larvae displaying morphological abnormalities were excluded from the motor assays. The zebrafish larvae were washed three times in E3 medium to remove residual particles by being gently transferred in E3 using a Pasteur pipette. The washed zebrafish were then transferred to a 96-well plate. Motor function was then analyzed as described in detail in our previous work[170,171]. Briefly, a video stream of zebrafish moving in the wells of a 96-well plate was captured at two frames/s. Video recordings were analyzed using the open source *LSRtrack* and *LSRanalyze* MATLAB scripts that we reported and extensively validated previously[170-172]. All video recordings were taken at the same time of the day (between 2-5 pm).

4.2.9 Zebrafish nickel uptake

Nickel uptake was determined by collecting surviving embryos and larvae upon termination of the experiment to measure cumulative metal uptake. Briefly, larvae were transferred to clean 12-well plates in groupings by dose, rinsed 5 times in fresh E3 medium to rinse residual external particles from surface of the zebrafish, euthanized using 10% sodium hypochlorite and rinsed 5 times with E3 media. Residual medium was then removed and zebrafish were dried in air. A dissolving procedure by Borgmann et al.[173] was used beginning with addition of nitric acid (12.5 µL/fish, 70%, Fischer Scientific) followed by at least one week digestion followed by addition of hydrogen peroxide (10 µL/fish, 30%, JTBaker) and 24 hours digestion. Resulting solutions were diluted up to 8 mL and the Ni concentration was measured via ICP-AES. The number of rinse cycles was determined by repeating washes until the nickel uptake measurement became

independent of the number of washes. Furthermore, an independent experiment was conducted with fluorescent CENs, confirming the absence of detectable CENs attached to the zebrafish larvae exterior after five washes.

4.2.10 Statistics

Data for each of the assays were parametrically distributed. To compare the effects of multiple different concentrations of each nanomaterial with embryo buffer in the same experiment, we employed one-way ANOVA followed by Dunnett's test[107]. * indicates $p \leq 0.05$ and *** indicates $p \leq 0.001$. Three independent experiments were conducted for each zebrafish endpoint with 12-18 fish per condition.

4.3 RESULTS

4.3.1 Characterization of Ni/SiO_2 CENs

Transition electron microscopy (TEM) images of the Ni-containing CENs are shown in Figure 18, and material characteristics are summarized in Table 4. For all three CENs, the nickel NPs are similar in size (~1- 2 nm) and nickel content is ~9-12 wt%. The composite NPs are spherical and ~40-55 nm. The silica porosity and surface area are also similar, with surface areas of ~200-300 m^2/g and average silica pore diameters of ~0.7 nm (0Figure 52). The silica microstructure is amorphous and the embedded nickel particles are crystalline (0Figure 53). All three materials share common chemical compositions and have similar dimensions, and differ in nanostructure

alone. Occasional necking between adjacent particles in TEM indicates the presence of some aggregation in the synthesized material (likely due to formation of oxygen bridges during thermal treatment). To assess agglomeration in the zebrafish E3 medium (49 mM NaCl, 1.6 mM KCl, 3.3 mM $CaCl_2$, 3.3 mM $MgSO_4$, pH 7.4), CENs were dispersed in E3 medium solution by sonication, and agglomerate sizes were measured using dynamic light scattering (DLS, Table 4). After dispersion in E3 media, all three CENs agglomerate to similar sizes.

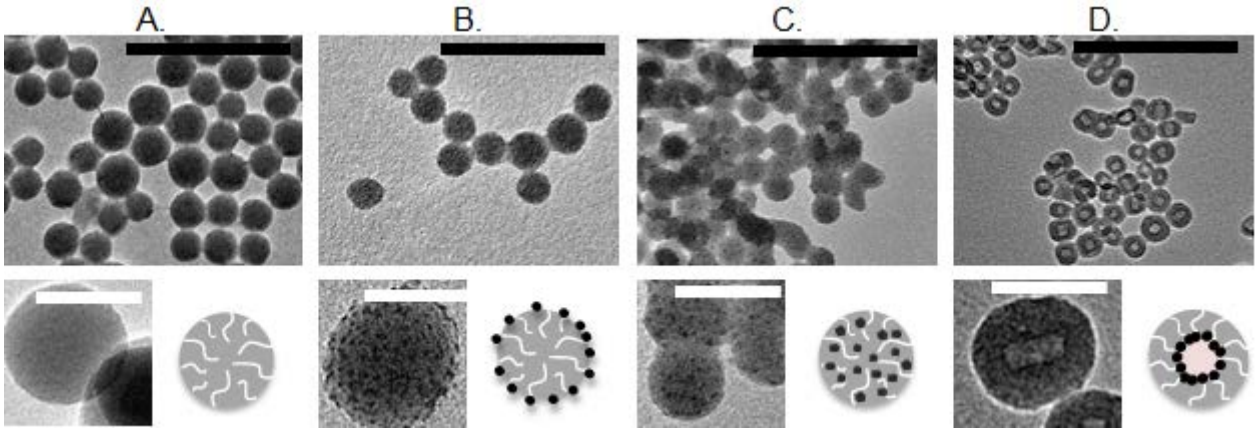

Figure 18. TEM images of typical (a.) metal-free SiO_2, (b.) Ni-SiO_2, (c.) nhNi@SiO_2 and (d.) hNi@SiO_2 samples. Scale bars are 200 nm for larger images (black) and 50 nm for smaller pictures (white).

Table 4. Ni loading (from EDX), Ni particle size (from TEM)(dry) CEN particle size (from TEM), and CEN agglomerate size suspended in E3 medium (from DLS) for hNi@SiO2, nhNi@SiO2, and Ni-SiO2 CENs shown in Figure 18.

CEN	Ni loading (wt% Ni)	D_p, Ni particle (nm), n= # particles counted	D_p, primary particle (nm), n= # particles counted	Mean size in E3 medium suspension, (nm)
hNi@SiO_2	9.0 ± 0.9	< 2	43.26 ± 7.2, n=105	301 ± 22
nhNi@SiO_2	9.6 ± 0.4	2.5 ± 0.4, n=55	41.2 ± 8.5, n=102	292 ± 27
Ni-SiO_2	11.9 ± 3.2	2.1 ± 0.4, n=73	54.5 ± 8.2, n=112	322 ± 77

4.3.2 Ni^{2+} dissolution

Dissolution of metal ions from metal NPs is an important mechanism mediating the toxicity of metals[30,109,110,164], including nickel[66,111]. Therefore we asked if purely metal dissolution from the CENs into the medium correlated directly with toxicity to suggest a mechanistic link[174]. Nickel dissolution was determined by dispersing 200 mg Ni/L of CEN in E3 zebrafish embryo medium for five days. 200 mg Ni/L was chosen as it was the highest concentration used to analyze zebrafish larvae malformations and motility toxicity. This concentration also provides the maximum nickel ion dissolution expected over the course of the study. At specific time points, the CENs were separated using centrifugal ultrafiltration, and inductively coupled plasma atom emission spectroscopy (ICP-AES) was used to determine the amount of ionic nickel. For all

materials, the rate of dissolution was initially rapid (one and four hour time point), but gradually slowed after the first 24 hours (Figure 19). Ni-SiO_2 CENs showed the highest Ni ion dissolution (16.1 mg Ni/L) while hNi@SiO_2 (5.04 mg Ni/L) and nhNi@SiO_2 (4.3 mg Ni/L) CENs exhibited similar Ni ion concentrations at day five. However, the initial dissolution rate of hNi@SiO_2 was almost double the nhNi@SiO_2 dissolution rate. To furthermore assess potential differences in dissolution of the particles after uptake by the zebrafish embryos and larvae, i.e. to mimic the acidic conditions that the CEN will experience during endocytosis (i.e. in a lysosome), we also studied dissolution in a low pH environment (pH=4.5). Dissolution was determined as described previously, but the E3 medium pH was adjusted to 4.5 by adding 0.1 M HCl dropwise over 15 minutes (~1-2 mL) until the monitored pH reached 4.5. While this cannot perfectly mimic the lysosome environment, these experiments yield insight into differences in dissolution due to pH differences alone, which is expected to be the main factor impacting dissolution behavior. As expected, all three CENs experienced significant enhanced nickel ion dissolution (over 75% total nickel) compared to the experiments at neutral pHs (Figure 20)[175]. However, the qualitative behavior and relative ranking of the dissolution rates between the three CEN remained unchanged.

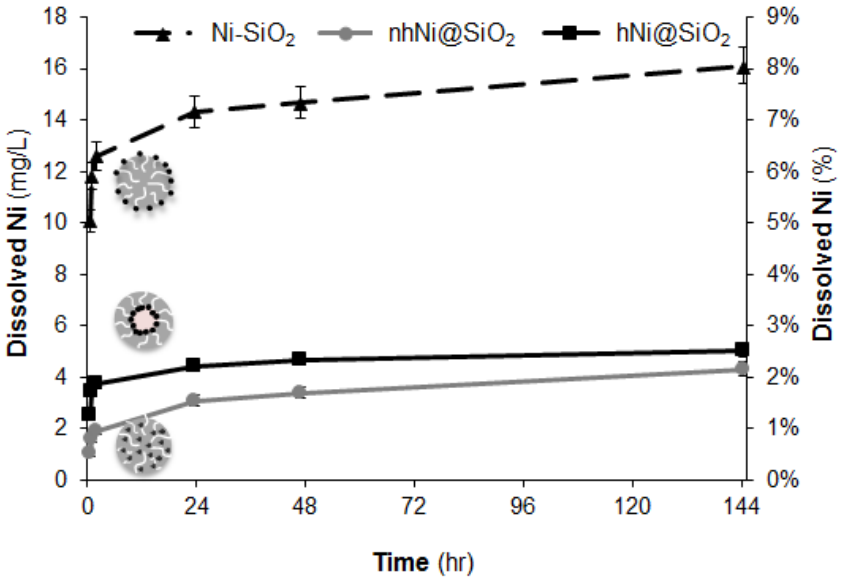

Figure 19. Nickel amount dissolved and percent dissolution of Ni-containing CEN in E3 medium at room temperature for 5 days with a starting concentration of 200 mg Ni/L. Ni-SiO_2 had the highest Ni^{2+} dissolution.

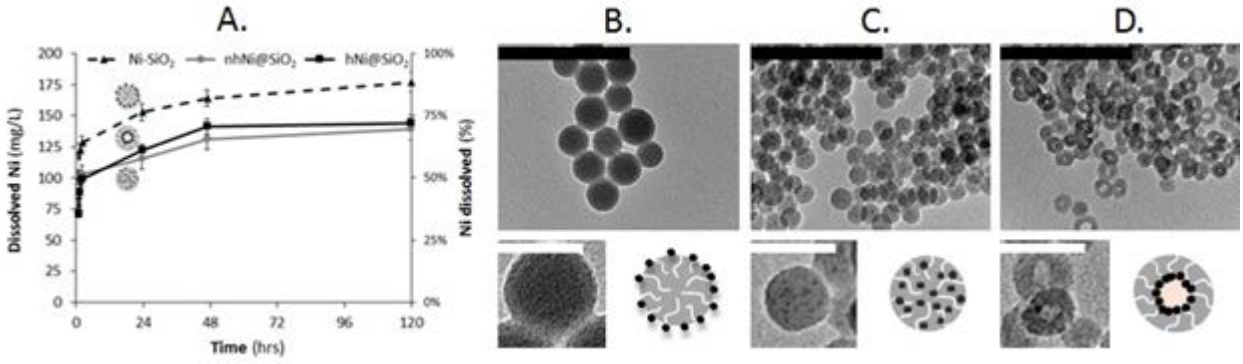

Figure 20. A. Quantitative 200 mg Ni/L CEN nickel ion dissolution in E3 with a pH=4.5 over 120 hours. Representative TEM images B. Ni-SiO_2 C. nhNi@SiO_2 and D. Ni-SiO_2.

4.3.3 SiO_2 dissolution

Silica dissolution could compromise the nanomaterial stability in the aqueous media, alter the size and shape of the CEN, and ultimately cause the metal NPs to be released from the protective silica matrix into the medium or the zebrafish larvae, affecting the CEN's toxicity. Therefore, silica dissolution was studied over five days by dispersing 200 mg Ni/L CENs in E3 media. TEM images were taken after the full five day exposure of the CENs, and silica dissolution was quantified at numerous time points using a colorimetric assay (Figure 21)[168]. hNi@SiO_2 showed the highest dissolution (114 mg SiO_2/L, ~6.7% total SiO_2), followed by nhNi@SiO_2 (55.9 mg SiO_2/L, 3.3% total SiO_2), and Ni-SiO_2 (19.2 mg SiO_2/L, 1.9% total SiO_2). In agreement with the overall low dissolution, TEM shows only minor change in particle morphology. There is no discernible change in the decoration of the surface of Ni-SiO_2 CENs with nickel NPs, and while some change in sphericity of the nhNi@SiO_2 CEN and a slight thinning of the silica shell of the hNi@SiO_2 CENs indicates some SiO_2 dissolution, these changes remain minor and do not appear to affect the Ni NPs overall. An acidic environment, such as in the lysosome during nanomaterials uptake by the fish, further reduces silica dissolution to < 0.2% (Figure 22)[176].

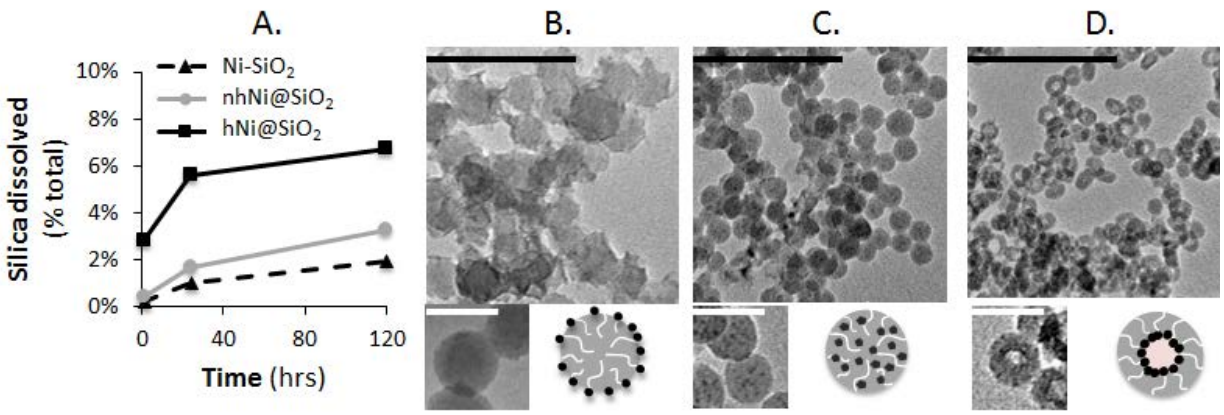

Figure 21. A. % total SiO_2 dissolution from CENs dispersed in E3 medium for five days at room temperature with a starting concentration of 200 mg Ni/L. TEM images on day five of B. Ni-SiO_2, C. nhNi@SiO_2 and D. hNi@SiO_2. Scale bars are 200 nm for larger images (black) and 50 nm for smaller pictures (white). All three CENs exhibited minimal silica dissolution.

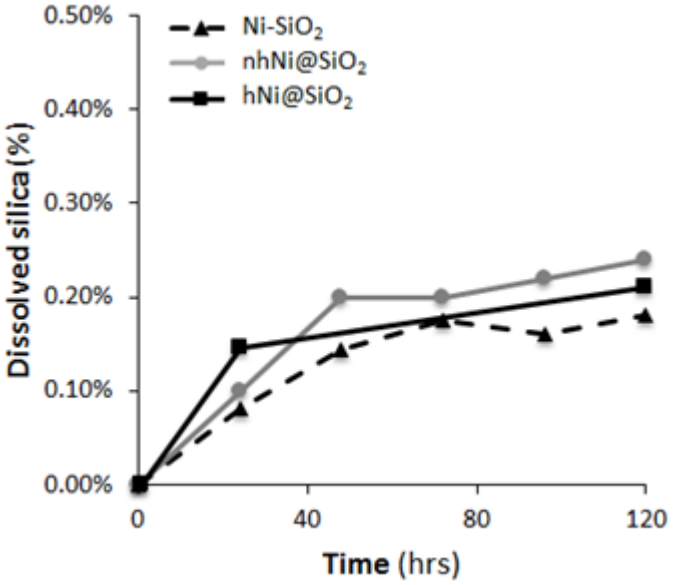

Figure 22. Relative dissolution of silica (shown as percentage of total initial silica amount) for 200 mg Ni/L CENs dispersed in E3 media with pH adjusted to 4.5 to mimic the lysosome environment.

4.3.4 Ni/SiO_2 CEN settling

Settling modifies the effective concentration in solution adjacent to the zebrafish, which at early developmental time points lie at the bottom of the wells[112]. 200 mg Ni/L CENs were dispersed in E3 medium and UV-visible spectroscopy was used to measure settling directly over five days (Figure 23). nhNi@SiO_2 (68.5% decrease in absorbance over five days) settled significantly less than hNi@SiO_2 and Ni-SiO_2 (> 90% decrease in absorbance over five days).

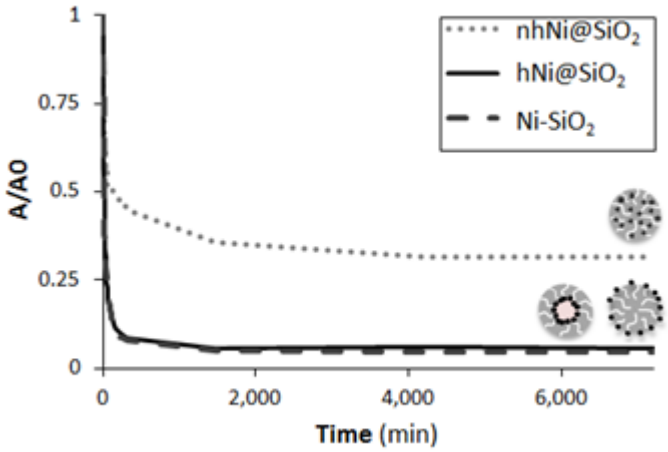

Figure 23. CEN Settling behavior measured via UV-vis spectroscopy over five days, shown as time-dependent absorbance (at λ- 287 cm^{-1}, normalized to the initial absorbance A_0 for each material). Initial concentration was 200 mg Ni/L. nhNi@SiO_2 settled the least out of the three CENs.

4.3.5 Toxicity of Ni/SiO_2 CENs in zebrafish

To evaluate the toxicity of different Ni/SiO_2 NP configurations, we exposed developing zebrafish embryos to 10 – 400mg Ni/L of CENs dispersed in E3 embryo medium, from 24 hours (Prim-5 stage)[144] to 5 days post-fertilization. It has been reported previously that the chorion can act as a barrier for uptake of metal nanoparticles[177,178]. Consequently, in order to eliminate differences in chorionic penetration of nanoparticles as a variable from our studies, zebrafish embryos were dechorionated mechanically at 24 hours post-fertilization (hpf). Dechorionation is a standard method widely used in multiple labs worldwide for microscopy in live zebrafish. It is well-established that dechorionation does not itself adversely affect zebrafish development or health[179].

4.3.6 Zebrafish survival

Survival (defined as a visible heart beat) was monitored daily until five days post-fertilization (dpf) (Figure 24). E3 medium containing $NiCl_2$ was used as a positive control for toxicity related to dissolved Ni^{2+}; E3 medium without additives was used as a negative control. Pure (nickel-free) silica NPs dispersed in E3 medium was used as a control to distinguish toxic effects of the silica support. In all experiments, we compared CEN, Ni^{2+}, silica-only and E3-only exposures in identical dechorionated zebrafish embryos assigned to each group randomly, so that any differences between experimental groups are attributable unequivocally to the chemical exposure. 99% zebrafish embryos survived to 5dpf in E3 medium alone, or in E3 medium containing silica NPs at a concentration up to 2,700 mg SiO_2/L. This corresponds to the amount of silica present at the highest concentration of CEN tested. As expected, $NiCl_2$ was toxic in a

concentration-dependent manner; the calculated LC_{50} for Ni^{2+} in this assay was 235 mg/L. In contrast, 95% embryos survived to 5dpf during exposure to all concentrations of CENs, including similar or higher total amounts of total (metallic + ionic) nickel to the $NiCl_2$ group.

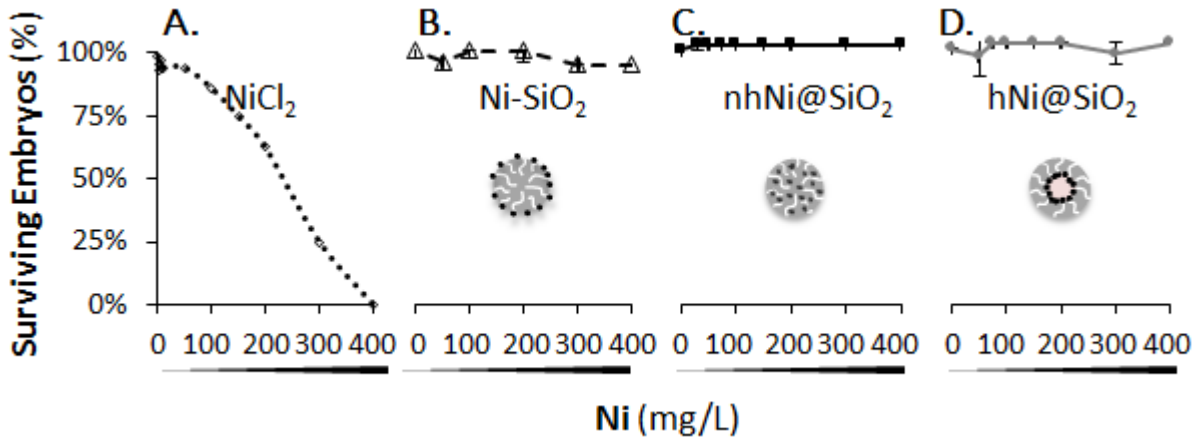

Figure 24. Zebrafish larvae survival (%) after exposure to 5-400 mg Ni/L for A. $NiCl_2$ B. Ni-SiO_2 C. nhNi@SiO_2 and D. hNi@SiO_2 on 5dpf. Error bars are error of sum squares (SSE). More than 95% zebrafish embryo survived following exposure to CENs at all concentrations tested.

4.3.7 Zebrafish larvae malformations

Malformations were evaluated as an indicator of developmental toxicity. Metal NPs have previously been reported to cause a range of developmental defects in zebrafish larvae including abnormal spinal curvature, pericardial and abdominal edema[160,161]. Zebrafish embryos were mechanically dechorionated at 24hpf and exposed to 10-200 mg Ni/L of CENs dispersed in E3 media. The embryos were monitored for the appearance of malformations over the next four days (Figure 25), including abnormal curvature of the spine and body (lordosis, kyphosis and

scoliosis), pericardial and abdominal edema, and failure of swim bladder inflation (representative images and quantification of the frequency of different malformations is detailed in Figure 57 and

Table 7). One or more malformations were seen in a high proportion of zebrafish embryos exposed to $NiCl_2$ (200 mg Ni/L: 88.3% ± 6.1%), whereas the malformation rate for embryos exposed to CENs containing a similar amount of Ni did not differ significantly from E3-only control (200 mg Ni/L nhNi@SiO_2: 10.4% ± 11.2%; 200 mg Ni/L hNi@SiO_2: 5.7% ± 6.1%; 200 mg Ni/L Ni-SiO_2: 0.0% ± 0.0%; E3 medium only: 2.5% ± 2.0%; $p<0.001$ $NiCl_2$ versus E3-only control, one-way ANOVA with Dunnett's *post hoc* test).

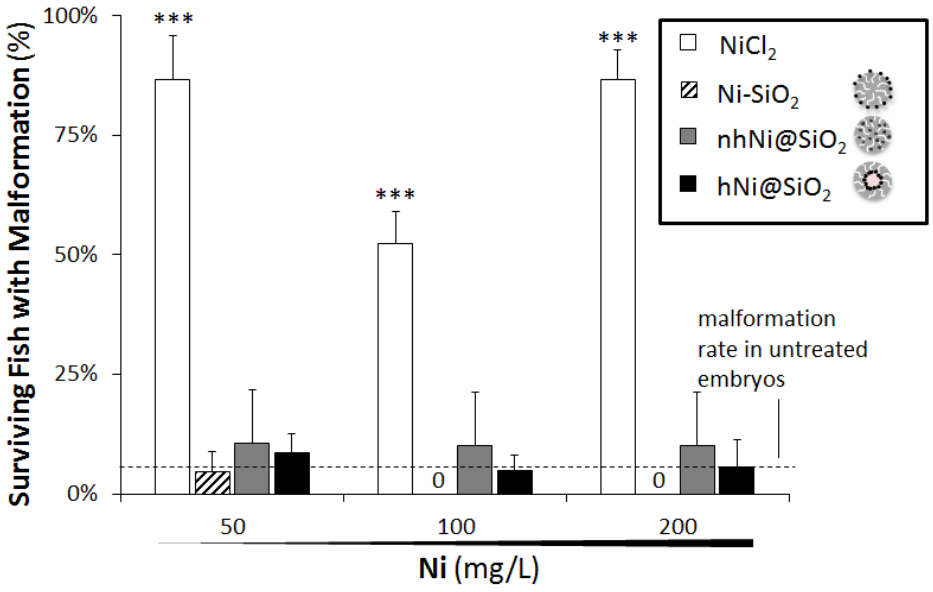

Figure 25. Malformations observed in surviving zebrafish larvae for $NiCl_2$ and CENs on 5dpf. Malformation rate for unexposed control zebrafish larvae was 2.5% (indicated by the dashed line). Note that no malformations were observed for Ni-SiO_2 at higher concentrations. ***$p\geq0.001$ for one way ANOVA followed by Dunnett's t-test, error bars are SSE. No significant development of malformations after exposure to Ni/SiO_2 CENs.

4.3.8 Zebrafish larval motor function

The absence of detectable differences in toxicity between the CENs in survival or malformation assays prompted us to measure a functional endpoint that is sensitive to disruptions in neurological development. Previous reports indicate that nickel can act as a neurotoxin which would be expected to adversely affect motor function in developing zebrafish larvae[180-182]. Zebrafish larval motor behavior can be quantified in multiple larvae simultaneously, thereby allowing statistically robust determination of how toxicants alter motor physiology[170,172,183]. Three patterns of altered larvae locomotor behavior with increasing toxicant concentration have been reported previously: (i) a monotonic decrease in total larval displacement/time with increasing toxicant concentration[154,163]; (ii) a monotonic increase in displacement/time with increasing toxicant concentration[184]; and (iii) a biphasic relationship in which locomotor activity first increases at lower concentrations and after reaching a maximum, decreases at higher concentrations[185].

Embryos were mechanically dechorinated at 24hpf and exposed to Ni CENs for three days. Before the onset of exposure at the Prim-5 developmental stage (24hpf)[144], zebrafish embryos do not show spontaneous movement, which is first seen at Prim-30 (36hpf). By 5dpf, zebrafish larvae show rapid and regular spontaneous swimming behavior[172]. We therefore measured spontaneous propulsive movements at 5dpf, to evaluate the development of swimming behavior during CEN exposure. At 4dpf surviving zebrafish larvae were collected and transferred to E3 medium with no additives. All zebrafish larvae with morphological abnormalities (compared with normal healthy zebrafish larvae under light microscopy) were excluded from the motor assays. Consequently, the motor assays are informative about the development of locomotor function, rather than mechanical consequences or morphological

malformation involving the body shape, trunk muscles or fins. Using our previously reported methods, we quantified zebrafish larval motor function at 5dpf in 96-well plates for one hour in bright white light (200 Lux brightness, 4900K color temperature) (Figure 26)[170-172], and determined their mean velocity (V_M = total displacement of the larval centroid over the course of the recording/ time period of observation). CEN-exposed animals were compared with controls derived from the same pool of dechorionated embryos, so that differences between the treatment groups were attributable unequivocally to chemical exposures rather than any baseline difference between animals. Compared with E3-only controls, pure nickel free SiO_2 NPs, did not affect larval motility at any concentration tested (Figure 27). Ni^{2+} salt provoked an increase in V_M at concentrations up to 100 mg Ni/L (Figure 26A). At higher concentrations (100-300 mg Ni/L) V_M declined below baseline measurements (detailed $V_M \pm$ SE and p-values for all materials and concentrations can be found in 0). Ni-SiO_2 CEN caused a monotonic increase in V_M with increasing concentration through the concentration range measured (Figure 26B). Zebrafish embryos exposed to nhNi@SiO_2 exhibited no change in larval V_M over the concentration range tested (Figure 26C). hNi@SiO_2 provoked similar changes in motility to $NiCl_2$ (Figure 26D); V_M increased from baseline up to a concentration of 100 mg Ni/L and then decreased again at higher concentrations. Together, these data show that developmental exposure to silica alone or nhNi@SiO_2 did not provoke abnormalities in this assay. In contrast, hNi@SiO_2 and $NiCl_2$ provoked similar abnormalities to one another and Ni-SiO_2 showed an intermediate phenotype. These data consequently allow us assign the following ranking to the toxicity of Ni CENs in the development of zebrafish larval motor function: hNi@SiO_2 > Ni-SiO_2 > nhNi@SiO_2.

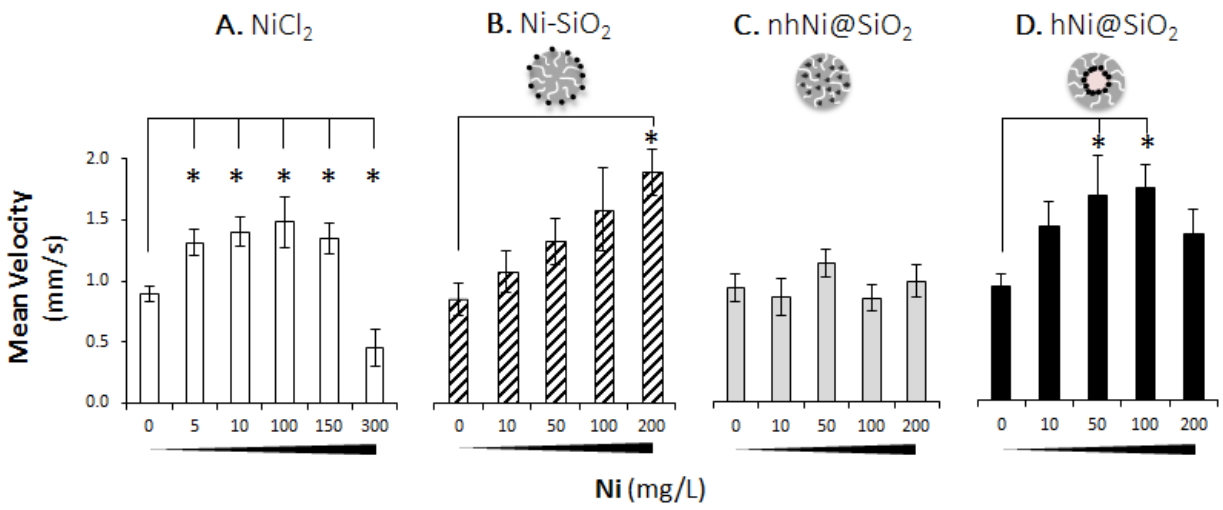

Figure 26. Zebrafish larval mean velocity (mm/s) after exposure to 0-200 mg Ni/L A.) $NiCl_2$ analogous salt and, B.) Ni-SiO_2, C.) nhNi@SiO_2 and D.) hNi@SiO_2 CENs. * indicates $p \geq 0.05$ for one-way ANOVA followed by Dunnett test, error bars SSE compared to E3 control. $NiCl_2$, hNi@SiO_2 and Ni-SiO_2 caused a change in zebrafish larval mean velocity over the tested concentrations.

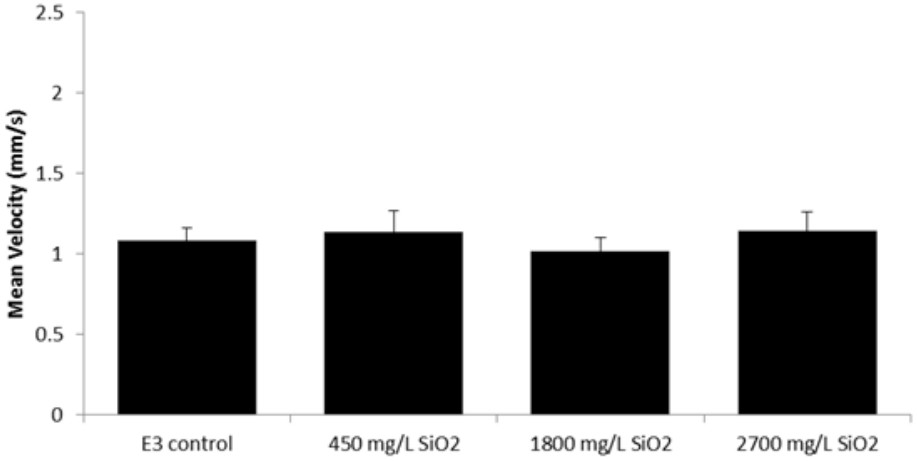

Figure 27. Zebrafish mean velocity (mm/s) after exposure to 0-2700 mg SiO_2/L. * indicates $p \geq 0.05$ for one-way ANOVA followed by Dunnett test, error bars SSE.

4.3.9 Zebrafish nickel uptake

To determine how toxicity was correlated with nickel uptake, we measured tissue Ni concentrations in zebrafish embryos and larvae exposed to one of the three CENs or Ni^{2+}. Zebrafish embryos were exposed to 50 mg Ni/L of either CEN or Ni^{2+} for 24-120 hours. After exposure, the zebrafish embryos and larvae were thoroughly washed five times and digested to allow measurement of tissue Ni content by ICP-AES. An 'uptake efficiency' was calculated after 48 or 96 hours of exposure as the measured nickel content per fish divided by the calculated available nickel ion concentration from NP dissolution (Figure 19). If only ionic Ni was taken up into the zebrafish larvae, the CEN uptake efficiency would be similar to the nickel salt.

The uptake efficiency was significantly higher for CENs than for Ni salt at both time points (Figure 28). This increased uptake indicates that the total Ni tissue content was derived from both uptake of ion and uptake of metal, indicating that CENs were likely taken up into the zebrafish larvae. Overall, the zebrafish embryos exposed to $NiCl_2$ had a higher internal nickel content than the zebrafish embryos exposed to Ni CENs (Figure 29). After exposure to $NiCl_2$, the zebrafish Ni content increased over the first 24 hour exposure, but then reached a plateau and was steady over the next 72 hours. When comparing the three CENs, over the first 48 hour exposure, the zebrafish embryos exposed to Ni-SiO_2 and hNi@SiO_2 showed a higher nickel content than zebrafish embryos exposed to nhNi@SiO_2. From 72-96 hour exposure, the total nickel content after exposure to Ni-SiO_2 and hNi@SiO_2 CENs decreased, pointing towards a nickel elimination mechanism[186]. In contrast, the internal nickel present after exposure to nhNi@SiO_2 showed an increase from 48 to 96 hour exposure. The zebrafish embryos exposed to nhNi@SiO_2 exhibited a continuous increase in internal nickel over the full 96 hour exposure and by 120 hpf had the highest nickel content out of all three CENs.

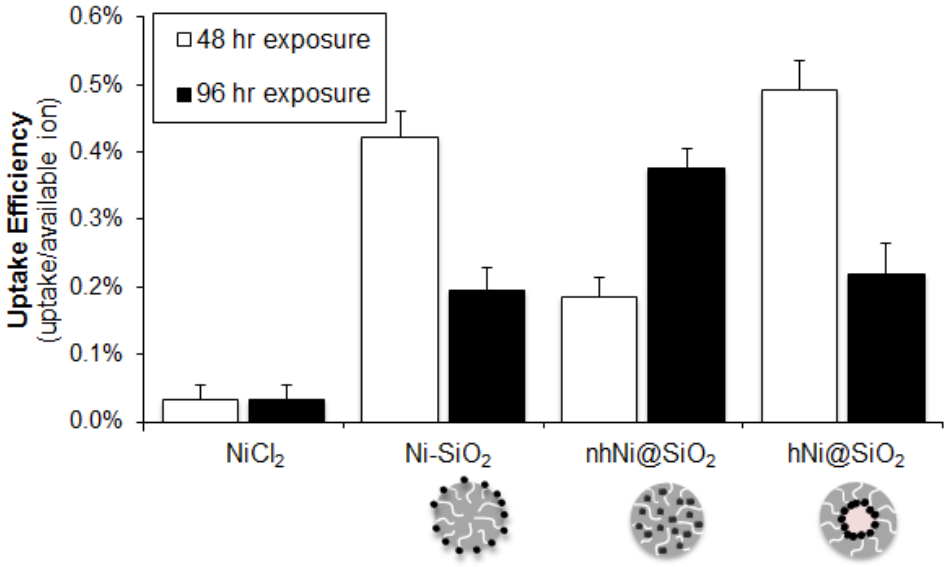

Figure 28. Zebrafish uptake efficiency of $NiCl_2$ and CENs after 50 mg Ni/L exposure for 48 hours and 96 hrs.

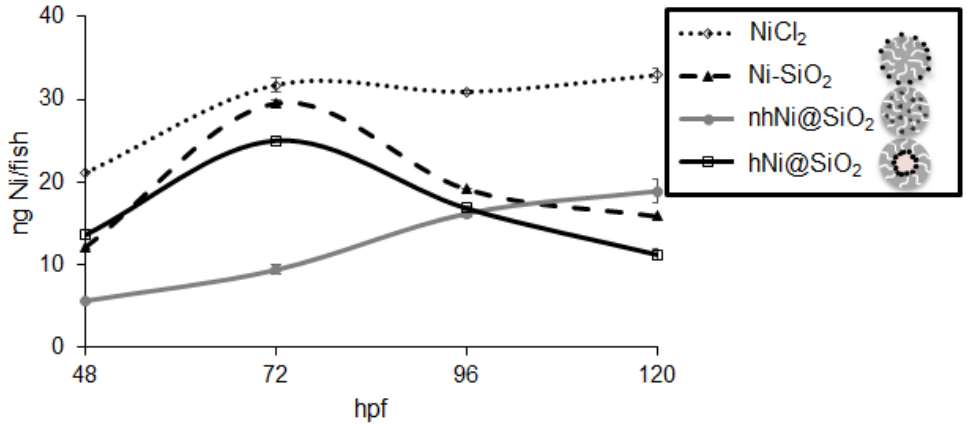

Figure 29. Zebrafish nickel uptake at 48, 72, 96, 120 hpf after exposure to 50 mg Ni/L $NiCl_2$, Ni-SiO_2, nhNi@SiO_2 and hNi@SiO_2.

4.4 DISCUSSION

The present study aimed to utilize high-throughput zebrafish assays to study the toxicity of Ni/SiO_2 CENs and understand structure-toxicity correlations that emerge from differing nanoconfigurations. Although they are simple and robust assays, we did not detect differences in survival or morphology between that were dependent on NP configuration, since all three CENs showed no difference from controls in either mortality or the presence of developmental malformations. In comparison, previous studies by Ispas et al. reported an LD50 of 200-300 mg Ni/L for 30-100 nm bare (i.e. unsupported) nickel NPs in similar 5-day zebrafish experiments[66]. The much smaller size of the Ni NPs in our study (~1-2 nm vs 30-100 nm) might be predicted to enhance toxicity as a consequence of the higher reactivity of smaller nanoparticles due to more under-coordinated, reactive surface sites, larger surface area, faster dissolution, etc. The absence of detectable mortality attributable to CEN in the present study strongly suggests that the silica embedding/deposition mitigates toxicity. Unfortunately, synthesizing 1-2 nm Ni nanoparticles free from residual synthesis chemicals—such as polymers[187], surfactants[188] and other chemicals[189] which would alter uptake and dissolution behavior and hence toxicity—without significant agglomeration and sintering of the particles is non-trivial. A direct comparison of the toxicity of bare Ni NPs as a function of size down into the sub-10 nm range has consequently not yet been achieved. However, our results provide initial support for the idea that embedding Ni NPs in a silica core significantly reduces their toxicity. This strategy potentially could be exploited in order to mitigate the toxicity of metal nanoparticles without impeding their functionality and thus has great potential to provide safer nanomaterials, for example, for use in chemical plants and in the fuel processing industry. These industries utilize metal NPs as

catalysts and rely on supports to provide catalyst stability and thus could utilize these embedding strategies to reduce occupational hazard due to metal NP exposure.

In contrast to survival and morphology endpoints, the development of zebrafish larval motor function during CEN exposure provided an assay that distinguished the effects of the three different CENs. In this assay, hNi@SiO_2 and Ni-SiO_2 exhibited evidence of developmental toxicity while nhNi@SiO_2 exposure throughout the concentration range tested did not alter development of motor function. The mechanism underlying the biphasic nature of the relationship between toxicants and the complex composite endpoint of whole organism motor function is not understood, though there has been at least one prior report of similar zebrafish motility behavior after exposure to alcohol[185]. However, it is clear that 'toxicity' is not a simple linear measurement in this assay and care must be taken to evaluate a sufficient concentration range of test compound to establish the nature of the relationship between concentration of toxicant and motor performance. Our study also suggests that it may be necessary to use multiple morphological and physiological endpoints in parallel to detect abnormalities provoked by novel putative toxicants, since evaluation of only morphology or survival in this study would have missed potentially significant abnormalities triggered by CENs.

Our physicochemical characterization of the CENs allowed us to identify properties that affect the toxicity of nanomaterials. First, the observed differences in nickel dissolution behavior can be traced back to the structural differences between the three CENs: For Ni-SiO_2, the external nickel NPs are directly exposed to the bulk medium and are therefore subject to fast dissolution. In contrast, the nickel NPs in hNi@SiO_2 (which can be considered an "inverted" configuration of the Ni-SiO_2) are exposed only to the solution inside the cavity of the silica shell. The small liquid volume contained in the central cavity likely develops a rapid increase in Ni^{2+}

concentration from Ni NP dissolution, which slows further dissolution. Exchange of the liquid volume in the central cavity with the bulk solution surrounding the CEN through the microporous silica walls assures continued, but slow, dissolution. Finally, the Ni NPs in nhNi@SiO_2 are tightly embedded into the porous silica matrix, reducing not only the liquid volume into which Ni dissolves but also the surface area of the Ni NPs directly exposed to the solution. Furthermore, compared with hNi@SiO_2, the silica pores of nhNi@SiO_2 are significantly longer as they extend throughout the silica particle, rather than just through the walls. These factors likely combine to retard dissolution by reducing the effective solvent volume, exposed NP surface area and rate of solvent exchange between pores and the surrounding media. However, if toxicity were entirely dependent on Ni^{2+} dissolution into the media, these results suggest that Ni-SiO_2 should be significantly more toxic than either hNi@SiO_2 or nhNi@SiO_2, yet we found hNi@SiO_2 to be more toxic than Ni-SiO_2. Furthermore, the maximum Ni^{2+} concentration that resulted from dissolution of Ni from the CENs into the medium was 16 mg Ni/L – the corresponding concentration of $NiCl_2$ did not provoke abnormalities, and so toxicity cannot be explained solely by ion dissolution from the CENs into the media.

Silica dissolution was found to be minor for all three CENs. While silica dissolution may affect toxicity for longer exposures times (past five days when the silica matrix may show more substantial dissolution), silica dissolution does not pose a toxicity concern during these subacute exposures as the silica structures prove to be sufficiently robust.

In contrast, the developmental toxicity associated with hNi@SiO_2 and Ni-SiO_2 correlated with their settling behavior. Rapid settling is predicted to result in a higher effective CEN concentration towards the bottom of the well. Since zebrafish embryos lie at the bottom of the

well until they become motile, an elevated concentration of CENs at the bottom of a well could potentially lead to higher CEN uptake in the zebrafish during early development[142]. After development of spontaneous motility after 36hpf, larval zebrafish start to spend less time at the bottom of the well. The more toxic CENs we tested (hNi@SiO_2 and Ni-SiO_2) showed rapid settling, consistent with the idea that enhanced exposure earlier during development (24 – 48hpf) accounted for the detected abnormalities of motor function at 5dpf. Possible explanations for sensitivity of motor function to disruption during early development might include blood-brain barrier formation that might exclude metal ions from the CNS at later time points or disruption of the formation of circuits essential for motor function during a critical window early in development. Regardless, alterations in effective exposure caused by settling are an important additional variable in the evaluation of CENs that settle and should be taken into account in future studies.

Interestingly, hNi@SiO_2 proved to be more toxic than the other two CENs, even though Ni-SiO_2 showed faster dissolution in E3 medium and caused zebrafish total nickel concentration to be higher. Our assay for measuring zebrafish Ni content does not differentiate ionic from metallic Ni. We predict that Ni dissolution inside a zebrafish will differ significantly from the external solution because the pH differs and there is a high concentration of proteins within the zebrafish that could form a corona around the CENs. These corona would be expected to limit dissolution of Ni from Ni-SiO_2 by coating the external nickel NPs, whereas the nickel NPs embedded inside hNi@SiO_2 might be protected by the silica matrix from protein capping, resulting in enhanced dissolution inside the animal. If toxicity were dependent on Ni^{2+} inside the zebrafish, this is a possible mechanism by which hNi@SiO_2 shows enhanced toxicity compared with the other structures we studied.

4.5 CONCLUSION

Our results demonstrate that zebrafish embryos provide a useful screening model for evaluating CEN toxicity during vertebrate development by combining established (zebrafish larval survival and malformations) and novel (zebrafish larval locomotor function) methods for detecting phenotypes. Based on these assays, we found that Ni/SiO_2 CENs were significantly less toxic than the corresponding ionic metal and might offer a potential path towards mitigating NP toxicity (formal proof of the latter awaits the development of suitable techniques for the synthesis of size-controlled nickel NPs smaller than 10nm without capping agents). Our results highlight the importance of conducting a thorough physicochemical characterization of nanomaterials in the biological system of interest as an inherent part of the toxicity assessment. While ex-situ characterization (i.e., TEM, XRD, BET surface area, etc.) is necessary to evaluate baseline CEN properties, it is not sufficient to elucidate size- and structure-dependent effects that occur in the test media, such as settling, agglomeration, and dissolution. Based on these characterizations of CENs in biological media, our results suggest that modification of the effective exposure might be more important for determining NP toxicity than “nano-chemistry” effects. Overall, we propose that CENs may offer a relatively straightforward stepping stone towards the rational design of safer nanomaterials.

5.0 DEVELOPMENTAL TOXICTY OF NI/SIO_2 CENS USING ZEBRAFISH HATHCING ASSAYS

5.1 INTRODUCTION

Due to their small size, nanomaterials show unique properties compared to traditional bulk materials and hence are rapidly emerging in consumer products and industrial applications[14]. However, these unique properties can also lead to new toxicities[1,15,109,190,191], which motivates an urgent need to develop *in vivo* methods that allow for sensitive, high-throughput evaluation of nanomaterial toxicity[83]. Zebrafish (*Danio rerio*) have emerged as a convenient and powerful model for high-throughput evaluation of nanomaterials toxicity[83,110,140]. Their small size allows them to be housed in 96-well plates, well-suited for rapid screening. In addition, they are prolific breeders, laying 50-200 eggs per batch. Furthermore, zebrafish develop rapidly and externally, allowing direct observation of survival, morphology, and hatching. These can be employed as simple assay end-points in parallel with sensitive physiological measurements such as neurological function. Zebrafish are also uniquely placed as a model to provide insights into the harmful effects of industrial discharges on aquatic life. Consequently, zebrafish have been employed extensively in nanotoxicology research, using simple and robust end points such as mortality[66,111,151-154,163], hatching[34,110,140,154,155,158,159,163], malformation[34,110,140,154,159,160,163] and motor function[154,163,164].

Zebrafish hatching in particular has emerged as a facile, quick, and sensitive assay that is routinely used in evaluation of developmental toxicity of nanomaterials [34,110,140,154,155,158,159,163,192-196]. Two protocols are prevalent in the literature: a high-throughput method and a high-volume method. The high-throughput method monitors zebrafish hatching in a 96-well plate in which one zebrafish is placed in 0.1-0.3 mL of media[155,158,159]. This methodology offers many advantages for high-throughput screening by utilizing small well sizes, thus requiring smaller quantities of nanomaterials, allowing for highly parallelized evaluation, and lower space requirement compared to a more conventional 24-well plate assays. The high-volume protocol, in contrast utilizes a 24-well plate with two mL/zebrafish[34,110,140,154,163,197] and is an established protocol extensively used to study toxicity of chemicals[198-200].

In practice, nanoparticles (NPs) are rarely used as independent structures because they tend to aggregate and/or sinter, resulting in deactivation and loss of their desired nano-specific properties. To overcome deactivation, nano-enabled materials are often designed as multi-component materials in which the nanoparticles are embedded in a support structure[72-75]. These NP/support configurations, often referred to as complex engineered nanomaterials (CENs), are widely expected to constitute the next generation of nanomaterials. However, there are only few nanotoxicity studies conducted to date on these CENs[77,78,87].

In the present chapter, we evaluated three CEN structures to determine how NP embedding in a support may affect toxicity. In the first CEN structure Ni NPs are deposited on the external surface of a porous, amorphous silica NP (Ni-SiO_2), in the second structure Ni NPs are embedded within the porous amorphous silica NP (nhNi@SiO_2), and in the third structure the Ni NPs are embedded in the central cavity of a hollow, porous, and amorphous silica shell (hNi@SiO_2). Previously, we studied the toxicity of these nanomaterials utilizing dechorionated

zebrafish assays, including zebrafish survival, development of malformations and larval motility behavior. This study showed that the Ni-SiO_2 and hNi@SiO_2 CENs were toxic and altered zebrafish larval motility behavior, while the nhNi@SiO_2 had no observable toxicity (Chapter 4.0). In this current Chapter, we aimed to corroborate the previous findings and confirm the suitability of (much faster and more convenient) hatching assays for CEN toxicity assessment.

5.2 METHODS

5.2.1 CEN synthesis

The Ni/SiO_2 CENs synthesis was reported previously (Chapter 4.2.1). For the present study, some of the CENs were fluorescently tagged with an Alexa Fluor 488 NHS ester dye (Thermo Fisher Scientific). 0.2 g CEN was dispersed in 1:1 H2O:HCl. 50 µL (3-Aminopropyl)trimethoxysilane, and 50 µL 0.0155 M Alexa Fluor 488 NHS Ester were added and the mixture was allowed to stir for 2 hours. The CENs were separated using centrifugation and washed three times in DI water.

5.2.2 CEN characterization

CEN size and morphology were characterized via transition electron microscopy (TEM, JEOL-2000FX electron microscope). ImageJ software (http://rsb.info.nih.gov/ij/) was used to measure the particle sizes obtained from TEM. Ni/SiO_2 elemental composition was determined using scanning Electron Microscopy (SEM, JEOL JSM-6510LV/LGS with Oxford Inca) equipped with EDX at a beam voltage of 15kV. Surface area and porosity were determined by Brunauer

Emmett Teller (BET) analysis using a Micromeritics ASAP 2020 surface area and porosity analyzer. Pre-treatment consisted of 2-3 hour degassing at 200^{o}C under vacuum. Typically, a 6-point BET analysis was used for total surface area measurement and an 84-point N_2 Barrett-Joyner-Halenda (BJH) analysis with Halsey thickness curve correction and Kruk-Jaroniec-Sayari correction for pore size and volume determination.

5.2.3 Zebrafish testing

Zebrafish studies were carried out in accordance with NIH guidelines for animal care and use and with approval from the University of Pittsburgh Institutional Animal Care and Use Committee. Strain AB wild-type adult zebrafish were crossed to generate embryos for experiments. All nanotoxicity experiments were conducted in embryos and larvae up to 5 days post-fertilization. Zebrafish embryos were raised in E3 medium at 28.5 °C in a 14:10 h light:dark cycle (white light at 200 Lux). Dried CEN powder was weighed, added to E3 media, and sonicated 20 min. Serial dilutions were then prepared volumetrically. The solutions were re-dispersed by sonication for 1-2 minutes immediately prior to addition to the well. To conduct exposure assays, 4 hours post fertilization (hpf) embryos were left in their chorion and transferred to a well of a polystyrene multi-well plate. Zebrafish embryos were incubated for 5 days at 28.5^{o}C and analyzed visually each day for survival, developmental malformations and hatching. Each condition used 12-18 embryos and was repeated in three independent experiments. For high-throughput hatching tests, one zebrafish embryo was placed per well of a 96-well plate with 0.3 mL CEN solution. For high-volume hatching tests, one zebrafish embryo was placed per well of a 24-well plate with 2 mL CEN solution.

5.2.4 NH_3 concentration

NH_3 concentration was determined using a colorimetric assay that formed indophenol using sodium salicylate[201]. At the determined time point, the zebrafish media was collected and pooled to obtain a 3 mL sample. The sample was diluted to 35 mL, and 5 mL of a 40% sodium salicylate solution was added, followed by 3 mL 1.93% NaOCl in 0.1M NaOH solution, followed by 5 mL of 2% $K_4Fe(CN)_6*3H_2O$ + 10% $Na_3Citrate*2H_2O$ in 0.1 M NaOH. The solution was vortexed after each addition and then incubated in the dark for two hours. Absorbance at 660 nm was read using a DU 720 UV/vis spectrophotometer. A calibration curve was determined using NH_3SO_4 in E3 media.

5.2.5 CEN settling

CENs were dispersed in E3 medium and deposited in a cuvette to a liquid height of either 3.5 cm or 1.75 cm. CEN absorbance was measured by UV-Visible spectroscopy (Beckman Coulter DU720). Path length was 1 cm and wavelength was 287 nm. CEN aggregate size was determined using Stokes' law[130]. Settling velocities were calculated from sedimentation traces as half the height divided by the specific time point[202].

5.2.6 Microscopy

CEN aggregate location was determined by exposing the zebrafish to fluorescently tagged CENs using the protocol described above. After exposure, zebrafish were carefully washed twice before being manually dechorionated. The zebrafish were then imaged. Microscopy was carried out after tricaine anaesthesia to prevent movement. Anaesthetized larvae were embedded in 3% low melting point agarose in E3 buffer and imaged using an inverted microscope.

5.3 RESULTS AND DISCUSSION

5.3.1 Ni/SiO_2 CEN characterization

Three Ni/SiO_2 complex engineered nanomaterials (CENs) were synthesized using a reverse microemulsion sol-gel synthesis: Ni NPs deposited on an amorphous silica NP (Ni-SiO_2), Ni NPs embedded throughout a porous silica NP (nhNi@SiO_2), and Ni NPs encapsulated in a hollow core surrounded by a porous silica shell (hNi@SiO_2). Figure 30 shows representative TEM images of the Ni/SiO_2 CENs; key material characteristics are summarized in

Table 5. The Ni NPs size for all three CENs is ~2- 3 nm, and the size of the composite CENs is ~40-55 nm. The Ni content is ~9-12 wt%. The CENs also have similar surface areas (~200-300 m^2/g), and average silica pore diameters of ~0.7 nm. All three materials hence have near-identical chemical compositions and similar dimensions but differ in nanostructure only.

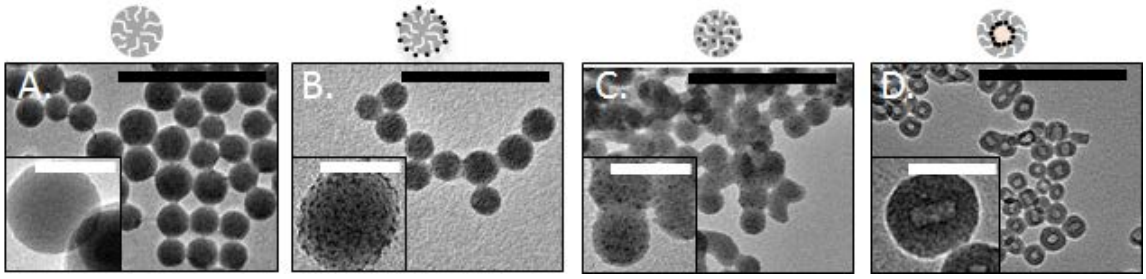

Figure 30. TEM images of Ni/SiO_2 CENs. A. Nickel-free SiO_2, B. Ni-SiO_2, C. nhNi@SiO_2, D. hNi@SiO_2. Black scale bars are 200 nm. White scale bars are 50 nm.

Table 5. Ni weight loading, diameter of Ni NP, diameter of CEN.

CEN	Ni loading [wt% Ni]	D_p, Ni NP [nm], n= # particle	D_p, CEN [nm], n= # particle
Ni-SiO_2	9.0 ± 0.9	< 2, n=72	43.26 ± 7.2, n=105
nhNi@SiO_2	9.6 ± 0.4	2.5 ± 0.4, n=55	41.2 ± 8.5, n=102
hNi@SiO_2	11.9 ± 3.2	2.1 ± 0.4, n=73	54.5 ± 8.2, n=112

5.3.2 Toxicity studies

We had previously assessed the toxicity of the same three Ni/SiO_2 CENs by monitoring the effect of these CENs on zebrafish larvae survival, development of malformations and larval motility behavior (Chapter 4.0). None of the CENs caused zebrafish larvae death or development of malformations over a wide concentration range of 0-400 mg Ni/L. However, the Ni-SiO_2 and hNi@SiO_2 CENs caused changes in the larval motility behavior, while the nhNi@SiO_2 CEN did not alter larval motility. The difference in observed toxicity could be attributed to the different settling behavior of these three nanomaterials. To further corroborate these findings, we employed the simple, widely used hatching assay to monitor possible developmental toxicity associated with these Ni/SiO_2 CENs.

5.3.3 Zebrafish embryo hatching in high-throughput assay depends on CEN structure

Zebrafish embryo hatching has been used widely as a facile, high-throughput screening assay for evaluating the toxicity of nanomaterials[34,110,140,154,155,158,159,163,192-196]. To evaluate the developmental toxicity associated with our Ni/SiO_2 CENs, we hence assessed the effect of these CENs on zebrafish embryo hatching. We utilized a high-throughput protocol in which one four hours post fertilization (hpf) zebrafish embryo was placed in each well of a 96-well plate loaded with 300 μL CEN solution. The zebrafish embryos were monitored over the next five days to observe hatching (Figure 31). Zebrafish embryos in pure E3 media were used as a control. 70% of the control zebrafish had hatched on day three, and 100% of the zebrafish had hatched by day five. After exposure to 200 mg of Ni/L Ni-SiO_2 or hNi@SiO_2, the zebrafish successfully hatched by day four and displayed a slight acceleration in hatching compared to the control zebrafish. Zebrafish embryos exposed to 200 mg Ni/L nhNi@SiO_2 experienced a strong delay in hatching (6.6% hatched at 72 hpf and 80% at 120 hpf).

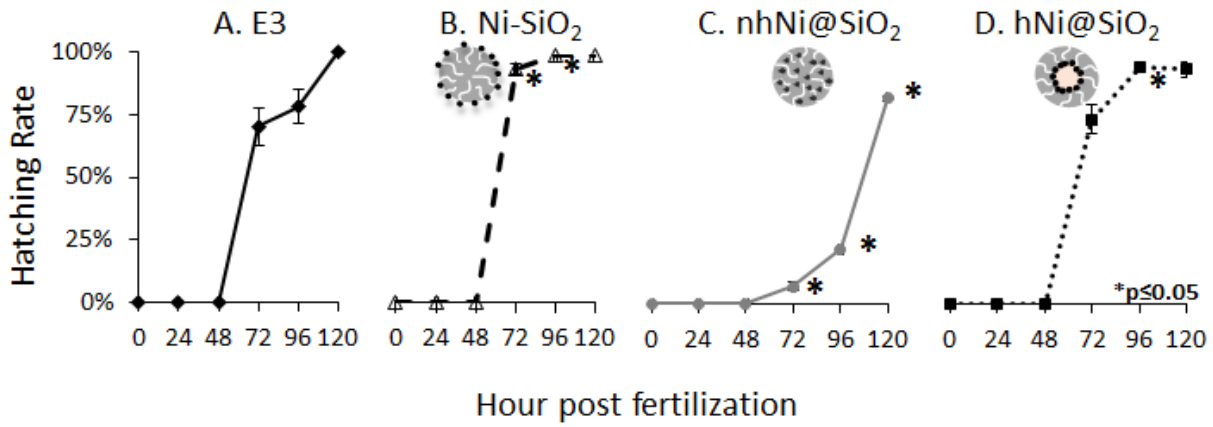

Figure 31. Zebrafish hatching rate over five days utilizing a high-throughput protocol in which one 4hpf zebrafish was placed per well in a 96-well plate. Hatching was monitored over five days after exposure to A. E3 media B. 200 mg Ni/L Ni-SiO_2 C. 200 mg Ni/L nhNi@SiO_2 and D. 200 mg Ni/L hNi@SiO_2. * indicates $p \leq 0.05$ for Dunnett's test.

These results suggest toxicity differences based on structure: the Ni-SiO_2 and hNi@SiO_2 CENs did not alter zebrafish hatching, while the nhNi@SiO_2 CEN significantly decreased zebrafish hatching. Interestingly, these results are contradictory to our previous results that indicated nhNi@SiO_2 was the least toxic of the three materials with no detectable toxicity in all tested assays (Chapter 4.3). However, further careful assessment of the present results shows an unexpected slight delay in hatching for the control zebrafish, which are expected to have fully hatched by 72hpf[179]. We hypothesized that this delay could be due to the high-throughput protocol: The small well volumes in the 96-well plate could lead to a buildup of excreted metabolites to toxic levels, which could cause a delay in hatching.

5.3.4 Eliminating toxic waste buildup

To confirm and eliminate the origin of the unexpected hatching delay for the control fish, we adjusted the media volume per zebrafish systematically from 0.3 mL –2.0 mL and again monitored hatching over five days (Figure 32). At 48hpf, the zebrafish hatching rate increased from 0 to 12.5% and finally to 50% as the media volume increased from 0.3 to 0.5 and 0.6 mL/zebrafish. There was no further statistically significant change in hatching rate with further increase of the media volume from 0.6 – 2 ml/zebrafish. The same trend was observed for hatching at 72hpf: Hatching rates increased with increase in media volume from 0.3-0.6 mL/fish with no further change above 0.6 mL/fish. Hence, these results confirm our hypothesis that small well volumes can result in toxic concentrations of metabolites, and suggest that a minimum of 0.6 mL E3/fish must be used in order to eliminate this effect.

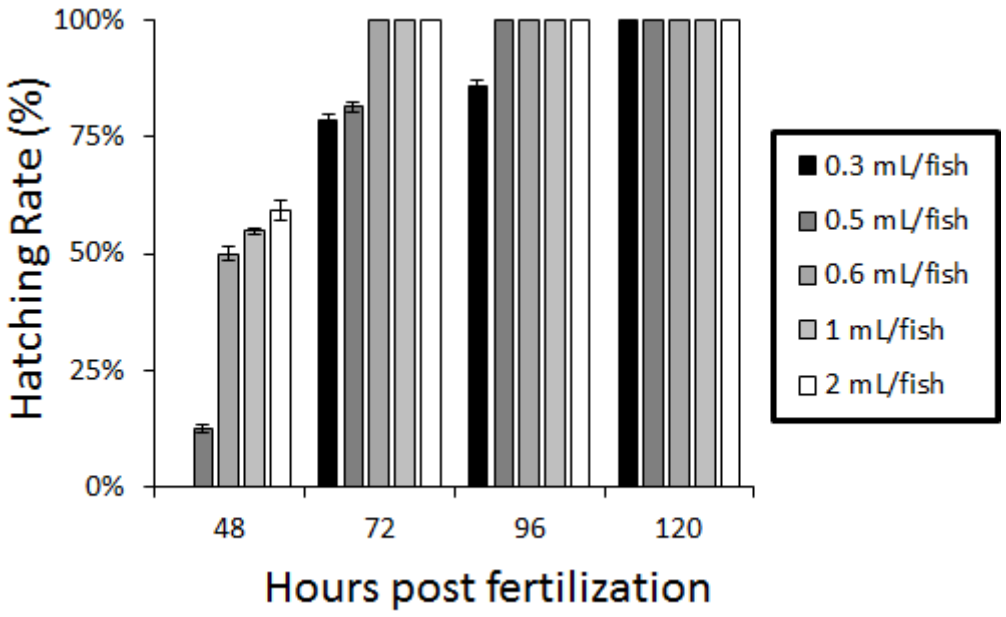

Figure 32. 4hpf zebrafish hatching rate over five days as E3 volume was varied from 0.3 - 2 mL/fish.

This “self-inhibition” in hatching for the control zebrafish is likely due to the presence of excreted waste metabolites, including ammonia[203,204]. Excess amino acids and proteins are metabolized and excreted, rather than stored by the animal. While terrestrial animals metabolize these nitrogenous waste into urea or uric acid, teleost fish excrete up to 90% of their nitrogenous waste as ammonia[205]. Thus, as the experiment progresses, the small media volume per well in the 96-well plate should build up an increasingly high concentration of ammonia. To test this, the ammonia concentration in the well during zebrafish hatching was determined at 72hpf using a colorimetric assay[201]. As expected, a significant NH_3 concentration was detected for the smallest media volumes, which decreased with increasing volume (Figure 33A). To further corroborate if this NH_3 concentration caused the observed toxicity, we monitored the hatching rate of zebrafish placed in a 24-well plate with 2 mL of E3 spiked with an ammonia concentration of 0.075 mol/L (i.e. the NH_3 concentration detected in 96-well plate). The zebrafish indeed exhibited a significant decrease in hatching upon NH_3 addition with a hatching rate similar to that for zebrafish in the 96-well plate (Figure 33), supporting the hypothesis that the delay in hatching was indeed due to the build-up of NH_3 in the well.

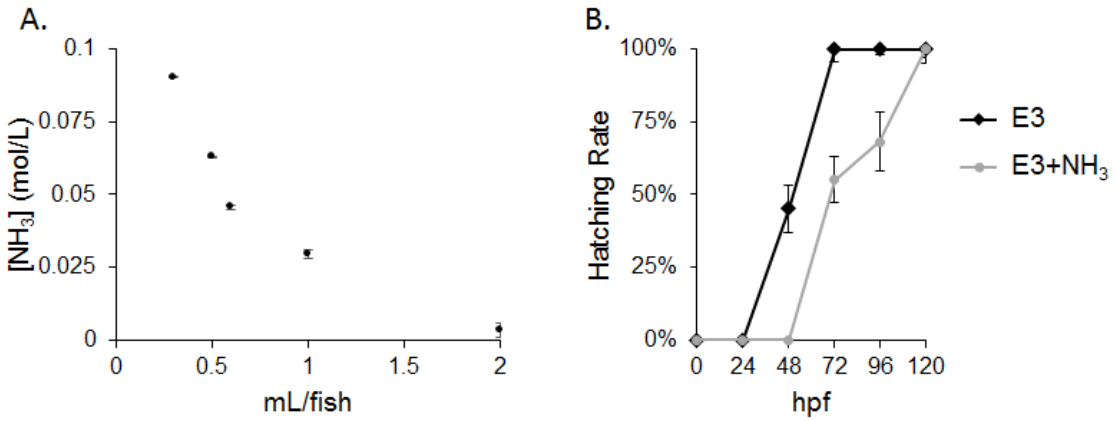

Figure 33. A. NH_3 concentration in the well as the media volume was varied from 0.3-2 mL/fish on 72hpf. B. Hatching rate for 4hpf zebrafish placed in a 24-well plate exposed to E3 media (black) or E3 medium spiked with 0.075 M NH_3 (grey).

This inherent toxicity could possibly be eliminated, while maintaining use of a high-throughput methodology, by changing the media every day. However, this is not a feasible option when conducting nanotoxicity studies. It is difficult, if not impossible, to assure removal of all nanomaterial when changing media due to nanomaterials settling and strong adhesion to the chorion and the well walls. This renders exact control of the nanomaterial exposure impossible as the experiment proceeds over time and multiple media exchanges. Thus, to eliminate this toxicity, i.e. to eliminate false positives that result from excretion of metabolites rather than from nanomaterials exposure, we transitioned to a high-volume methodology in order to assess the true effect of the CENs on hatching.

5.3.5 Zebrafish hatching in high-volume assays is independent of CEN structure

The effect of the Ni/SiO_2 CENs on zebrafish hatching was analyzed next utilizing a high-volume protocol to eliminate the inherent hatching inhibition due to excreted NH_3. One zebrafish was placed in each well of a 24-well plate with two mL CEN media solution (Figure 34). 50% of the control zebrafish hatched by 48hpf and all zebrafish had hatched by 72hpf, as expected for healthy control zebrafish. After exposure to 200 mg Ni/L CENs, all three materials induced a delay in hatching at 48hpf. However, by 72hpf, 100% of the zebrafish had hatched. Contrary to the previous, high-throughput results, there was hence no toxicity difference based on structure when this high-volume protocol was used. Furthermore, the Ni-SiO_2 and hNi@SiO_2 CEN resulted in similar zebrafish hatching rates independent of the protocol used. In contrast, the nhNi@SiO_2 CEN caused less severe hatching delay when using the high volume protocol compared to the high-throughput protocol. This suggests the Ni-SiO_2 and hNi@SiO_2 CENs were able to counter the NH_3 toxicity present in the high-throughput protocol.

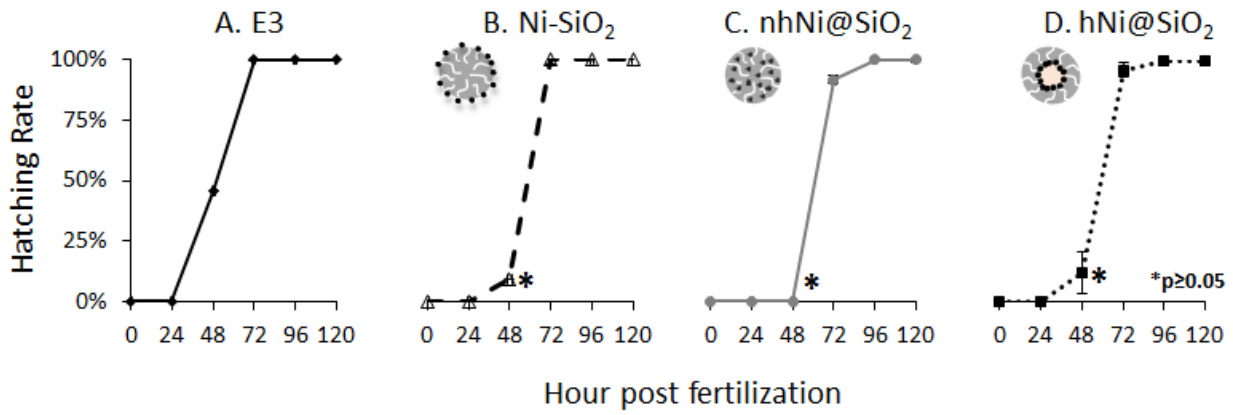

Figure 34. Hatching rate for 4hpf zebrafish placed in 2 mL/fish over five days after exposure to A. E3 media B. 200 mg Ni/L Ni-SiO_2 C. nhNi@SiO_2 and D. hNi@SiO_2. *p≤0.05 for Dunnett's test.

5.3.6 Zebrafish exposure to CENs decreased NH_3 concentration

The fact that zebrafish exposed to hNi@SiO_2 or Ni-SiO_2 CENs showed slightly accelerated hatching compared to the control, independent of the protocol, i.e. independent of the volume used suggests that these CENs are able to counter the toxicity associated with the excretion of NH_3. We therefore measured the NH_3 concentration in the well after zebrafish exposure to 200 mg Ni/L CENs for 72 hours in a 96-well plate. Figure 35 shows the measured concentrations, normalized to the NH_3 concentration in the control zebrafish well (0.09M). In all cases, the ammonia concentration in the well dropped significantly compared to that for the control, but the reduction was strongly depending on the CEN. The ammonia concentration after zebrafish exposure to Ni-SiO_2 CENs was reduced to 11% compared to the control (0.0099M), while that for zebrafish exposed to hNi@SiO_2 was ~36% of the control (0.032M), and ammonia concentration after zebrafish exposure to nhNi@SiO_2 was 64% of the control (0.058M). We

hypothesized that this reduction in NH_3 concentration may be due to one of three reasons: 1) Formation of a $Ni(NH_3)_6$ complex, which reduces the free NH_3 concentration; 2) NH_3 decomposition, catalyzed by the Ni NPs; and 3) reduction of the zebrafish's metabolism due to exposure to the CENs and hence reduced NH_3 production.

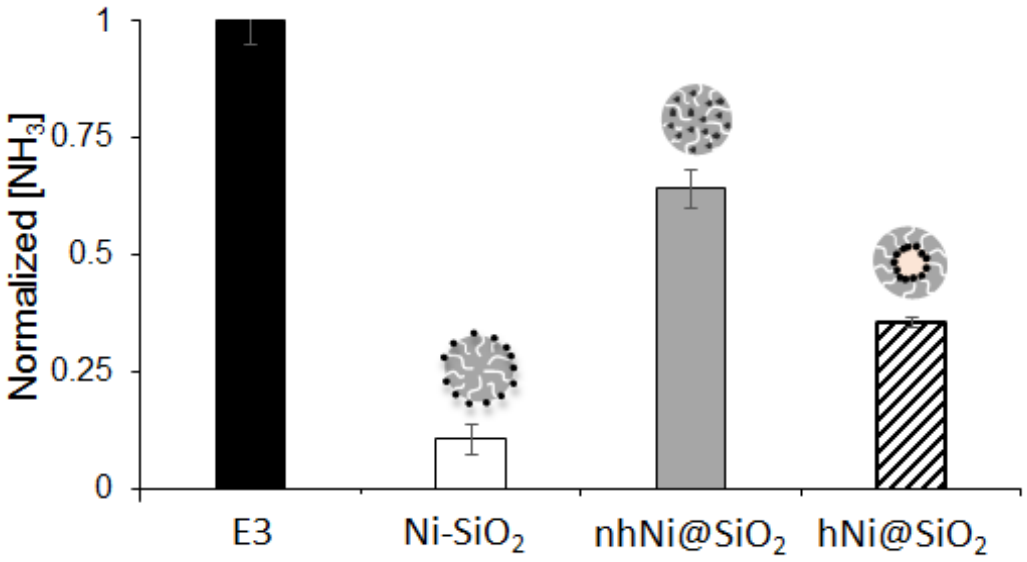

Figure 35. NH_3 concentration after 4hpf zebrafish exposure to 200 mg Ni/L CENs for 72 hours in a 96-well plate. NH_3 concentration is normalized to the NH_3 concentration in control zebrafish wells.

Ni^{2+} and NH_3 are known to react and form a $Ni(NH_3)_6$ complex which is often utilized in the synthesis of Ni NPs[206-209]. Hence, Ni^{2+} ions, dissolved from the CENs, could interact with the excreted NH_3 to form this $Ni(NH_3)_6$ complex and thus remove free, toxic NH_3. However, a quick examination of the stoichiometry of the complex allows us to discard this hypothesis: The control zebrafish produced 27 µmol NH_3 (Figure 33A). Maximum Ni^{2+} dissolution from the CENs (15 mg Ni/L for the Ni-SiO_2 CEN, shown previously in Figure 20) would yield 0.0766

μmol Ni^{2+} in a 300 μL well volume. Based on the 1:6 stoichiometric ratio of Ni:NH_3 in the $Ni(NH_3)_6$ complex, this would bind 0.460 mol of NH_3, i.e. it would lead to a less than 2% reduction in NH_3 concentration. However, the NH_3 concentration in the experiments was reduced by more than 90%. Thus, this effect would be unable to cause the observed reduction in NH_3 concentration.

Next, Ni is known to be a catalyst for NH_3 decomposition [210,211]. While the reaction rates tend to be extremely slow at room temperature, even a slow catalytic decomposition might be significant for the low concentration present in the well. To evaluate the possible decomposition of NH_3, we dispersed the CENs in E3 spiked with 0.075 mol/L NH_3 (in the absence of zebrafish). After three days the CENs were separated and the NH_3 concentration was determined (Figure 36). No change in NH_3 concentration was observed. Thus, the CENs were not acting significantly as catalysts for NH_3 decomposition at the experimental conditions. However, this experiment excludes the interaction between the CENs and the enzymes secreted from the zebrafish that are used for NH_3 detoxification[212]. Thus it could be possible that the CENs affect these enzymes behavior. However, it is likely that the NPs would either bind or reduce the effectiveness of these enzymes, which would lead to an increase in NH_3 concentration. Hence, it is unlikely that the CENs are interfering and binding the enzymes excreted by the zebrafish that aid in NH_3 detoxification.

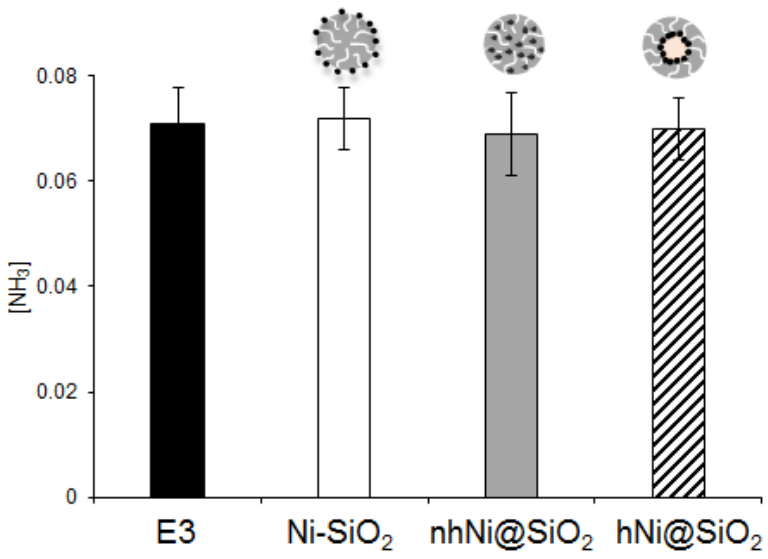

Figure 36. NH_3 concentration after CENs were dispersed in E3 media spiked with 0.075 mol/L NH_3 for three days.

Finally, for our CENs, the observed reduction in NH_3 correlates well with the ranking of the nanomaterials in terms of Ni dissolution (Ni-SiO_2 >> hNi@SiO_2 > nhNi@SiO_2). Previous studies indeed suggest that Ni NPs cause an inhibition in hatching due to dissolved Ni^{2+}, as supported by elimination of the toxicity when chelating the dissolved Ni^{2+} [192]. Therefore, we evaluated NH_3 concentrations in the well after zebrafish were exposed to different $NiCl_2$ concentrations (3, 5, 15 mg Ni/L), corresponding to the Ni^{2+} concentrations expected from CEN dissolution (Figure 37). A strong decrease in NH_3 concentration with increasing Ni^{2+} concentration was observed, and the observed NH_3 concentrations were in good agreement with the NH_3 concentration measured after exposure to CENs (Figure 35). This hence strongly supports the hypothesis that dissolved Ni^{2+} poisoned the zebrafish, resulting in a reduction in metabolism and hence a reduction in excreted NH_3.

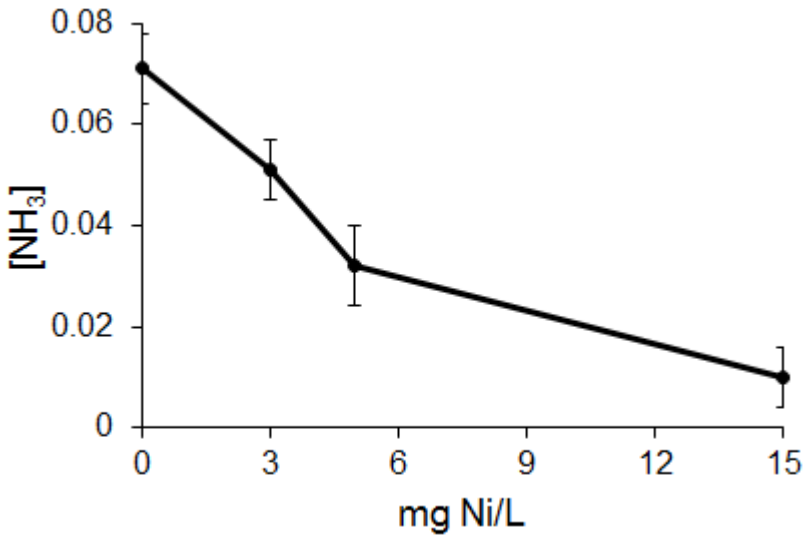

Figure 37. NH_3 concentration in well after 4hpf zebrafish were exposed to 0-15 mg Ni/L $NiCl_2$ for 72 hour in a 96-well plate.

Overall, at this point the following picture emerges: The small well volume in the 96-well plate resulted in the build-up of toxic levels of excreted NH_3, even for the control zebrafish. However, dissolved Ni^{2+} from the CENs, a second toxin for the CEN-exposed zebrafish, reduced the zebrafish metabolism and thus caused a reduction in NH_3 production. This mitigated the self-poisoning from the excreted NH_3. Thus, the Ni-SiO_2 and hNi@SiO_2 CENs falsely appeared non-toxic in the high-throughput hatching assay since one toxin (Ni^{2+}) compensated the effect of the other toxin (NH_3), while the control fish experienced the unmitigated effect of the "self-poisoning" from NH_3 secretion. When the self-poisoning was removed by transitioning to an increased well volume (in the 24-well plates), the true toxicity of the Ni/SiO_2 CENs became apparent in delayed hatching at 72hpf.

5.3.7 Well height determines aggregate size which influences transport through the chorion

The explanations so far cannot explain why the nhNi@SiO_2 CEN was more toxic than the control zebrafish in the 96-well plate. While this CEN shows the lowest dissolution among the CENs and hence should result in the least mitigation of the "self-poisoning", this cannot explain an *increase* in toxicity over the control. Hence, the toxicity associated with this CEN cannot be due solely to Ni^{2+} dissolution but must be due to another distinguishing characteristic of this nanomaterial. In chapter 4.0 with these three CENs, we found aggregation and settling to be a critical parameter that affected toxicity. Among the three CENs, the nhNi@SiO_2 CEN was the most stable in the water column, i.e. it showed the smallest aggregate sizes and lowest settling rate. Therefore, we hypothesized that the toxicity observed for nhNi@SiO_2 in the 96-well plate could be due to differences in aggregate size between the three CEN.

The chorion is known to act as a barrier for NP interactions with the zebrafish embryo[177,178]. This barrier will be increasingly effective with increasing particle size. Hence, one should expect that with increasing aggregate size the CENs will less able to penetrate the chorion. The CEN with the smallest aggregate sizes (nhNi@SiO_2) should be able to interact much more efficiently with the embryo, resulting in enhanced toxicity. However, this effect alone cannot explain why the increased toxicity of this material was entirely removed when transitioning from the 96-well plate to the 24-well plate, i.e. with increase in well volume. Note, however, that with increasing well volume, the media height also increases. This results in an increase in the number of CENs in any (differential) water column above the zebrafish, and a longer settling path for the CEN. These factors can be expected to increase the size of the aggregates formed in that differential well volume during settling. Thus, the smaller aggregates

in the 96-well plate would be more likely to penetrate the chorion than the larger aggregates in the 24-well.

To confirm this hypothesis, we examined the settling rates in CEN solutions with two different heights and determined the aggregate size using Stokes' law (Figure 38)[130]. The results confirm that nhNi@SiO_2 indeed formed smaller aggregate sizes in the lower water column, with a majority of the CEN not aggregating at all (i.e. remaining at size ≤50 nm). In contrast, Ni-SiO_2 and hNi@SiO_2 CENs settled in similar ways in both water column heights. Ni-SiO_2 showed a minor shift to smaller aggregate sizes for the shorter well height, while hNi@SiO_2 showed similar aggregate size distribution for both heights, suggesting a critical aggregate size was formed. The settling behavior and calculated aggregate sizes hence agree with our hypothesis.

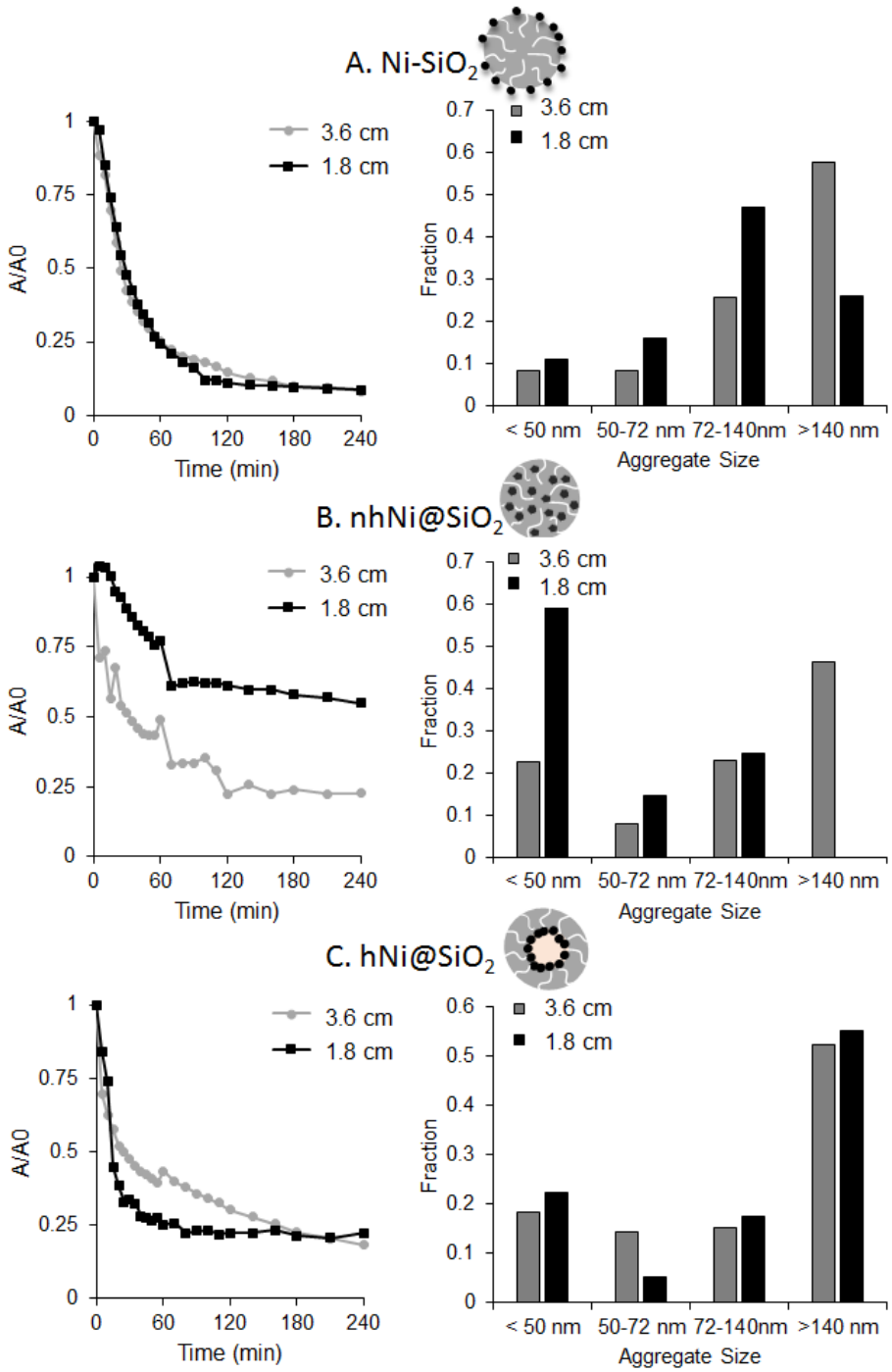

Figure 38. Settling rates (shown as relative UV-vis absorption intensity vs time; left column) and aggregate size distribution (determined by Stokes' law; right column) for A. Ni-SiO_2 B. nhNi@SiO_2 C. hNi@SiO_2 dispersed in E3 media for two different well volumes.

To further support the hypothesis that the difference in aggregate size indeed affects the ability of the CENs to cross the zebrafish chorion, we determined the CEN location by exposing the zebrafish to fluorescently tagged CENs. After a 72 hour exposure, the chorion was mechanically removed and the embryo was imaged in fluorescent microscopy (Figure 39). The zebrafish exposed to the hNi@SiO_2 and Ni-SiO_2 CEN in the 96-well plate shows little evidence of CENs, indicating that the large fraction of hNi@SiO_2 and Ni-SiO_2 CENs that formed large aggregates was indeed unable to penetrate the chorion and interact with the fish. In contrast, the zebrafish exposed to the nhNi@SiO_2 in the 96-well plate showed a significant coverage with CEN, indicating that the small aggregates and non-aggregated particles for this CENs were able to cross the chorion. While these CENs dissolve less Ni^{2+} than the other two CENs, dissolution will hence occur inside the chorion and thus increase the direct exposure of the embryo. At this increased exposure, the toxicity of Ni^{2+} appears to overwhelm the compensating effect of the NH_3 mitigation and the true Ni toxicity becomes apparent in the observed delay in hatching. In contrast to this, the zebrafish exposed to nhNi@SiO_2 in the 24-well plate showed no CENs adhering to the zebrafish, again confirming that the increasing aggregate size with increasing media height results in reduced or even entirely hindered penetration of the chorion, thus eliminating the severe hatching delay observed in the 96-well plate.

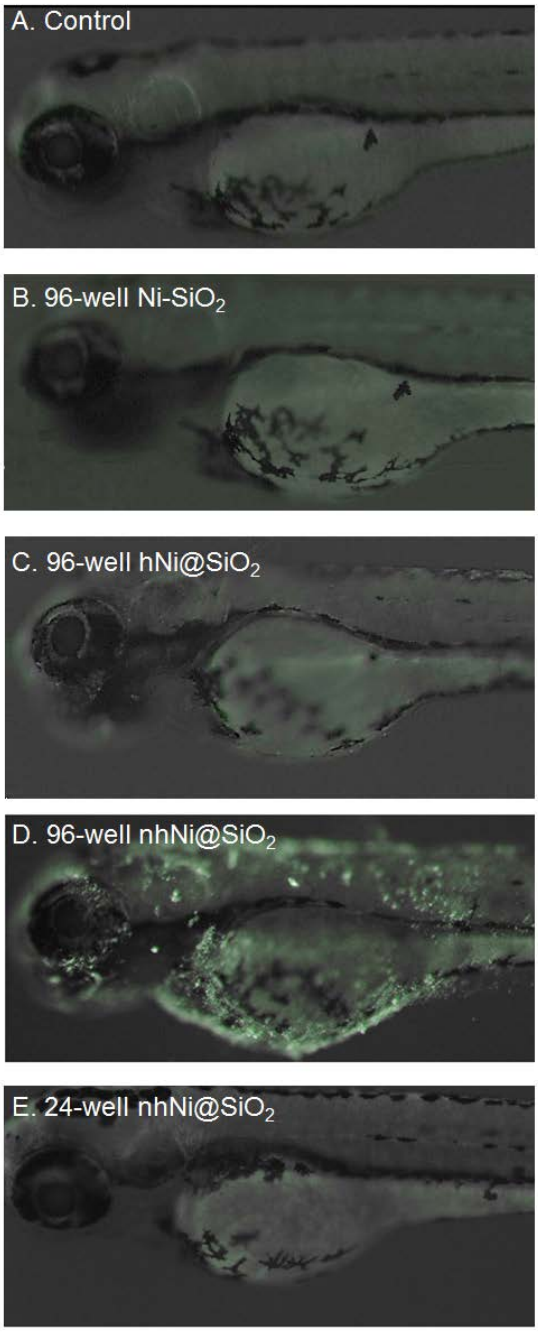

Figure 39. Fluorescent images of zebrafish exposed to 200 mg Ni/L fluorescently tagged CENs for 72 hours. The zebrafish were collected in their chorion, washed and then dechorionated manually before imaging. A. Control zebrafish in a 96-well plate B. Zebrafish exposed to Ni-SiO_2 in a 96-well plate. C. Zebrafish exposed to nhNi@SiO_2 in a 96-well plate. D. Zebrafish exposed to hNi@SiO_2 in a 96-well plate. E. Zebrafish exposed to nhNi@SiO_2 in a 24-well plate.

5.4 SUMMARY AND CONCLUSIONS

High-throughput zebrafish hatching assays are widely used for nanotoxicity studies since they allow high parallelization by utilizing 96-well plates, saving time and space, and enabling evaluation with very small amounts of nanomaterial. However, the results from the present study indicate that great care needs to be taken in order to avoid spurious results from these high-throughput assays. The small media volume per zebrafish in 96-well plates can result in build-up of excreted metabolites which can mask the true nanomaterials toxicity in ways that are not necessarily predictable and may not even be immediately apparent, in particular as the field moves towards evaluation of more complex "next-generation" nanomaterials.

Thus, in our evaluation of three different complex engineered nanomaterials (CEN), we initially assessed two of these CEN falsely as non-toxic. However, further investigations showed that this apparent absence of toxicity was due to a compensation between two different toxins, and the CEN are in fact toxic to the zebrafish embryo. In the small well volume of the 96-well plate, the accumulation of excreted metabolites resulted in "self-poisoning" of the fish. However, Ni^{2+}, a toxin originating from dissolution of the embedded Ni NP in the Ni/SiO_2 CENs, appeared to reduce the zebrafish metabolism and hence reduced the concentration of toxic NH_3 (i.e. the excreted metabolite). Thus, the presence of two toxins resulted in a mutual mitigation of the toxic effect, giving rise to a false "safe" rating of the nanomaterials.

Furthermore, in agreement with our previous studies, we find that aggregate size of nanomaterials, which invariably aggregate to different degrees and sizes in various environments, is a critical factor in controlling nanomaterials toxicity. In the present chapter, aggregate size controlled the ability of the CENs to penetrate the chorion. Hence, the CEN with the smallest aggregate size showed the strongest toxic response. This was the case despite the

fact that this material shows the least Ni^{2+} dissolution, which is suspected to be the sole cause of toxicity for these nanomaterials.

However, aggregate size can be strongly affected by the height of the media column, i.e. the well size of the respective multiwall plate, as observed in the present study for the nhNi@SiO_2 CEN. Hence, the smaller effective size distribution in the lower media column (i.e. the smaller wells of the 96-well plate) resulted in enhanced ability of the nanomaterial to penetrate the chorion, and hence strong enhancement of the toxic response. Note that this difference in the observed response may not necessarily be a weakness of the assay: Instead, it suggests that developmental aquatic toxicity of nanomaterials is likely strongly affected by the specific exposure, and any one assay is hence highly unlikely to capture the "real", effective environmental toxicity. In order to fully capture the potential toxicity of any nanomaterial, one would hence have to assess the toxicity in various scenarios in order to capture the "worst case".

Overall, for the three Ni/SiO_2 CENs in the present study, we found significant toxicity only for the nhNi@SiO_2 under conditions where aggregate sizes remained small, due to the fact that only this nanomaterial was able to penetrate the chorion to a significant degree and hence directly expose the zebrafish embryo to enhanced Ni^{2+} doses from dissolution. Zebrafish exposed in larger well volumes (and hence to larger aggregates) and zebrafish exposed to the other two CENs (hNi@SiO_2 and Ni-SiO_2) experienced only a slight delay in hatching, suggesting only mild toxicity. While a direct comparison with non-embedded Ni NPs of similar size was not possible (since synthesis of such small Ni NPs requires the use of capping agents, which will again significantly alter NP uptake, dissolution, and toxicity), a comparison with the reported toxicity of larger Ni NPs[158,192,196] suggests that formation of such CEN in which (potentially

toxic) metal NPs are embedded into a (non-toxic) matrix could be an efficient way to mitigate NP toxicity in next-generation complex engineered nanomaterials.

6.0 EMBEDDING CU NPS IN SILICA SUPPORT REDUCES TOXICITY COMPARED TO CU NPS DEPOSITED ON SILICA SUPPORT

6.1 INTRODUCTION

Copper nanoparticles (NPs) have excellent thermophysical properties and thus have made important advances in electronics technology (semiconductors, electronic chips, heat transfer nanofluids)[213,214]. In addition, they have found other use in catalytic applications[215,216], solar cells and lithium batteries[217,218], and air and liquid filtration[219,220]. Furthermore, due to their biocidal properties they have been incorporated into face masks, wound dressings, socks and water purifiers[52-56,214]. However, copper NPs have been shown to be toxic in both *in vivo*[152,177,195,221-225] and *in vitro*[32,109,176,226-228] models.

Current studies focusing on the toxicity associated with (bare) Cu NPs found them to be ranked "moderately toxic" based on EPA guidelines[111,222,229]. These (bare) NP studies provide excellent insight into the possible toxicity associated with these materials. However, Cu NPs are being utilized in complex engineered materials (CENs), in which the Cu NP is embedded in a support matrix, to prevent deactivation of the material[51,56,230-232]. Yet, there have been limited studies to date focusing on the effect embedding the Cu NP has on toxicity. By studying how embedding the Cu NP in a support, compared to deposited on the surface, we can determine if nanoembedding is an effective strategy to designing safer Cu nanomaterials[28,90,91]. We

hypothesize that by combining the active toxic Cu NPs with a non-toxic amorphous silica support, we can aid in mitigating toxicity. This will be completed by reducing interaction with the environment and slowing Cu^{2+} dissolution, a known toxic source[166,167].

In this Chapter, we investigated the toxicity of two nanostructured copper-silica CENs: (i) copper NPs deposited on the external surface of an amorphous silica particle (Cu-SiO_2), and (iii) non-hollow core-shell materials (nhCu@SiO_2), which consist of Cu NPs embedded into porous amorphous silica shells. Utilizing these structures we will study how embedding alters the CENs physicochemical properties and thus affects toxicity. In order to test this, the CENs were subjected to thorough physicochemical characterization, including the determination of Cu^{2+} dissolution, SiO_2 dissolution and aggregation properties. The toxicity of these materials were then evaluated in zebrafish larvae, using four complementary endpoints: survival[66,111,151-153], developmental morphology[160,161], hatching[34,110,140,154-159], and motor function[68,162-164]. The first three are considered robust, established assays in nanotoxicology, whereas motor function is a novel and recently emerging assay for evaluating nanotoxicity.

6.2 METHODS

6.2.1 Cu/SiO_2 CEN synthesis

Non-hollow Cu@SiO_2 (nhCu@SiO_2) materials were synthesized using a one-pot reverse microemulsion synthesis developed in our laboratory. First, 50 mL of cyclohexane (≥99%) and 10.5 g surfactant Brij 58 (≥99% polyethylene glycol hexadecyl ether, Mn ~1124, Sigma-Aldrich) were refluxed at 50^{o}C until the surfactant was fully dissolved. 1.5 mL of 1 M $CuCl_2$ was then

added drop-wise. Next, 5 g of tetraethylorthosilicate (TEOS, ≥99%) was added, followed by 3 mL of ammonium hydroxide (30%). After two hours of aging for silica growth, particles were precipitated with 2-propanol, collected via centrifugation, washed three times with iso-propanol, and dried in air. The crushed powder was then calcined in a Thermolyne 79300 tube furnace for 2 hours at 500^{o}C in air.

For surface-deposited Cu-SiO_2, copper-free spherical silica spheres were first synthesized using the microemulsion nhCu@SiO_2 procedure above but replacing aqueous Cu salt with 1.5 mL deionized (DI) water. Following calcination of the Cu-free silica, a deposition-precipitation method, modified from Deng et al.[105], was used to deposit very small and near-monodisperse Cu NPs on the surface of the calcined silica spheres. 0.6 g of SiO_2 NPs were dispersed in 15 mL of DI water by sonication, X M Cu salt solution was added (0.52 g $CuCl_2$ in 10 mL DI water), and the mixture was again sonicated for 20 min. Ammonium hydroxide (30%) was then added drop-wise over 20 min until the pH of the solution was ~9.5. The resulting material was mixed for 20 min, centrifuged, dried, calcined at 300^{o}C in air, rinsed twice in DI water, dried, and calcined again at 300^{o}C in air.

6.2.2 CEN size, morphology and surface area characterization

CEN size and morphology were characterized with transition electron microscopy (TEM, JEOL-2000FX electron microscope). Particle measurements of TEM images were done using ImageJ software (http://rsb.info.nih.gov/ij/). Scanning Electron Microscopy (SEM) equipped with EDX was used at beam voltage of 15kV to determine elemental composition. Surface area and porosity were determined by Brunauer Emmett Teller (BET) analysis using a Micromeritics ASAP 2020 surface area and porosity analyzer. Pre-treatment consisted of 2-3 hr degassing at

200^{o}C under vacuum. Typically, a 6-point BET analysis was used for total surface area measurement and an 84-point N_2 Barrett-Joyner-Halenda (BJH) analysis with Halsey thickness curve correction and Kruk-Jaroniec-Sayari correction for pore size and volume determination.

6.2.3 CEN aggregation size characterization

CEN aggregate size in E3 medium (49 mM NaCl, 1.6 mM KCl, 3.3 mM $CaCl_2$, 3.3 mM $MgSO_4$, pH 7.4) was determined by dynamic light scattering (DLS, Zetasizer Series Nano-ZS). E3 medium was chosen as it is the zebrafish medium used for the toxicity studies. The samples were first dispersed by sonication and then ~1 mL of dispersed solution was added to a cuvette. The refractive index of silica was used for all measurements.

6.2.4 CEN Cu^{2+} dissolution

The degree of Cu^{2+} dissolution from the CENs in E3 medium was determined at specific time points. Six mL dispersions (3 mg Cu/L) were prepared in E3 media. CENs were removed from the dispersions by centrifugation followed by filtration (Amicon 10,000 molecular weight cut-off filters, ~3.1 nm). HNO_3 (Sigma, 70%) was added dropwise to the filtrate to a concentration of 3 wt%. Dissolved Cu^{2+} was measured under radial detection by inductively coupled plasma atomic emission spectroscopy (ICP-AES, Thermo Electron Corporation iCAP6500 Duo Series ICP-OES Spectrometer). Standards were formulated from a stock standard solution (Fischer Scientific) with 3 wt% HNO_3 in deionized water to generate a standard curve.

6.2.5 CEN SiO_2 dissolution

Dissolved silica concentration was measured using the ASTM D859-00 standard test method for silica in water[168]. Briefly, 10 mL dispersions (3 mg Cu/L) were prepared in E3 media. At specific time points the CENs were removed by centrifugation followed by filtration. 0.2 mL of HCl (1:1 water:acid) and 0.4 mL of ammonium molybdate (75 g/L, Sigma-Aldrich) was added in succession to the collected sample. After five minutes, 0.3 mL of oxalic acid (100 g/L, Sigma-Aldrich) was added. 0.4 mL of amino-naphthol-sulfonic acid (0.5 g 1-amino-2-naphthol-4-sulfonic acid + 150mL DI water + 1 g Na_2SO_3 + 30 g $NaHSO_3$) was added after 1 minute. After ten minutes the absorbance was read at 815 nm using UV-Visible spectroscopy. A blank was prepared using E3 medium without CENs.

6.2.6 Nanomaterial suspension preparation

Dried CEN powder was weighed, added to E3 media, and sonicated 20 min. Serial dilutions were then prepared volumetrically. The solutions were re-dispersed by sonication for 1-2 minutes immediately prior to addition to the well.

6.2.7 Zebrafish studies

Zebrafish studies were carried out in compliance with all federal and local regulations, in accordance with NIH guidelines for animal care and use and with full approval from the University of Pittsburgh Institutional Animal Care and Use Committee. Embryos for experiments were generated by crossing healthy adult WT strain AB zebrafish of 4 – 12 months of age. The

afternoon before mating, zebrafish were placed in breeding tanks with false bottoms, and dividers to separate males and females. On the morning of mating the divider was removed at 08:00 when the zebrafish facility lights are illuminated to allow breeding. Timed embryos were collected within the first hour of breeding. The embryos were washed in system water and then E3 buffer and transferred to 10cm plates containing E3 buffer with methylene blue (0.0001% w/v). A maximum of 30 embryos were housed in each dish. Plates were kept at 28.5°C in an incubator with white light illumination (color temperature 4900K; brightness 200 Lux) on a light-dark cycle (14 hours light:10 hours dark, light starts at 08:00).

6.2.8 Zebrafish embryo test (survival, morphology, hatching)

At 4 hours post fertilization (hpf), zebrafish embryos were left in their chorion and transferred to a well of a polystyrene multi-well plate. One zebrafish was placed in one well of a 24-well plate with two mL CEN solution. Zebrafish were incubated for five days at 28.5^{o}C and analyzed visually each day for survival, developmental malformations and hatching. 12-18 embryos were tested for each condition and per was repeated in three independent experiments.

6.2.9 Zebrafish larval motility behavior

24 hpf zebrafish embryos were mechanically dechorionated and placed in one well of a 24-well plate with two mL CEN solution. The chorion was removed to eliminate differences in exposure due to different hatching behaviors. Surviving larvae were collected on day four, zebrafish larvae displaying morphological abnormalities were excluded from the motor assays. The zebrafish larvae were washed three times in E3 medium to remove residual particles by being gently

transferred in E3 using a Pasteur pipette. The washed zebrafish were then transferred to a 96-well plate. Motor function was then analyzed as described in detail in our previous work [170,171]. Briefly, a video stream of zebrafish moving in the wells of a 96-well plate was captured at 2 frames/s. Video recordings were analyzed using the open source *LSRtrack* and *LSRanalyze* MATLAB scripts that we reported and extensively validated previously[170-172]. All video recordings were taken at the same time of the day (between 2-5 pm).

6.2.10 Zebrafish copper uptake

Zebrafish Cu uptake was determined by collecting surviving embryos and larvae upon termination of the experiment to measure cumulative metal uptake. Briefly, larvae were transferred to clean 12-well plates in groupings by dose, rinsed 5 times in fresh E3 medium to rinse residual external particles from surface of the zebrafish, euthanized using 10% sodium hypochlorite and rinsed five times with E3 media. Residual medium was then removed and zebrafish were dried in air. A dissolving procedure by Borgmann et al.[173] was used beginning with addition of nitric acid (12.5 µL/fish, 70%, Fischer Scientific) followed by at least one week digestion followed by addition of hydrogen peroxide (10 µL/fish, 30%, JTBaker) and 24 hours digestion. Resulting solutions were diluted up to 8 mL and the Cu concentration was measured via ICP-AES. The number of rinse cycles was determined by repeating washes until the copper uptake measurement became independent of the number of washes.

6.2.11 Statistics

Data for each of the assays were parametrically distributed. To compare the effects of multiple different concentrations of each nanomaterial with embryo buffer in the same experiment, we employed one-way ANOVA followed by Dunnett's test[107]. * indicates $p \leq 0.05$. Three independent experiments were conducted for each zebrafish endpoint with 12-18 fish per condition.

6.3 RESULTS

6.3.1 Characterization of Cu/SiO_2 CENs

Two Cu/SiO_2 complex engineered nanomaterials (CENs) were synthesized using a reverse microemulsion sol-gel synthesis: Cu NPs externally deposited on a silica support (Cu-SiO_2) and Cu NPs embedded throughout a SiO_2 support (nhCu@SiO_2). Transition electron microscopy (TEM) images of the Cu/SiO_2 CENs are shown in Figure 40, and material characteristics are summarized in Table 6. Both materials share common chemical compositions and have similar dimensions, and differ in nanostructure alone. For both CENs, the copper NPs are similar in size (~2-3 nm) and copper content is ~10-12 wt%. The CENs are spherical and ~40 nm. Additionally, the surface area are similar, (~100-150 m^2/g). Agglomerate size was assessed by dispersing the CEN in zebrafish E3 medium (49 mM NaCl, 1.6 mM KCl, 3.3 mM $CaCl_2$, 3.3 mM $MgSO_4$, pH 7.4) by sonication, and agglomerate sizes were measured using dynamic light scattering (DLS,

Table 6). After dispersion in E3 media, the Cu-SiO_2 aggregated to larger sizes than the nhCu@SiO_2.

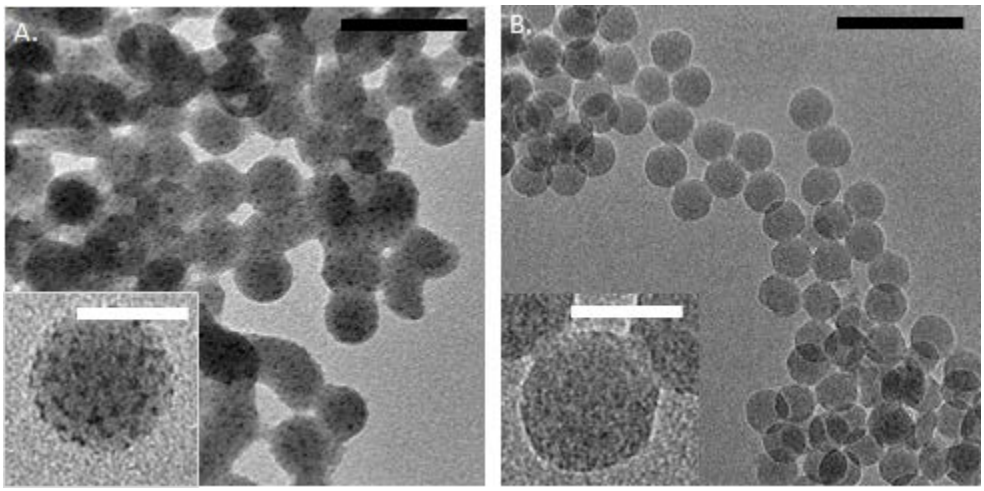

Figure 40. TEM images of typical (a.) Cu-SiO_2, (b.) nhCu@SiO_2 samples. Scale bars are 100 nm for larger images (black) and 50 nm for insets (white).

Table 6. Cu loading (from EDX), Cu NP size (from TEM)(dry) CEN particle size (from TEM), CEN agglomerate size suspended in E3 medium (from DLS) and surface area for Cu-SiO_2 and nhCu@SiO_2, shown in Figure 40.

CEN	Cu loading (wt% Cu)	D_p, Cu particle (nm), n= # particles counted	D_p, primary particle (nm), n= # particles counted	Mean size in E3 medium suspension, (nm)	Surface area (m^2/g)
Cu-SiO_2	9.8 ± 0.5	2.2 ± 0.3, n=100	45.2 ± 7.5, n=120	1091 ± 102	140.4
nhCu@SiO_2	10.5 ± 0.7	2.4 ± 0.4, n=104	51.5 ± 6.2, n=120	653.14 ± 59.5	99.4

6.3.2 Cu^{2+} dissolution

Ion dissolution from metal NPs is an important mechanism mediating the toxicity of metals[30,109,110,164], including copper[31,226]. Therefore, we investigated the metal dissolution from the CENs into the E3 medium. This will determine if toxicity is directly correlated with the Cu^{2+} ion shedding[174]. Cu^{2+} dissolution was determined by dispersing 3 mg Cu/L of CEN in E3 zebrafish embryo medium for five days. 3 mg Cu/L was chosen as it was a concentration in the middle of the tested range for toxicity studies and had greater than 70% zebrafish survival for all tested materials (see Figure 43). At specific time points, centrifugal ultrafiltration was used to separate the CENs, and inductively coupled plasma atom emission spectroscopy (ICP-AES) was used to determine dissolved Cu^{2+} concentration. Cu-SiO_2 CENs showed the highest Cu^{2+} dissolution (0.11 mg Cu/L) while nhCu@SiO_2 (0.017 mg Ni/L) CEN exhibited a much lower Cu^{2+} dissolution (Figure 41). Cu-SiO_2 displayed a constant dissolution of Cu^{2+} over 72 hours, but gradually slowed from 72-96 hours. In contrast, the nhCu@SiO_2 rapidly dissolved the first 24 hours and slowed for the next 96 hours.

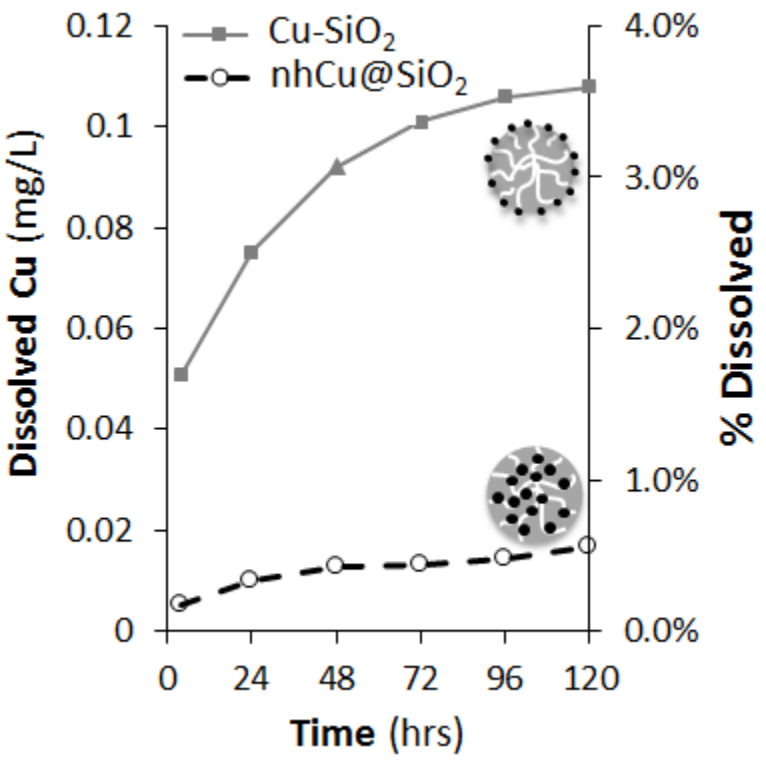

Figure 41. Dissolved Cu^{2+} and percent dissolution of Cu/SiO_2 CENs in E3 media at room temperature for 120 hours with a starting concentration of 3 mg Cu/L.

6.3.3 SiO_2 dissolution

Silica dissolution could compromise the CENs stability in the aqueous media, alter the size and shape of the CEN, and ultimately cause the Cu NP to be released from the protective silica matrix into the medium or the zebrafish larvae. Therefore, silica dissolution was quantified using a colorimetric assay over five days by dispersing 3 mg Cu/L CENs in E3 media (Figure 42)[168]. $nhCu@SiO_2$ (0.839 mg SiO_2/L, 3.1% total SiO_2) showed a higher dissolution than the $Cu\text{-}SiO_2$ (0.289 mg SiO_2/L, 1.1% total SiO_2) CEN. However, both CENs exhibit minimal silica

dissolution (<4%) and hence silica dissolution was not expected to release Cu NPs from the silica matrix.

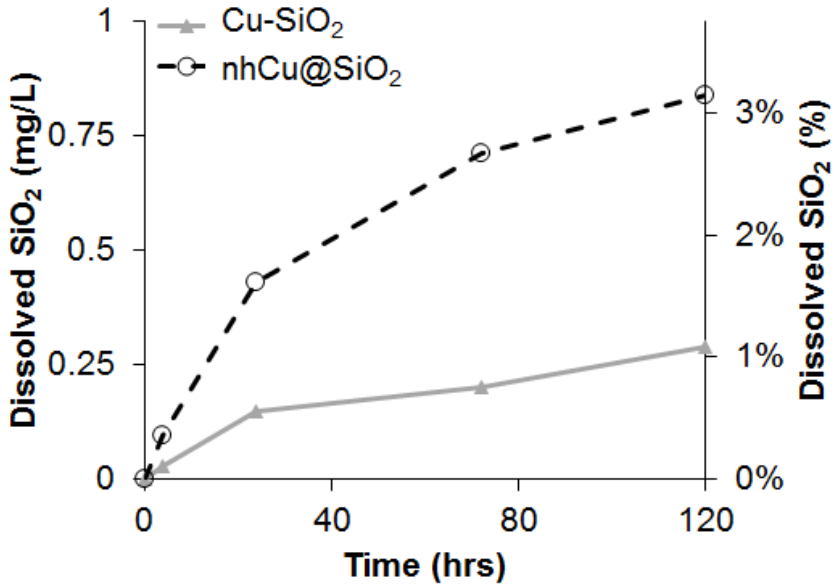

Figure 42. A. Dissolved silica (mg SiO_2/L and % total SiO_2) from 3 mg Cu/L CENs dispersed in E3 medium for five days at room temperature.

6.3.4 Toxicity of Cu/SiO_2 CENs

To evaluate the effect nanoembedding has on toxicity, 4hpf zebrafish embryos were exposed to 0.1 – 10 mg Cu/L of CENs dispersed in E3 embryo medium for five days. E3 medium containing $CuCl_2$ was used as a positive control for toxicity related to dissolved Cu^{2+}; E3 media without additives was used as a negative control. The toxicity of the SiO_2 support was tested previously and it was determined that there was no toxicity associated with these NPs (Chapter 4.0). Hence,

any observed toxicity was related to the Cu NPs. Survival (defined as a visible heart beat) was monitored daily until 5 days post fertilization (dpf) (Figure 43A).

6.3.5 Zebrafish survival depends on CEN structure

As expected, $CuCl_2$ was toxic in a dose-dependent manner; the calculated LC_{50} for Cu^{2+} was ~2.5 mg/L. The Cu-SiO_2 CEN caused a dose-dependent decrease in zebrafish survival; the calculated LC50 was 5 mg Cu/L. In contrast, 92% of the zebrafish embryos exposed to nhCu@SiO_2 CEN survived over the tested concentration range (0-10 mg Cu/L). There was a clear toxicity ranking: $CuCl_2$ was the most toxic and caused a higher mortality rate than the than the Cu-SiO_2 CEN which caused more zebrafish death than the nhCu@SiO_2 CEN. However, when survival was plotted again the dissolved Cu^{2+} concentration (extrapolated from Figure 41), the Cu-SiO_2 CEN was more toxic than the $CuCl_2$ salt (Figure 43B). This indicates a nano-specific effect: the toxicity associated with the Cu-SiO_2 CEN cannot be explained purely by Cu^{2+} dissolution in the media.

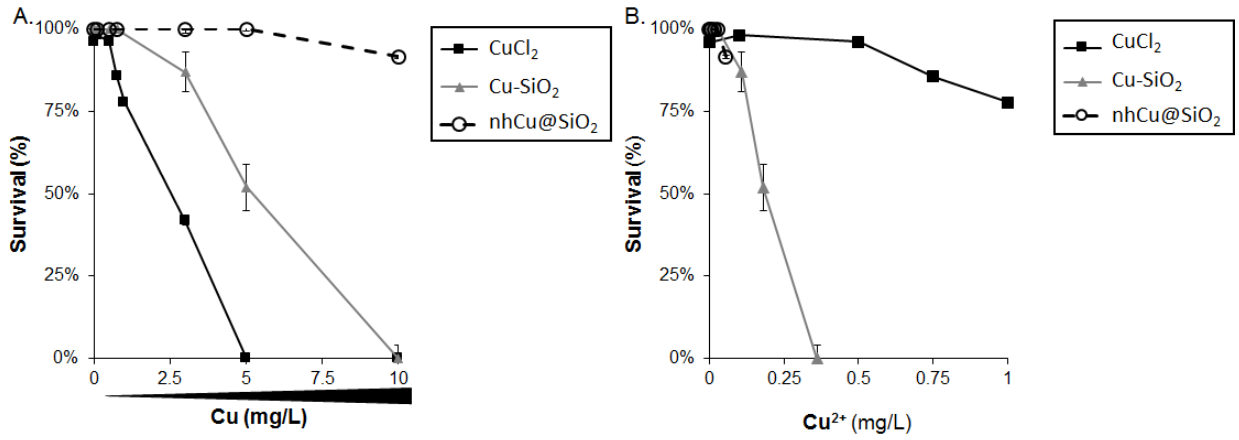

Figure 43. Zebrafish larvae survival (%) after exposure to A. 0-10 mg Cu/L for $CuCl_2$ or Cu-SiO_2 or nhCu@SiO_2 on 5dpf. B. Survival was plotted against the dissolved Cu^{2+} concentration present in the well. Error bars are error of sum squares (SSE).

6.3.6 Cu materials did not cause development of zebrafish larvae malformations

Metal NPs have previously been reported to cause a range of developmental defects in zebrafish larvae including abnormal spinal curvature, pericardial and abdominal edema[160,161]. Therefore, we evaluated the development of malformations as an indicator of developmental toxicity. 4hpf zebrafish embryos were left in their chorion and exposed to 0-5 mg Cu/L of $CuCl_2$ or CENs dispersed in E3 media. The embryos were monitored for the appearance of malformations over the next five days (Figure 44), including abnormal curvature of the spine and body (lordosis, kyphosis and scoliosis), pericardial and abdominal edema, and failure of swim bladder inflation (representative images is detailed in **Error! Reference source not found.**Figure 57). Overall, the development of malformations for embryos exposed to 0-5 mg Cu/L Cu/SiO_2 CENs or $CuCl_2$ did not differ significantly from E3-only control. Hence, evaluating the development of

malformations was not a sensitive endpoint for evaluating developmental toxicity of the Cu materials.

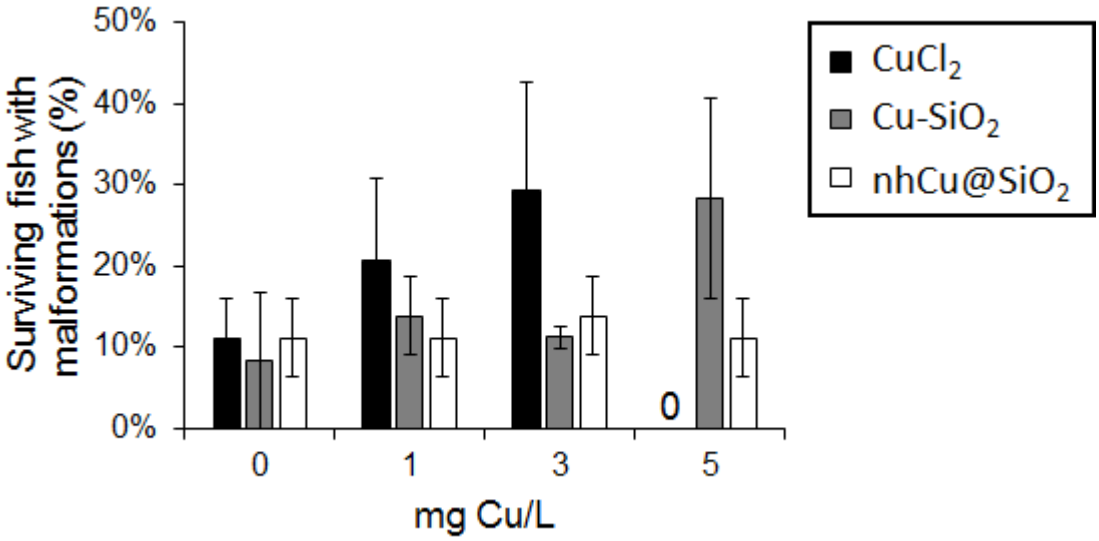

Figure 44. Malformations observed in surviving zebrafish larvae exposed to $CuCl_2$ or Cu/SiO_2 CENs on 5dpf. Note that there were no surviving fish for 5 mg Cu/L $Cu\text{-}SiO_2$. *$p \geq 0.05$ for one way ANOVA followed by Dunnett's t-test, error bars are standard deviation.

6.3.7 Zebrafish hatching dependent on Cu structure

Evaluating the effect nanomaterials have on zebrafish hatching is a quick, facile assay that is used extensively in nanotoxicity studies to determine developmental toxicity. Therefore, we examined the inhibition in zebrafish hatching due to the Cu/SiO_2 CENs. 4hpf zebrafish (left in their chorion) was exposed to 0-10 mg Cu/L and monitored daily until 5dpf. The hatching rate was calculated by normalizing the number of hatched zebrafish by the total number of surviving

zebrafish. Figure 45 indicates the hatching rate on 72hpf for zebrafish exposed to 0-10 mg Cu/L. 100% of the control zebrafish had hatched by 72hpf. Zebrafish exposed to $CuCl_2$ had the highest delay in hatching (< 0.1 mg Cu/L delayed 50% of the zebrafish from hatching), followed by Cu-SiO_2 CEN (0.1 mg Cu/L delayed 50% of the zebrafish from hatching) and, lastly, nhCu@SiO_2 (0.75 mg Cu/L delayed 50% of the zebrafish from hatching) had the least effect on the hatching rate (Figure 45A). The toxicity ranking due to inhibition in hatching agrees with the toxicity ranking based on zebrafish survival. However, when the toxicity was plotted again the dissolved Cu^{2+} concentration, both CENs were more toxic than the $CuCl_2$ salt. As previously seen with survival, this suggests the presence of a nano-specific effect. The dissolved media Cu^{2+} concentration cannot solely explain the observed toxicity.

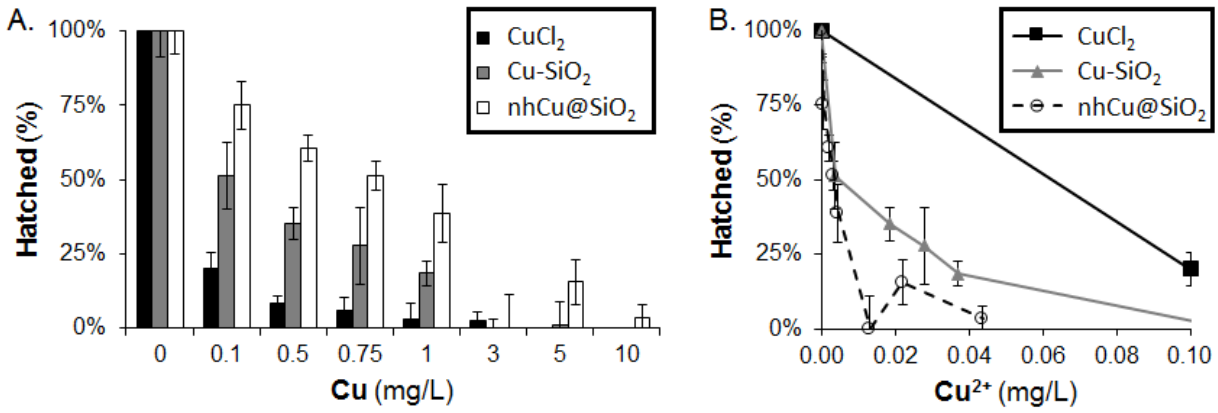

Figure 45. 72 hpf hatching rate for zebrafish exposed to 0-10 mg Cu/L $CuCl_2$, Cu-SiO_2, or nhCu@SiO_2. All tested concentrations were significant compared to the control (error bars are standard deviation, significance was determined using one way ANOVA followed by Dunnett's test).

6.3.8 Cu/SiO_2 CENs affect zebrafish larval motor function in dark portions

Previous reports indicate that copper can act as a neurotoxin which would be expected to adversely affect motor function in developing zebrafish larvae[233,234]. Additionally, zebrafish larval motor behavior can be quantified in a 96-well plate, thereby allowing statistically robust determination of how toxicants alter motor physiology[170,172,183]. The chorion has been previously reported to possibly act as a barrier for uptake of metal NPs[177,178]. Consequently, in order to eliminate differences in chorionic penetration of NPs as a variable from our studies, zebrafish embryos were mechanically dechorionated at 24 hours post-fertilization (hpf). In parallel, survival rates for 24hpf dechorionated zebrafish exposed to the Cu/SiO_2 CENs were monitored. The survival rates were similar, thus the toxicity associated with zebrafish survival was independent of the presence of the chorion.

Embryos were mechanically dechorinated at 24hpf and exposed to Cu CENs or $CuCl_2$ for four days. Spontaneous propulsive movements was measured on 5dpf to evaluate the development of swimming behavior during CEN exposure. At 5dpf surviving zebrafish larvae were collected and transferred to E3 medium with no additives for two hours. All zebrafish larvae with morphological abnormalities (compared with normal healthy zebrafish larvae under light microscopy) were excluded from the motor assays. Consequently, the motor assays are informative about the development of locomotor function, rather than mechanical consequences or morphological malformation involving the body shape, trunk muscles or fins. Three patterns of altered larvae locomotor behavior with increasing toxicant concentration have been reported previously: (i) a monotonic decrease in total larval displacement/time with increasing toxicant concentration[154,163]; (ii) a monotonic increase in displacement/time with increasing toxicant

concentration[184]; and (iii) a biphasic relationship in which locomotor activity first increases at lower concentrations and after reaching a maximum, decreases at higher concentrations[185,235,236].

Using our previously reported methods, we quantified zebrafish larval motor function at 5dpf in 96-well plates for one hour in bright white light and three 20 minute light/dark cycles (200 Lux brightness, 4900K color temperature)[170-172], and determined their mean velocity (V_M = total displacement of the larval centroid over the course of the recording/ time period of observation). All three copper materials did not cause any significant change in larval motility during the one hour light exposure (Figure 46). In contrast, all three materials provoked abnormalities in the zebrafish larval motility behavior during the dark portion of the cycle (Figure 47). $CuCl_2$ caused a monotonic increase in V_M from 0.1-0.75 mg Cu/L and then exhibited a decrease in V_M from 1-3 mg Cu/L. Cu-SiO_2 exhibited this same trend, with an elevated V_M from 0.1-0.5 mg Cu/L and a decrease in V_M from 0.5-3 mg Cu/L. Robust motility analysis was not possible for these materials past 3 mg Cu/L due to zebrafish death. Lastly, zebrafish exposed to nhCu@SiO_2 exhibited an increase in V_M from 0.1-1 mg Cu/L and a decrease in V_M from 3-10 mg Cu/L. It is difficult to develop a ranking of these materials based on the changes in motility due to the response being u-shaped rather than a monotonic increase or decrease in V_M. But, it allowed toxicity to be detected at lower concentrations than hatching or survival.

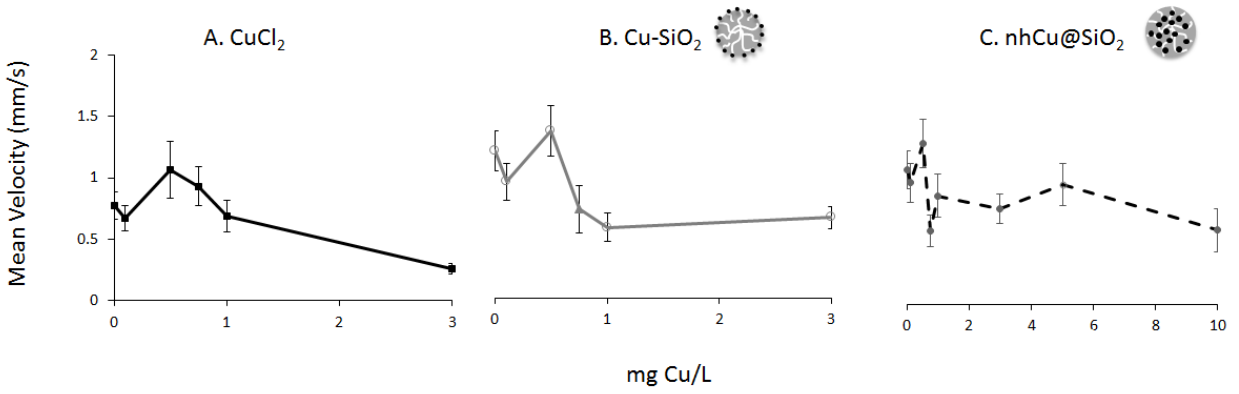

Figure 46. Zebrafish larval mean velocity (mm/s) after exposure to 0-10 mg Cu/L A.) $CuCl_2$ analogous salt and, B.) Cu-SiO_2, C.) nhCu@SiO_2. Shown as average VM and error bars are SSE.

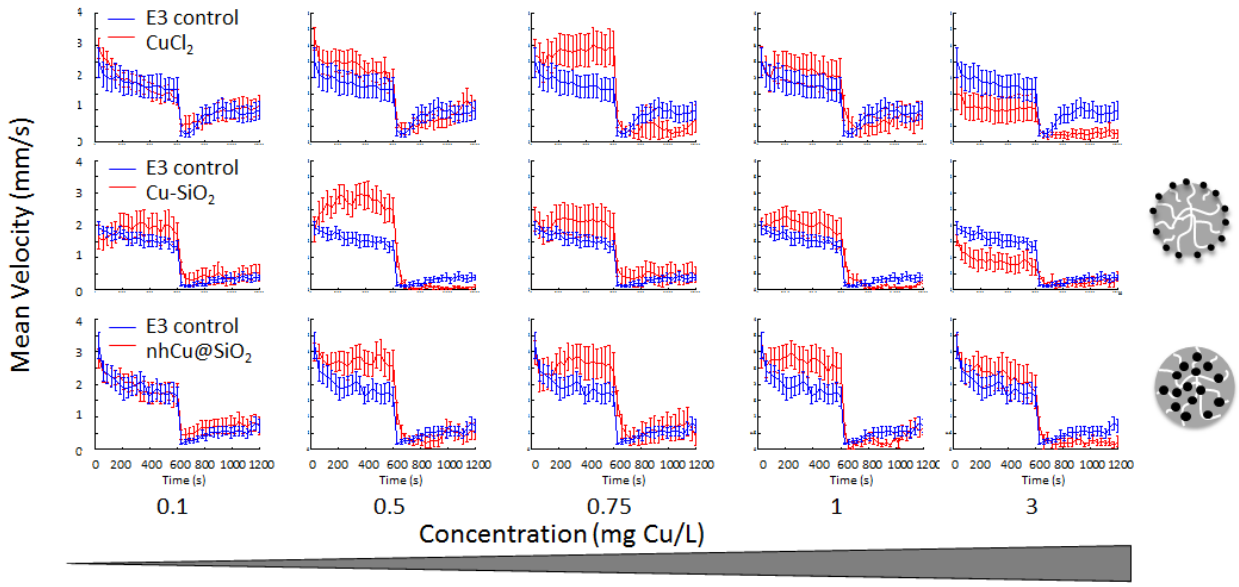

Figure 47. Average zebrafish larval mean velocity over the three cycles (dark from 0-600 sec; light from 600-1200 sec) after exposure to 0-10 mg Cu/L A.) $CuCl_2$ analogous salt and, B.) Cu-SiO_2, C.) nhCu@SiO_2. Shown as average VM and error bars are SSE.

6.3.9 Structure does not affect zebrafish copper uptake

To determine if toxicity was correlated with total copper uptake into the zebrafish, we measured tissue Cu concentrations in zebrafish larvae exposed to the copper materials. Zebrafish embryos were exposed to 3 mg Cu/L of either CEN or $CuCl_2$. Both 4 hpf chorionated zebrafish and 24hpf dechorionated zebrafish were used. After exposure, the zebrafish embryos and larvae were thoroughly washed five times and digested to allow measurement of tissue Cu content by ICP-AES. Figure 48 shows the total Cu content after 96 hour exposure to the copper materials. For both 4hpf chorionated zebrafish and 24 hpf dechorionated zebrafish, there was no significant differences in Cu uptake depending on the material. The 4hpf chorionated zebrafish had a higher Cu uptake than the 24 hpf dechorionated zebrafish. This was expected since the fish were exposed to the Cu materials for an additional 20 hours.

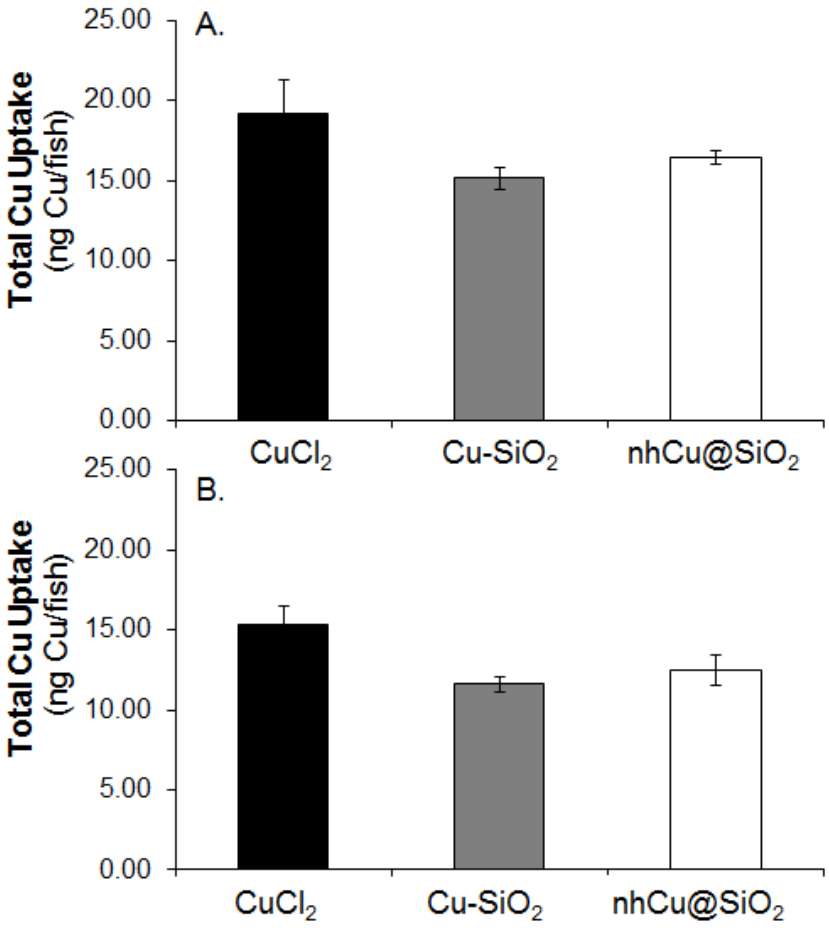

Figure 48. Cu uptake at 96hpf after exposure to 3 mg Cu/L $CuCl_2$, Cu-SiO_2 and nhCu@SiO_2 for A. 4hpf zebrafish left in the chorion and B. 24hpf mechanically dechorionated zebrafish.

6.4 DISCUSSION

This present study aimed to utilize high-throughput zebrafish assays to study the toxicity of Cu/SiO_2 CENs and understand the effect nano-embedding had on toxicity. It was clear from the zebrafish assays that the Cu-SiO_2 CEN was more toxic than the nhCu@SiO_2 CEN. The Cu-SiO_2 CEN caused a higher rate of zebrafish death and a more significant delay in zebrafish hatching.

In addition, both CENs were a developmental neurotoxin. Interestingly, the CENs did not affect larval motility behavior in the light, but, only disrupted larval motility behavior in the dark. This inverted U shape in the dark (but not in the light) was also observed when zebrafish were exposed to cocaine and d-amphetamine[236]. However, there is no clear evidence what this means developmentally for the zebrafish.

Overall, embedding the Cu NP in a SiO_2 NP led to a safer nanomaterial than the externally deposited Cu NPs. This can be possibly due to reducing Cu^{2+} dissolution or limiting interaction between the Cu NPs and the environment. Indeed, the Cu NPs deposited on the external SiO_2 NPs had ~6X higher dissolution than the Cu NPs embedded in the SiO_2 NPs. This is likely due to the external Cu NPs being directly exposed to the E3 media. The saturation concentration is hence kept low and the Cu^{2+} dissolution does not reach equilibrium quickly and Cu NP is able to keep dissolving. In contrast, the Cu NP embedded in the silica support experiences a slower dissolution because the Cu^{2+} equilibrates with the media inside the pore which reaches equilibrium much faster. It is then dependent on the media to diffuse out of the pores. This is a much slower process, than the external NPs which are exposed to the bulk media, and leads to a reduction in Cu^{2+} concentration in the media. While the Cu^{2+} dissolution ranking (Cu-SiO_2 > nhCu@SiO_2) agrees with the toxicity rankings ($CuCl_2$ > Cu-SiO_2 > nhCu@SiO_2), the dissolved Cu^{2+} concentration cannot solely explain the observed toxicity (Figure 43A and Figure 45A). When the survival and hatching rates were plotted against the dissolved Cu^{2+} concentration present in the well, both CENs exhibited a more toxic response than the correlating salt. Thus, a nano-specific toxicity mechanism is at play that relies on the uptake of the CENs. Other reports suggest the toxicity of their Cu NPs is dependent on this same nano-specific effect[152,223].

Interestingly, the zebrafish total Cu uptake was similar for all three materials. This suggests that the differences in toxicity is not due to an enhanced uptake of a specific material. Rather suggests the toxicity is related to the type of Cu (ionic or metallic) present in the organism. Unfortunately, we are not able to differentiate between ionic copper and metallic copper. However, based on previous *in vitro* studies, Cu NPs are shown to be toxic via a Trojan horse mechanism[226-228]. In addition, a Trojan horse mechanism can explain the observed toxicity differences. The surface deposited Cu NPs are expected to dissolve Cu^{2+} at a faster rate than the Cu NP embedded in the silica. This rapid and more complete dissolution is in agreement with the elevated toxicity with these materials. Furthermore, this dissolution could occur in different organs in the zebrafish. Naively, we would expect the Cu^{2+} salt and Cu CENs to be located in different organs/tissues of the zebrafish due to different transport mechanisms. Moreover, it would not be a far reach to hypothesize the two CENs are transported to different organs/tissues. Due to differences in the surface chemistry (Cu-terminated versus SiO_2-terminated), there could be different uptake, and transportation throughout the zebrafish.

6.5 CONCLUSIONS

Our results demonstrate that zebrafish embryos provide a useful screening model for evaluating CEN toxicity during vertebrate development by combining established (zebrafish larval survival and malformations) and novel (zebrafish larval locomotor function) methods for detecting phenotypes. Based on these assays, the Cu/SiO_2 CENs were toxic via a nano-specific mechanism, likely a Trojan horse mechanism. By embedding the Cu NPs in a silica shell, the

toxicity was significantly reduced compared to Cu NPs deposited on the silica surface. The embedded NPs are protected by the silica shell which leads to a decreased dissolution. Hence, it is likely the nhCu@SiO_2 CENs were less toxic due to a reduced Cu^{2+} concentration (the toxic source) inside the zebrafish. Comparatively, our Ni/SiO_2 nanomaterials toxicity is correlated with an increase in dosing of the two toxic materials. However, in this study we effectively showed that embedding the Cu NPs reduced toxicity while exposing the zebrafish to similar doses. Overall, embedding NPs in a support holds great promise when designing safer nanomaterials.

7.0 SUMMARY AND OUTLOOK

7.1 SUMMARY

In this work, we hypothesize that the design of complex engineered nanomaterials (CENs) will be instrumental in mitigating/reducing the toxicity of functional metal nanoparticles. We tested this hypothesis using a system of metal NPs combined with a non-toxic silica support NP, carefully synthesized into different configurations. The choice of the CEN design was based on catalyst materials developed by Dr. Veser's lab. These materials have potential use in the chemical industry.

The CENs physicochemical properties were rigorously characterized to understand how they influence toxicity. There was significant changes in dissolution and aggregation properties based on the materials structure, indicating a possible modulation of the toxic effects of these synthesized CENs. In order to evaluate the toxicity of the CENs we chose two alternate model systems: an *in vitro* cell culture system for mechanistic understanding of the pathway of toxicity and an *in vivo* zebrafish model for an evaluation of toxicity to a whole organism. It is important to note that the primary point of interest lies in human relevant toxicity of these NPs. Currently, no model system can completely represent human exposure, thus, it is critical to develop a thorough understanding of the interactions of the CENs with alternate model systems, which can be carefully extrapolated to predict human exposure.

7.1.1 Model systems for toxicity evaluation

By evaluating toxicity to both i*n vivo* and *in vitro* models, we can better understand the source of nanomaterials toxicity. Due to the simplicity of *in vitro* models, it is possible to identify the toxicity mechanism (including a Trojan horse mechanism). *In vivo* systems present physiologically relevancy due to the interactions between organs and cells. However, this increased complication in *in vivo* models makes it difficult to clearly identify the toxicity mechanisms. Thus, by studying the toxicity mechanism in *in vitro* systems, it is possible to gain insights into the toxicity mechanism of *in vivo* models.

We used a cell culture system to investigate the modes of cell-CEN interaction and the underlying toxicity mechanisms. Cell culture systems allow more controlled exposure, measured perturbations and investigation to facilitate the identification of the toxicity mechanism at play. Furthermore, due to the cell's small size, short experiment times, quick cell division cycle, and low cost, experiments can be run in an inexpensive, high-throughput manner. This provides a rapid, and critical, initial toxicity screening of nanomaterials. Specifically, 3T3 fibroblasts, murine skin cells, are a robust, inexpensive cell line that is a FDA standard test model for evaluating biomaterial safety. They have found wide-spread use in nanotoxicity studies. While 3T3 fibroblasts do not provide an accurate model for dermal exposure, they provide a robust and established system that allows mechanistic toxicity studies to be conducted. By utilizing 3T3 fibroblasts in our studies, we were able to understand how nano-embedding affected dissolution, which, in turn, affected toxicity.

Our study determined that the Ni/SiO_2 CENs were toxic via a Trojan horse mechanism. In this mechanism, the metal ions dissolved from the NPs incited toxicity, rather than interaction between the NP and the biological environment. Thus, the safest nanomaterial has minimal

intracellular ion dissolution. This was accomplished by embedding the metal NP into the silica shell. Furthermore, we were able to extrapolate this observation and design an even safer nanomaterial by increasing the shell thickness around the embedded NP. This increase in shell thickness slowed the ion dissolution further and eliminated toxicity to the 3T3 fibroblasts.

For an *in vivo* model we chose zebrafish as a well-characterized model of invertebrate organism. Zebrafish (*Danio rerio*) provide a rapid, inexpensive, high-throughput and well-characterized model to evaluate the toxicity of chemical structures in a vertebrate organism *in vivo*[110,139,140]. The zebrafish shares a common basic body plan with other vertebrates, including mammals, and many molecular mechanisms governing early embryogenesis are also shared[142-144]. Additionally, zebrafish are able to provide insights into the harmful effects of industrial discharges on aquatic life. In view of these advantages, zebrafish are already used to test the toxicity of chemicals and drugs[141,147-149]. Compared to other vertebrate models, zebrafish studies offer low cost[165], and high throughput toxicity screening assays. While zebrafish can offer insights into the teratogenic potential of test compounds in humans, it lacks human relevancy compared to other vertebrate model available for toxicity screening. Furthermore, the mode of exposure to the NP will likely be different in zebrafish as compared to human.

Our results showed that the CEN toxicity ranking was dependent on the zebrafish assay used. This was because the experimental aquatic system greatly affected the nanomaterials' aggregate size. This change in aggregate size modified the CENs settling rate which modified CEN exposure to the zebrafishes. Overall, this change in zebrafish exposure made it difficult to elucidate how the Ni NP embedding affected toxicity. However, it exhibited the critical need to understand and characterize the nanomaterials in their test environment.

The Ni/SiO_2 CENs exhibited a low toxicity and would be classified as "practically nontoxic" by the U.S. EPA guidelines[237]. Thus, while the Ni NPs acted as an excellent model for systematically studying the effect embedding had on toxicity, these nanomaterials are a low risk material. Occupational exposure limits for nickel and nickel compounds in the United States have been set from 0.007-1.5 mg Ni/m^3, depending on the regulatory body and material type[238,239]. However, there have been past exposures to Ni materials from 3.5-382 mg Ni/m^3 [240,241]. Our tested concentration in both the *in vivo* and *in vitro* work are well above the permissible occupational exposure limits and exposures that would be expected. However, it was necessary to use these concentrations to study the effect nanoconfiguration had on toxicity.

The changes in Ni/SiO_2 CEN settling behavior (and hence zebrafish exposure) was due to the high concentrations used in the experiments. Thus, we moved to a more toxic material, copper. Using this material we were able to probe the effect NP embedding had on toxicity, while maintaining similar zebrafish exposure to the CENs. For all tested toxicity assays, the Cu NPs embedded in the silica showed a lower toxicity than the Cu NPs deposited on the surface of the silica NP. At this point, we do not have a clear proof for the origin of the toxicity of this material. However, given our prior results with Ni-based nanomaterials (discussed above), and prior evidence in the literature[176,226,227,242], we hypothesize that the observed toxicity is again due to metal dissolution. Hence, changes in Cu dissolution, due to the CEN structure, led to changes in toxicity.

Overall, Cu NPs pose a potential risk to human health due to their widespread use in consumer products and elevated toxicity. Cu NPs and our $Cu\text{-}SiO_2$ CENs would be classified as "moderately toxic" by the U.S EPA guidelines. Interestingly, the structure that embedded the Cu NPs in the silica shell would be classified as "slightly toxic" by the U.S. EPA guidelines. Thus,

we were able to actually change the toxicity classification by embedding the Cu NP in the silica NP. The occupational exposure limits for copper are 1 mg/m^3. However, there have been few reports to date determining the actual environmental and occupational exposure to copper and copper oxide NPs. However, the widespread use of Cu NPs in many fields, combined with its toxic behavior, suggests that this nanomaterial has potential health concerns in the future.

Humans are most likely to be exposed to nanomaterials via inhalation or dermal pathway[95]. Thus, both of our tested toxicity models are not well-suited for studying the toxicity linked to specific exposure pathways. Rather, our studies provided toxicity results in a high-throughput manner that can be used to prioritize further toxicity tests. While other vertebrate models, like rats and mice, may be a more relevant toxicity model, in terms of both human relevancy and modeling possible NP exposure, than our tested models, they still have their limitations. These limitations include the studies' high cost, low-throughput nature, long experiment times and the possibility of false negatives results due to the nature of the experiments[243]. Overall, there is no perfect toxicity model. There is a trade-off between human relevancy with high-throughput toxicity screening. Thus, there is a need to understand how different models can be utilized to carefully and thoroughly screen for nanomaterials' toxicity. By initially screening for nanomaterials toxicity with high-throughput models (e.g. cell or zebrafish models), potential hazardous nanomaterials can be identified and screened with higher cost, more relevant models (like mice or rats). Thus, we would eliminate the need to use expensive, long term studies on every nanomaterial that has a potential risk to human health.

7.1.2 Safer nanomaterials

Many comprehensive nanotoxocity studies suggest that soluble metal/metal oxide NPs are toxic via a Trojan horse mechanism[29,30,65,120,229,244,245]. The NP acts as a delivery vehicle to the cell or organ. Once delivered, the NP releases ions which cause toxicity. Thus, the observed toxicity is due to the metal ions, and not related to direct interactions between the metal NP and the biological environment. Agreeing with these previous reports, the observations in our studies can be explained through dissolution-mediated toxicity. Our Ni/SiO_2 CENs were clearly toxic to the 3T3 fibroblasts via a Trojan horse mechanism: The intracellular Ni^{2+} concentration directly correlated with toxicity. Furthermore, we hypothesize that the CENs are toxic to the zebrafish via a Trojan horse mechanism. By embedding the NP in the silica shell, we slowed the ion dissolution within the zebrafish which led to a reduction in toxicity.

Clearly, we can see that when designing safer metal/metal oxide nanomaterials, it is imperative to minimize the ion dissolution. While a specific design may ensure a lower toxicity, it may, in turn, mitigate the NPs' functionality. Hence, the newly designed "safer" nanomaterial would not be a potential alternate. However, if a nanomaterial is designed for optimal functionality, there may be an elevated toxicity that leads to the product being discontinued in future applications. For example, our group has previously studied the Ni/SiO_2 CENs for multiple industrial applications including catalytic partial oxidation of methane (CPOM) and CO methanation[246]. These results show that the embedded CENs lead to better conversion than the surface deposited CENs. Thus, for this specific application, the safest nanomaterials actually represents the CEN that has optimized performance and functionality. In contrast, often the functionality for Cu NPs is related to the dissolved Cu^{2+}. The dissolved Cu^{2+} from the NP provides antifungal and bacteriostatic properties that are used in water treatment, antifouling

coatings by the paint industry and implant coatings[247-250]. However, this is also the source of toxicity. Thus, if a safer nanomaterial is designed by reducing Cu^{2+} dissolution, the NPs functionality may be hampered.

Overall, when designing safer nanomaterials, we need to find a balance between safety and functionality. This will require research, reiteration and collaboration from both the toxicologist and product/industry designers to understand how to accomplish this. This is a complicated problem, and requires thorough understanding of both the nanomaterials use and potential toxicity. Identifying the potential toxicity though is beyond studying the toxicity on a single cell line or model. It includes identifying the at-risk population to determine the correct models to use for toxicity screening.

In this work, we studied the effect embedding had on dissolution (and thus toxicity). However, there are other methods to stabilize the metal NP and reduce dissolution. These other potential methods include doping, alloying with another active metal NP, or binding to a support with strong metal-support interactions. Systematic studies will need to be conducted to determine which methods are efficient at reducing dissolution for specific metal NPs. Furthermore, the ion dissolution behavior needs to be considered for different test mediums. This includes characterizing the NP's ion dissolution in medium with organic substances to mimic aqueous exposures, medium supplemented with proteins to mimic biological fluids, and medium with an acidic pH to mimic lysosomes (an organelle that nanomaterials are often taken up through). By understanding how the NPs act in these media, we can begin to design nanomaterials that reduce dissolution.

7.2 OUTLOOK

7.2.1 Applying structure-toxicity correlations to other CENs

Our studies indicated that dissolved Ni^{2+}, rather than the NP itself, is the likely toxic source for Ni NPs. Hence, this structure-toxicity correlation could be expanded to other Ni complex engineered nanomaterials by alloying or doping. Ni is often alloyed with other metals, i.e. NiFe alloys used in catalytic and electromagnetic applications[61,251-253], and by systematically studying the effect of alloying, a safe structure may be determined that minimizes Ni^{2+} dissolution while still providing functionality. Furthermore, doping could be used to stabilize the NP and reduce dissolution while possibly not interfering with functionality.

7.2.2 Metal-support interactions

Metal NPs are often immobilized on oxide supports to protect against sintering and deactivation. These NP-support interactions affect the NPs activity by altering their morphology and electronic structure[254-257]. The support has shown to greatly influence a reactions' products, stability, conversion and yield[72,258-260]. These changes in NP properties, due to the support, can be expected to also influence the nanomaterials toxicity.

In the present dissertation we studied the toxicity associated with metal NPs on an inert amorphous SiO_2 support. Future work can study the toxicity associated with metal NP on different supports. By rationally changing the support, structure-toxicity correlations can be designed based on the adhesion energy between the support and NP[261]. This would including how the support influences physicochemical characteristics (ion dissolution, aggregation,

settling). By taking a systematic approach, we will be able to understand how a NPs support can influence toxicity. These correlations can be used to rationally design nanomaterials while still maintaining functionality.

Moreover, CeO_2 NPs are widely used in catalytic applications as a support due to their reducible nature[72,251,262-265]. They stabilize NPs at high temperature and provide better reactivity and conversion. In addition, CeO_2 NPs have found widespread use in biological applications including neurodegenerative disease regenerability[266], as an anti-inflammatory agent[267], and for cancer treatment[268]. Due to CeO_2 NPs ability to transition between the Ce^{3+} and Ce^{4+} oxidative states, the NPs have shown to actually protect cells from reactive oxygen species (ROS)[269-273]. Metal NPs have been shown to be toxic due generation of ROS[90,97,242,244,274-278]. Hence, by utilizing CeO_2 as a support, it is possible the CeO_2 NP could protectant against the ROS generated by the metal NP. Thus, the support NP may be able to counter the active metal NP's toxicity. Therefore, in future work, it would be interesting to investigate if toxicity can be mitigated by coupling a protective NP with a toxic ROS-generating NP.

7.2.3 Cell ability to recover from nanomaterial toxicity

In Chapters 2.0 and 3.0 , we showed that the Ni/SiO_2 CENs were toxic to 3T3 fibroblasts via a Trojan horse mechanism. Moreover, the localization of the Ni^{2+} inside the lysosomes led to a decrease in toxicity compared to a Ni^{2+} salt. However, not every exposure to nanomaterials is expected to be a constant exposure. Rather, we expect there to be a short exposure, followed by removal of the NPs (i.e. removed sunscreen loaded with ZnO NPs, took off socks using Ag NPs to wash). However there is a possibility the NP toxicity will persist. In preliminary studies, when the Ni^{2+} salt was removed, the cell was able to recover and return to normal metabolic activities

(Figure 49). However, in the presence of the nhNi@SiO_2 CEN, even though the toxin is removed and the cell is not taking up more CENs, the existing CEN is still localized in the cell and is continuing to shed ions, leading to a further reduction in toxicity (Figure 50). Thus, the exposure is persisting inside the cells are not expected to recover from this toxicity. Hence, in future work, it is important to study how this toxicity mechanism persists and design nanomaterials that are not only safe during exposures, but have limited persistency after the exposure is removed.

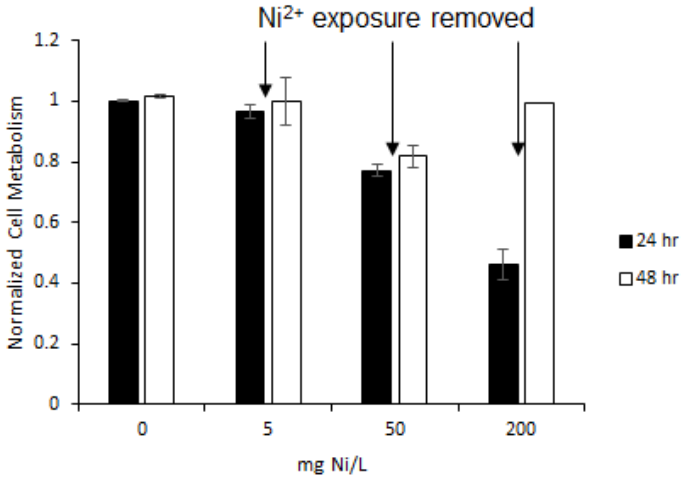

Figure 49. Cell metabolism (normalized to control at 24 hour) for 24 hour after exposure to 0-200 mg Ni/L $NiCl_2$. At 24 hours the media with $NiCl_2$ was replaced with 3T3 media with no toxins. The cell metabolism for 48 hour after a 24 hour recovery period is also presented.

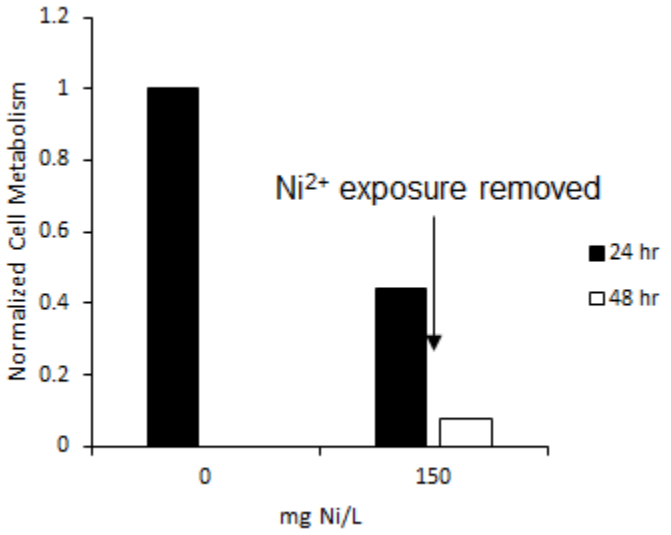

Figure 50. Cell metabolism (normalized to control at 24 hour) for 24 hour after exposure to 150 mg Ni/L nhNi@SiO_2. At 24 hours the media with nhNi@SiO_2 was replaced with 3T3 media with no toxins. The cell metabolism for 48 hour after a 24 hour recovery period is also presented.

7.2.4 Location of CENs in the zebrafish

In Chapter 4.0 , 5.0 and 6.0 , there were drastic toxicity differences to the zebrafish based on the surface termination (silica vs metal). We hypothesize that the different surface chemistries could lead to different uptake and translocation in the organism. Hence, we propose in the future to use fluorescently tagged CENs to aid in determining how the surface chemistry influences the location of the CENs in the zebrafish. Figure 51 shows fluorescently tagged Ni/SiO_2 CENs in the zebrafish after a four day exposure. The Ni-SiO_2 CENs are shown to be clearly located in the liver, while there is no presence of the nhNi@SiO_2 CEN in the zebrafish, suggesting a difference in accumulation based on the surface chemistries. This differences in translocation in the zebrafish may also be metal-dependent. Hence it would be crucial to study the location of the

CENs using multiple metals deposited on silica, in addition to embedded within silica. This will aid in gaining further insights into how to further design safer nanomaterials that aim for clearance pathways versus organs that accumulate NPs.

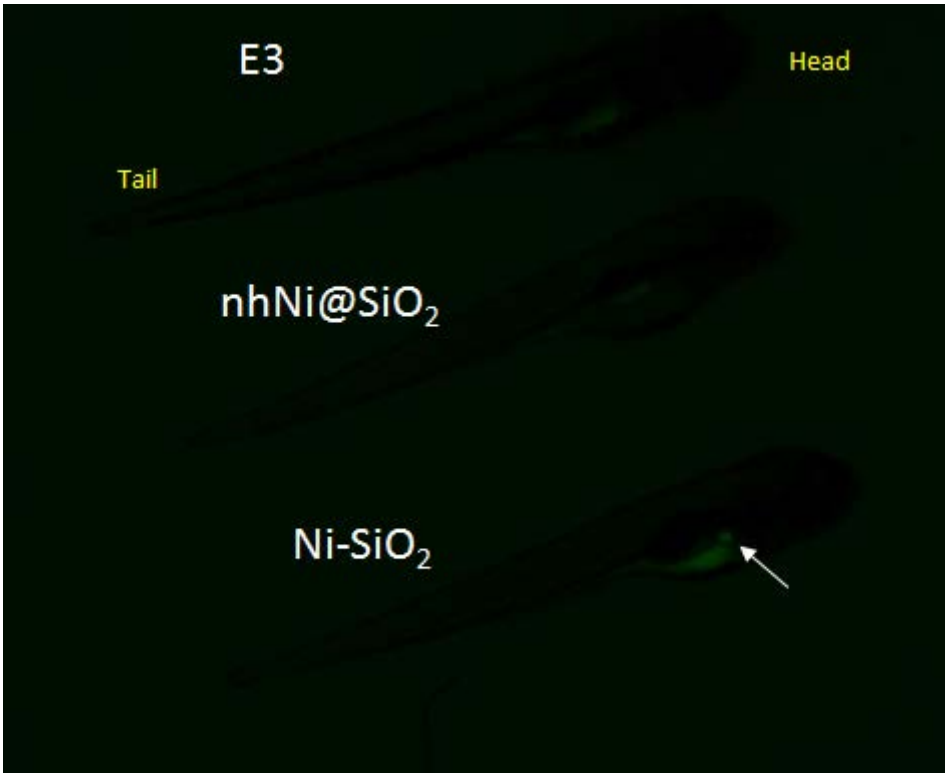

Figure 51. Fluorescent images of 24hpf zebrafish exposed to 200 mg Ni/L fluorescently tagged nhNi@SiO_2 or Ni-SiO_2 CENs for four days. The arrow indicates the liver and the presence of Ni-SiO_2 CENs in the liver.

APPENDIX

SUPPROTING INFORMATION

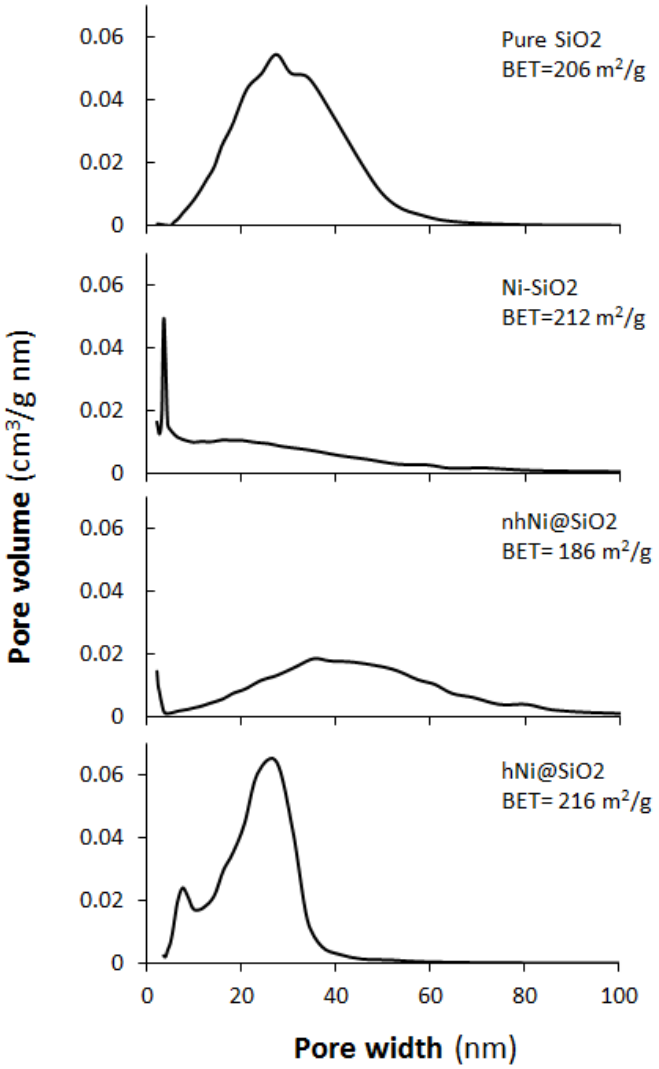

Figure 52. BET surface area and porosity for SiO_2, Ni-SiO_2, nhNi@SiO_2, hNi@SiO_2.

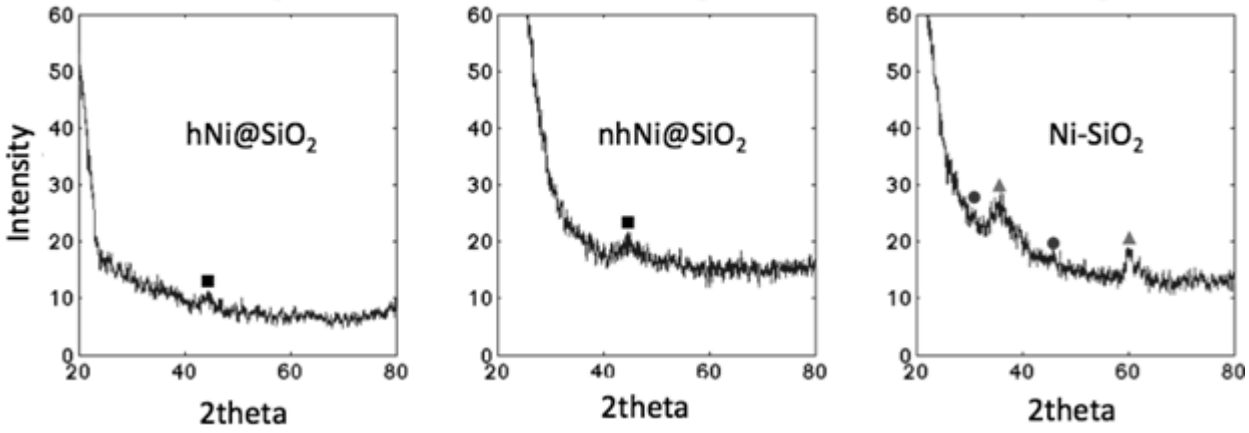

Figure 53. X-ray diffraction patterns of $hNi@SiO_2$, $nhNi@SiO_2$, and $Ni\text{-}SiO_2$. Square=Ni (04-0850), circle=NiO (78-0643), triangle=$NiSiO_3$ (43-00664).

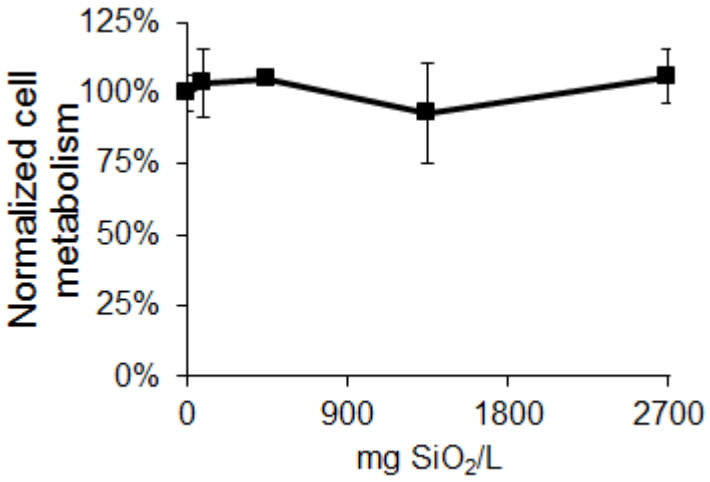

Figure 54. Cell metabolism (normalized to control) after exposure to 0-2700 mg SiO_2/L for 24 hours.

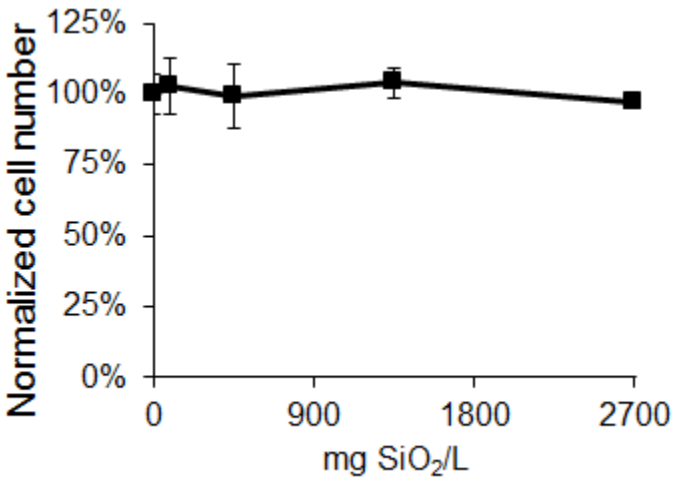

Figure 55. Cell number (normalized to control) after exposure to 0-2700 mg SiO_2/L for 24 hours.

The cell viability was analyzed by the LIVE/DEAD assay. Metabolically active cells convert calcein-AM to calcein, which fluoresces green. Ethidium homodimer-1 diffuses into dead cells, due to a compromised cell membrane, and fluoresces red. There were few apoptotic cells on the bottom of the well, as the cells no longer adhere to the well upon death. Figure 56 shows the LIVE/DEAD images after a 24 hour exposure to the Ni materials. The control condition consisted of predominantly viable cells. After exposure to $NiCl_2$, the cell number decreased as Ni concentration increased. The same trend was observed as the quantitative cell viability results: Ni-SiO_2 was the most toxic CEN and incurred the highest cell death, while the nhNi@SiO_2 CEN was the least toxic CEN with the lowest cell death. Overall, the trend is similar to the quantitative cell viability results.

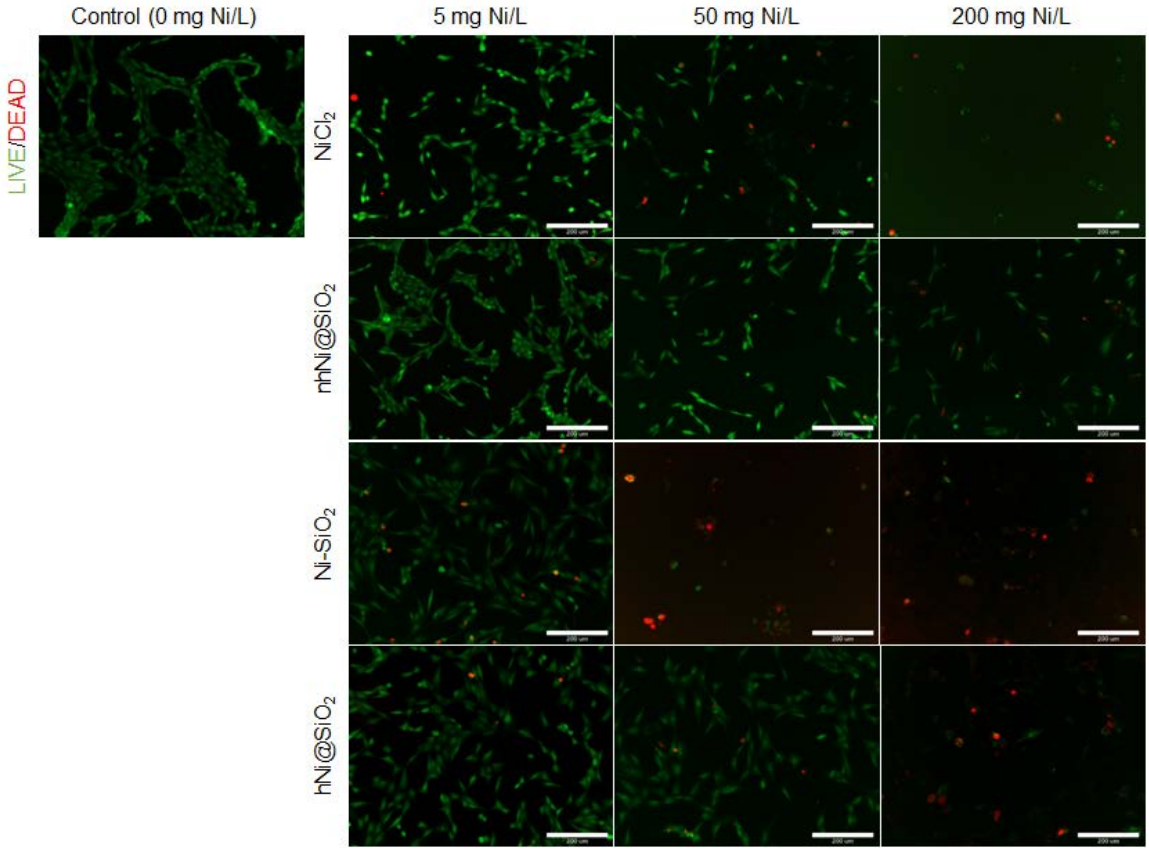

Figure 56. LIVE/DEAD images of 3T3 fibroblasts after 24 hour exposure to 0, 5, 50 and 200 mg Ni/L Ni materials.

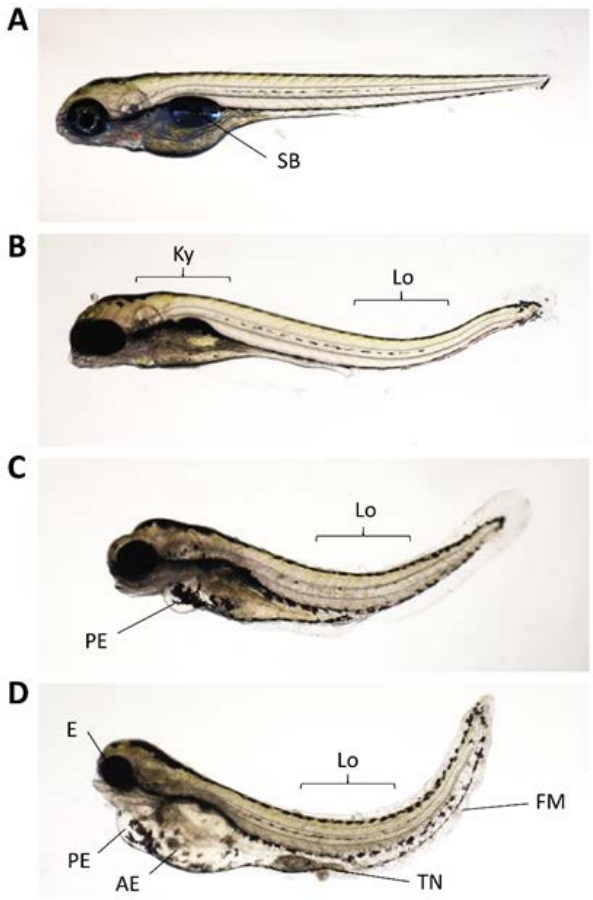

Figure 57. $NiCl_2$-induced developmental malformations. Examples are shown of zebrafish larval malformations present at 5 dpf, following exposure to $NiCl_2$ (50 mg Ni/L) for 4 days. A. Control, healthy zebrafish with normal morphology, including swim bladder (SB) formation. B. Zebrafish with abnormal spinal curvature including kyphotic (Ky) and lordotic (Lo) deformities. C. Zebrafish with more prominent lordosis (Lo) and pericardial edema (PE) D. Zebrafish with severe lordosis (Lo), pericardial edema (PE) abdominal edema (AE), tissue necrosis (TN), abnormal fin morphology (FM) and small eyes (E). Note panels B-D show failure of swim bladder formation; C and D also show shortened body length. C also shows lateral spinal curvature (scoliosis) seen as the caudal extremity of the body being out of the plane of focus of the micrograph.

Table 7. Frequency of malformations following developmental $NiCl_2$ exposure. The table shows the frequency (mean ± standard deviation) of abnormal spinal curvature, abdominal edema and pericardial edema after exposure to 50, 100 and 200 mg Ni/L $NiCl_2$ and CENs. Each individual zebrafish larva could show more than one malformation and all were recorded. The malformation rate was normalized to the number of surviving zebrafish. Note: after exposure to 100 and 200 mg Ni/L Ni-SiO_2 zebrafish developed no malformations.

Material/Concentration		Abnormal spinal curvature	Abdominal edema (AE)	Pericardial edema (PE)
Control	0 mg Ni/L	1.2± 1.1%	0 ± 0.0%	0± 0.0%
$NiCl_2$	50 mg Ni/L	58.3± 3.1%	13.7± 4.7%	48.0± 4.0%
	100 mg Ni/L	37.3± 2.5%	16.6± 2.6%	33.7± 5.1%
	200 mg Ni/L	66.3± 3.9%	35.3± 5.5%	62.7± 2.9%
Ni-SiO_2	50 mg Ni/L	2.8± 1.5%	0.3± 0.1%	0.3± 0.1%
	100 mg Ni/L	0± 0.1%	0± 0.0%	0± 0.0%
	200 mg Ni/L	0± 0.0%	0± 0.0%	0± 0.0%
nhNi@SiO_2	50 mg Ni/L	4.5± 3.8%	1.0± 0.5%	0.8± 0.1%
	100 mg Ni/L	4.8± 4.1%	0.6± 0.1%	0.6± 0.1%
	200 mg Ni/L	5.7± 6.2%	1.1± 1.0%	0.5± 0.3%
hNi@SiO_2	50 mg Ni/L	4.7± 5.1%	0.5± 0.1%	0.4± 0.1%
	100 mg Ni/L	2.5± 2.2%	0.2± 0.1%	0.2± 0.2%
	200 mg Ni/L	3.3± 1.6%	0.3± 0.2%	0.4± 0.2%

Detailed Mean Velocity

$NiCl_2$ salt: A non-monotonic, inverted, u-shaped concentration/mean velocity relationship was observed in (Figure 26A). Up to 100 mg/L, mean velocity increased with $NiCl_2$ concentration: 0 mg Ni/L: 0.895 ± 0.06 mm/s; 5 mg Ni/L: 1.32 ± 0.10 mm/s p=0.004; 10 mg Ni/L: 1.33 ± 0.09 mm/s p=0.006; 100 mg Ni/L: 1.49 ± 0.20 mm/s p=0.003; 150 mg Ni/L: 1.35 ± 0.13 mm/s p=0.032. At higher concentrations, $NiCl_2$ caused a decline in mean velocity below baseline measurements: 300 mg Ni/L: 0.46 ± 0.15 mm/s p=0.020; p is one ANOVA followed by Dunnett's test.

Ni-SiO_2: A monotonic increase in mean velocity was observed over the entire concentration range (Figure 26B): 0 mg Ni/L: 0.851 ± 0.12 mm/s; 10 mg Ni/L: 1.08 ± 0.17 mm/s p=0.801; 50 mg Ni/L: 1.32 ± 0.19 mm/s p=0.122; 100 mg Ni/L: 1.58 ± 0.34 mm/s p=0.081; 200 mg Ni/L: 1.90 ± 0.18 mm/s p=0.001; p is one-way ANOVA followed by Dunnett's test.

nhNi@SiO_2: No effect on mean velocity was observed over the entire concentration range tested (Figure 26C): 0 mg Ni/L: 0.937 ± 0.10 mm/s; 10 mg Ni/L: 0.860 ± 0.14 mm/s; 50 mg Ni/L: 1.14 ± 0.11 mm/s; 100 mg Ni/L: 0.85 ± 0.11 mm/s; 200 mg Ni/L: 0.99 ± 0.12 mm/s, p= 0.83; p is one-way ANOVA.

hNi@SiO_2: A mean velocity increase was observed up to a concentration of 100 mg/L (Figure 26D): 0 mg Ni/L: 0.950 ± 0.09 mm/s; 10 mg Ni/L: 1.45 ± 0.20 mm/s p=0.261; 50 mg Ni/L: 1.71 ± 0.31 mm/s p=0.032, 100 mg Ni/L: 1.77 ± 0.19 mm/s, p=0.042. At higher concentrations, mean velocity decreased towards baseline values: 200 mg Ni/L: 1.39 ± 0.20 mm/s p=0.264; p is one-way ANOVA followed by Dunnett's test.

BIBLIOGRAPHY

1. Nel A, Xia T, Mädler L, Li N. Toxic potential of materials at the nanolevel. *Science.* 2006;311(5761):622-627.

2. Casals E, Gonzalez E, Puntes V. Reactivity of inorganic nanoparticles in biological environments: insights into nanotoxicity mechanisms. *Journal of Physics D: Applied Physics.* 2012;45(44):443001.

3. Shukla R, Bansal V, Chaudhary M, Basu A, Bhonde RR, Sastry M. Biocompatibility of gold nanoparticles and their endocytotic fate inside the cellular compartment: a microscopic overview. *Langmuir.* 2005;21(23):10644-10654.

4. Shukla S, Priscilla A, Banerjee M, et al. Porous gold nanospheres by controlled transmetalation reaction: a novel material for application in cell imaging. *Chemistry of materials.* 2005;17(20):5000-5005.

5. Chen J, Saeki F, Wiley BJ, et al. Gold nanocages: bioconjugation and their potential use as optical imaging contrast agents. *Nano letters.* 2005;5(3):473-477.

6. Biella S, Prati L, Rossi M. Selective oxidation of D-glucose on gold catalyst. *Journal of catalysis.* 2002;206(2):242-247.

7. Ma Z, Dai S. Design of novel structured gold nanocatalysts. *Acs Catalysis.* 2011;1(7):805-818.

8. Nath N, Chilkoti A. A colorimetric gold nanoparticle sensor to interrogate biomolecular interactions in real time on a surface. *Analytical chemistry.* 2002;74(3):504-509.

9. Kim Y, Johnson RC, Hupp JT. Gold nanoparticle-based sensing of “spectroscopically silent” heavy metal ions. *Nano Letters.* 2001;1(4):165-167.

10. Tong S, Zhang C, Jiang C, et al. Improvement in the hole collection of polymer solar cells by utilizing gold nanoparticle buffer layer. *Chemical Physics Letters.* 2008;453(1):73-76.

11. Su Y-H, Ke Y-F, Cai S-L, Yao Q-Y. Surface plasmon resonance of layer-by-layer gold nanoparticles induced photoelectric current in environmentally-friendly plasmon-sensitized solar cell. *Light: Science & Applications.* 2012;1(6):e14.

12. Tian Y, Tatsuma T. Mechanisms and applications of plasmon-induced charge separation at TiO2 films loaded with gold nanoparticles. *Journal of the American Chemical Society.* 2005;127(20):7632-7637.

13. Luo J, Wang L, Mott D, et al. Core/shell nanoparticles as electrocatalysts for fuel cell reactions. *Advanced Materials.* 2008;20(22):4342-4347.

14. Roco MC. The long view of nanotechnology development: the National Nanotechnology Initiative at 10 years. *Nanotechnology Research Directions for Societal Needs in 2020*: Springer; 2011:1-28.

15. Oberdoester G. Nanotoxicology: An Emerging Discipline Evolving from Studies of Ultrafine Particles (vol 113, pg 823, 2005). *Environmental Health Perspectives.* 2010;118(9):A380-A380.

16. Buzea C, Pacheco II, Robbie K. Nanomaterials and nanoparticles: sources and toxicity. *Biointerphases.* 2007;2(4):MR17-MR71.

17. Li Y, Li J, Yin J, et al. Systematic influence induced by 3 nm titanium dioxide following intratracheal instillation of mice. *Journal of nanoscience and nanotechnology.* 2010;10(12):8544-8549.

18. Wang J, Zhou G, Chen C, et al. Acute toxicity and biodistribution of different sized titanium dioxide particles in mice after oral administration. *Toxicology letters.* 2007;168(2):176-185.

19. Wang J, Liu Y, Jiao F, et al. Time-dependent translocation and potential impairment on central nervous system by intranasally instilled TiO 2 nanoparticles. *Toxicology.* 2008;254(1):82-90.

20. He X, Zhang H, Ma Y, et al. Lung deposition and extrapulmonary translocation of nano-ceria after intratracheal instillation. *Nanotechnology.* 2010;21(28):285103.

21. Hirst SM, Karakoti A, Singh S, et al. Bio-distribution and in vivo antioxidant effects of cerium oxide nanoparticles in mice. *Environmental toxicology.* 2013;28(2):107-118.

22. Agency UEP. Research on Nanomaterials. 2016; https://www.epa.gov/chemical-research/research-nanomaterials. Accessed 09/27/2016, 2016.

23. Agency UEP. Control of Nanoscale Materials under the Toxic Substances Control Act. 2016; https://www.epa.gov/reviewing-new-chemicals-under-toxic-substances-control-act-tsca/control-nanoscale-materials-under. Accessed 09/27/2016, 2016.

24. OECD. OECD Guidelines for the Testing of Chemicals. 2013; http://www.oecd-ilibrary.org/content/package/chem_guide_pkg-en. Accessed 10/13/2016, 2016.

25. NIST. Assessing the Environmental, Health and Safety Impact of Nanoparticles. 2016; https://www.nist.gov/sites/default/files/documents/mml/bbd/cell_systems/16k_bio.pdf. Accessed 10/13/2016, 2016.

26. International A. *Annual book of ASTM standards.* ASTM International; 2004.

27. Hanna S, Cooksey G, Dong S, et al. Feasibility of using a standardized Caenorhabditis elegans toxicity test to assess nanomaterial toxicity. *Environmental Science: Nano.* 2016.

28. Oberdörster G, Maynard A, Donaldson K, et al. Principles for characterizing the potential human health effects from exposure to nanomaterials: elements of a screening strategy. *Particle and fibre toxicology.* 2005;2(1):8.

29. Ortega R, Bresson C, Darolles C, et al. Low-solubility particles and a Trojan-horse type mechanism of toxicity: the case of cobalt oxide on human lung cells. *Particle and fibre toxicology.* 2014;11(1):14.

30. Park E-J, Yi J, Kim Y, Choi K, Park K. Silver nanoparticles induce cytotoxicity by a Trojan-horse type mechanism. *Toxicology in Vitro.* 2010;24(3):872-878.

31. Aruoja V, Dubourguier H-C, Kasemets K, Kahru A. Toxicity of nanoparticles of CuO, ZnO and TiO 2 to microalgae Pseudokirchneriella subcapitata. *Science of the total environment.* 2009;407(4):1461-1468.

32. Kasemets K, Ivask A, Dubourguier H-C, Kahru A. Toxicity of nanoparticles of ZnO, CuO and TiO 2 to yeast Saccharomyces cerevisiae. *Toxicology in vitro.* 2009;23(6):1116-1122.

33. Xiong D, Fang T, Yu L, Sima X, Zhu W. Effects of nano-scale TiO2, ZnO and their bulk counterparts on zebrafish: Acute toxicity, oxidative stress and oxidative damage. *Science of the Total Environment.* 2011;409(8):1444-1452.

34. Zhu X, Wang J, Zhang X, Chang Y, Chen Y. The impact of ZnO nanoparticle aggregates on the embryonic development of zebrafish (Danio rerio). *Nanotechnology.* 2009;20(19).

35. Bondarenko O, Juganson K, Ivask A, Kasemets K, Mortimer M, Kahru A. Toxicity of Ag, CuO and ZnO nanoparticles to selected environmentally relevant test organisms and mammalian cells in vitro: a critical review. *Archives of toxicology.* 2013;87(7):1181-1200.

36. Morones JR, Elechiguerra JL, Camacho A, et al. The bactericidal effect of silver nanoparticles. *Nanotechnology.* 2005;16(10):2346.

37. Emam HE, Manian AP, Široká B, et al. Treatments to impart antimicrobial activity to clothing and household cellulosic-textiles–why "Nano"-silver? *Journal of Cleaner Production.* 2013;39:17-23.

38. Duran N, Marcato PD, De Souza GI, Alves OL, Esposito E. Antibacterial effect of silver nanoparticles produced by fungal process on textile fabrics and their effluent treatment. *Journal of biomedical nanotechnology.* 2007;3(2):203-208.

39. Samuel U, Guggenbichler J. Prevention of catheter-related infections: the potential of a new nano-silver impregnated catheter. *International Journal of Antimicrobial Agents.* 2004;23:75-78.

40. Jaroenworaluck A, Sunsaneeyametha W, Kosachan N, Stevens R. Characteristics of silica-coated TiO2 and its UV absorption for sunscreen cosmetic applications. *Surface and Interface Analysis.* 2006;38(4):473-477.

41. Popov A, Priezzhev A, Lademann J, Myllylä R. TiO2 nanoparticles as an effective UV-B radiation skin-protective compound in sunscreens. *Journal of Physics D: Applied Physics.* 2005;38(15):2564.

42. Smijs TG, Pavel S. Titanium dioxide and zinc oxide nanoparticles in sunscreens: focus on their safety and effectiveness. *Nanotechnol Sci Appl.* 2011;4(4):95-112.

43. Osmond MJ, Mccall MJ. Zinc oxide nanoparticles in modern sunscreens: an analysis of potential exposure and hazard. *Nanotoxicology.* 2010;4(1):15-41.

44. Kathirvelu S, D'souza L, Dhurai B. UV protection finishing of textiles using ZnO nanoparticles. *Indian Journal of Fibre & Textile Research.* 2009;34(9):267-273.

45. Rai M, Ingle A. Role of nanotechnology in agriculture with special reference to management of insect pests. *Applied microbiology and biotechnology.* 2012;94(2):287-293.

46. CDPR. (California Department of Pesticide Regulation) CDPR Database. 2016; http://apps.cdpr.ca.gov/cgi-bin/label/labq.pl?p_chem=175&activeonly=on. Accessed 10/13/2016, 2016.

47. Kiaune L, Singhasemanon N. Pesticidal copper (I) oxide: environmental fate and aquatic toxicity. *Reviews of Environmental Contamination and Toxicology Volume 213*: Springer; 2011:1-26.

48. Taghiyari HR, Moradi-Malek B, Kookandeh MG, Bibalan OF. Effects of silver and copper nanoparticles in particleboard to control Trametes versicolor fungus. *International Biodeterioration & Biodegradation.* 2014;94:69-72.

49. Matsunaga H, Kiguchi M, Evans P. Micro-distribution of metals in wood treated with a nano-copper wood preservative. Paper presented at: Proceedings International Research Group on Wood Protection Annual Meeting, IRG/WP2007.

50. Civardi C, Schwarze FW, Wick P. Micronized copper wood preservatives: An efficiency and potential health risk assessment for copper-based nanoparticles. *Environmental Pollution.* 2015;200:126-132.

51. Cioffi N, Ditaranto N, Torsi L, et al. Synthesis, analytical characterization and bioactivity of Ag and Cu nanoparticles embedded in poly-vinyl-methyl-ketone films. *Analytical and bioanalytical chemistry.* 2005;382(8):1912-1918.

52. Borkow G, Gabbay J. Putting copper into action: copper-impregnated products with potent biocidal activities. *The FASEB journal.* 2004;18(14):1728-1730.

53. Borkow G, Zatcoff RC, Gabbay J. Reducing the risk of skin pathologies in diabetics by using copper impregnated socks. *Medical hypotheses.* 2009;73(6):883-886.

54. Gabbay J, Borkow G, Mishal J, Magen E, Zatcoff R, Shemer-Avni Y. Copper oxide impregnated textiles with potent biocidal activities. *Journal of Industrial Textiles.* 2006;35(4):323-335.

55. Ren G, Hu D, Cheng EW, Vargas-Reus MA, Reip P, Allaker RP. Characterisation of copper oxide nanoparticles for antimicrobial applications. *International journal of antimicrobial agents.* 2009;33(6):587-590.

56. Bernstein M. Eliminating water-borne bacteria with pages from The Drinkable Book could save lives. *ACS.* 08/16/2015, 2015.

57. Liu X, Gurel V, Morris D, et al. Bioavailability of Nickel in Single-Wall Carbon Nanotubes. *Advanced Materials.* 2007;19(19):2790-2796.

58. Moisala A, Nasibulin AG, Kauppinen EI. The role of metal nanoparticles in the catalytic production of single-walled carbon nanotubes—a review. *Journal of Physics: condensed matter.* 2003;15(42):S3011.

59. Meyyappan M, Delzeit L, Cassell A, Hash D. Carbon nanotube growth by PECVD: a review. *Plasma Sources Science and Technology.* 2003;12(2):205.

60. Leite E, Carreño N, Longo E, Valentini A, Probst L. Synthesis of mesoporous silica with embedded nickel nanoparticles for catalyst applications. *Journal of nanoscience and nanotechnology.* 2002;2(1):89-94.

61. Bhavsar S, Najera M, Solunke R, Veser G. Chemical looping: To combustion and beyond. *Catalysis Today.* 2014;228:96-105.

62. Group TW. *The importance of nickel compounds: catalysts.* European Nickel Institute; 08/12/2015 2007.

63. Rostrup-Nielsen JR, Sehested J, Nørskov JK. Hydrogen and synthesis gas by steam-and C0 2 reforming. *Advances in catalysis.* 2002;47:65-139.

64. Chou K, Chang S, Huang K. Study on the characteristics of nanosized nickel particles using sodium borohydride to promote conversion. *ADVANCES IN TECHNOLOGY OF MATERIALS AND MATERIALS PROCESSING JOURNAL.* 2006;8(2):172.

65. Magaye R, Zhao J, Bowman L, Ding M. Genotoxicity and carcinogenicity of cobalt-, nickel-and copper-based nanoparticles (Review). *Experimental and therapeutic medicine.* 2012;4(4):551-561.

66. Ispas C, Andreescu D, Patel A, Goia DV, Andreescu S, Wallace KN. Toxicity and Developmental Defects of Different Sizes and Shape Nickel Nanoparticles in Zebrafish. *Environmental Science & Technology.* 2009;43(16):6349-6356.

67. Selim AA, Al-Sunaidi A, Tabet N. Effect of the surface texture and crystallinity of ZnO nanoparticles on their toxicity. *Materials Science & Engineering C-Materials for Biological Applications.* 2012;32(8):2356-2360.

68. Powers CM, Slotkin TA, Seidler FJ, Badireddy AR, Padilla S. Silver nanoparticles alter zebrafish development and larval behavior: distinct roles for particle size, coating and composition. *Neurotoxicology and teratology.* 2011;33(6):708-714.

69. Safi M, Sarrouj H, Sandre O, Mignet N, Berret J-F. Interactions between sub-10-nm iron and cerium oxide nanoparticles and 3T3 fibroblasts: the role of the coating and aggregation state. *Nanotechnology.* 2010;21(14):145103.

70. Hang MN, Gunsolus IL, Wayland H, et al. Impact of Nanoscale Lithium Nickel Manganese Cobalt Oxide (NMC) on the Bacterium Shewanella oneidensis MR-1. *Chemistry of Materials.* 2016;28(4):1092-1100.

71. Baek Y-W, An Y-J. Microbial toxicity of metal oxide nanoparticles (CuO, NiO, ZnO, and Sb 2 O 3) to Escherichia coli, Bacillus subtilis, and Streptococcus aureus. *Science of the total environment.* 2011;409(8):1603-1608.

72. Cao A, Lu R, Veser G. Stabilizing metal nanoparticles for heterogeneous catalysis. *Physical Chemistry Chemical Physics.* 2010;12(41):13499-13510.

73. Kirchhoff M, Specht U, Veser G. Engineering high-temperature stable nanocomposite materials. *Nanotechnology.* 2005;16(7):S401.

74. An K, Alayoglu S, Ewers T, Somorjai GA. Colloid chemistry of nanocatalysts: A molecular view. *Journal of colloid and interface science.* 2012;373(1):1-13.

75. Li Z, Li M, Bian Z, Kathiraser Y, Kawi S. Design of highly stable and selective core/yolk–shell nanocatalysts—A review. *Applied Catalysis B: Environmental.* 2016;188:324-341.

76. Lin W, Xu Y, Huang C-C, et al. Toxicity of nano-and micro-sized ZnO particles in human lung epithelial cells. *Journal of Nanoparticle Research.* 2009;11(1):25-39.

77. Xia T, Zhao Y, Sager T, et al. Decreased dissolution of ZnO by iron doping yields nanoparticles with reduced toxicity in the rodent lung and zebrafish embryos. *ACS nano.* 2011;5(2):1223-1235.

78. Sotiriou GA, Watson C, Murdaugh KM, et al. Engineering safer-by-design silica-coated ZnO nanorods with reduced DNA damage potential. *Environmental Science: Nano.* 2014;1(2):144-153.

79. Belharouak I, Sun Y-K, Liu J, Amine K. Li (Ni 1/3 Co 1/3 Mn 1/3) O 2 as a suitable cathode for high power applications. *Journal of Power Sources.* 2003;123(2):247-252.

80. Conry TE, Mehta A, Cabana J, Doeff MM. Structural Underpinnings of the Enhanced Cycling Stability upon Al-Substitution in LiNi0. 45Mn0. 45Co0. 1–y Al y O2 Positive Electrode Materials for Li-ion Batteries. *Chemistry of Materials.* 2012;24(17):3307-3317.

81. Goodenough JB, Kim Y. Challenges for rechargeable Li batteries†. *Chemistry of Materials.* 2009;22(3):587-603.

82. Klaper R. Cross species comparison of the impacts of nanomaterials: the role of molecular level differences due to environment and organism. ICEENN2016.

83. Nel A, Xia T, Meng H, et al. Nanomaterial Toxicity Testing in the 21st Century: Use of a Predictive Toxicological Approach and High-Throughput Screening. *Accounts of Chemical Research.* 2013;46(3):607-621.

84. Maurer-Jones MA, Lin Y-S, Haynes CL. Functional Assessment of Metal Oxide Nanoparticle Toxicity in Immune Cells. *Acs Nano.* 2010;4(6):3363-3373.

85. Pokhrel S, Nel AE, Maedler L. Custom-Designed Nanomaterial Libraries for Testing Metal Oxide Toxicity. *Accounts of Chemical Research.* 2013;46(3):632-641.

86. Gass S, Cohen J, Pyrgiotakis G, Sotiriou G, Pratsinis S, Demokritou P. Safer Formulation Concept for Flame-Generated Engineered Nanomaterials. *Acs Sustainable Chemistry & Engineering.* 2013;1(7):843-857.

87. Sadowski J, Guston DH. 'You caught me off guard': Probing the futures of complex engineered nanomaterials. *Journal of Nanoparticle Research.* 2016;18(7):208.

88. Joo SH, Park JY, Tsung C-K, Yamada Y, Yang P, Somorjai GA. Thermally stable Pt/mesoporous silica core–shell nanocatalysts for high-temperature reactions. *Nature materials.* 2009;8(2):126-131.

89. Philbert M, Alexeeff G, Bahadori T, et al. Review of Federal Strategy for Nanotechnology-Related Enviromental, Health, and Safety Research. The National Academic Press: Washington, DC; 2008.

90. Auffan M, Rose J, Bottero J-Y, Lowry GV, Jolivet J-P, Wiesner MR. Towards a definition of inorganic nanoparticles from an environmental, health and safety perspective. *Nature nanotechnology.* 2009;4(10):634-641.

91. Warheit DB. How meaningful are the results of nanotoxicity studies in the absence of adequate material characterization? *Toxicological sciences.* 2008;101(2):183-185.

92. Prakasham RS, Devi GS, Rao CS, Sivakumar V, Sathish T, Sarma P. Nickel-impregnated silica nanoparticle synthesis and their evaluation for biocatalyst immobilization. *Applied biochemistry and biotechnology.* 2010;160(7):1888-1895.

93. Jin P, Chen Q, Hao L, Tian R, Zhang L, Wang L. Synthesis and catalytic properties of nickel-silica composite hollow nanospheres. *The Journal of Physical Chemistry B.* 2004;108(20):6311-6314.

94. Boudjahem A, Monteverdi S, Mercy M, Bettahar M. Study of nickel catalysts supported on silica of low surface area and prepared by reduction of nickel acetate in aqueous hydrazine. *Journal of Catalysis.* 2004;221(2):325-334.

95. Zhao J, Shi X, Castranova V, Ding M. Occupational toxicology of nickel and nickel compounds. *Journal of Environmental Pathology, Toxicology and Oncology.* 2009;28(3).

96. Association NPER. *National Toxicology Program Proposal to List Nickel Nanoparticles in Future Editions of the RoC.* Durham: NiPERA Inc.;2013.

97. Ahamed M. Toxic response of nickel nanoparticles in human lung epithelial A549 cells. *Toxicology in Vitro.* 2011;25(4):930-936.

98. Ahmad J, Alhadlaq HA, Siddiqui MA, et al. Concentration-dependent induction of reactive oxygen species, cell cycle arrest and apoptosis in human liver cells after nickel nanoparticles exposure. *Environmental toxicology.* 2013.

99. Zhao J, Bowman L, Zhang X, et al. Metallic nickel nano-and fine particles induce JB6 cell apoptosis through a caspase-8/AIF mediated cytochrome c-independent pathway. *J nanobiotechnology.* 2009;7(2).

100. Ada K, Turk M, Oguztuzun S, et al. Cytotoxicity and apoptotic effects of nickel oxide nanoparticles in cultured HeLa cells. *Folia Histochemica et Cytobiologica.* 2011;48(4):524-523.

101. Park S, Lee YK, Jung M, et al. Cellular toxicity of various inhalable metal nanoparticles on human alveolar epithelial cells. *Inhalation toxicology.* 2007;19(sup1):59-65.

102. Guo D, Wu C, Li X, Jiang H, Wang X, Chen B. In vitro cellular uptake and cytotoxic effect of functionalized nickel nanoparticles on leukemia cancer cells. *Journal of nanoscience and nanotechnology.* 2008;8(5):2301-2307.

103. Pietruska JR, Liu X, Smith A, et al. Bioavailability, intracellular mobilization of nickel, and HIF-1α activation in human lung epithelial cells exposed to metallic nickel and nickel oxide nanoparticles. *Toxicological Sciences.* 2011:kfr206.

104. Ke Q, Davidson T, Kluz T, Oller A, Costa M. Fluorescent tracking of nickel ions in human cultured cells. *Toxicology and applied pharmacology.* 2007;219(1):18-23.

105. Deng X, Chen Z. Preparation of nano-NiO by ammonia precipitation and reaction in solution and competitive balance. *Materials Letters.* 2004;58(3–4):276-280.

106. Zhao J, Bertoglio BA, Devinney Jr MJ, Dineley KE, Kay AR. The interaction of biological and noxious transition metals with the zinc probes FluoZin-3 and Newport Green. *Analytical biochemistry.* 2009;384(1):34-41.

107. Dunnett CW. A multiple comparison procedure for comparing several treatments with a control. *Journal of the American Statistical Association.* 1955;50(272):1096-1121.

108. Powers CM, Yen J, Linney EA, Seidler FJ, Slotkin TA. Silver exposure in developing zebrafish (< i> Danio rerio</i>): Persistent effects on larval behavior and survival. *Neurotoxicology and teratology.* 2010;32(3):391-397.

109. Auffan M, Rose J, Wiesner MR, Bottero J-Y. Chemical stability of metallic nanoparticles: A parameter controlling their potential cellular toxicity in vitro. *Environmental Pollution.* 2009;157(4):1127-1133.

110. Zhu X, Zhu L, Duan Z, Qi R, Li Y, Lang Y. Comparative toxicity of several metal oxide nanoparticle aqueous suspensions to Zebrafish (Danio rerio) early developmental stage. *Journal of Environmental Science and Health Part a-Toxic/Hazardous Substances & Environmental Engineering.* 2008;43(3):278-284.

111. Griffitt RJ, Luo J, Gao J, Bonzongo JC, Barber DS. Effects of particle composition and species on toxicity of metallic nanomaterials in aquatic organisms. *Environmental Toxicology and Chemistry.* 2008;27(9):1972-1978.

112. Teeguarden JG, Hinderliter PM, Orr G, Thrall BD, Pounds JG. Particokinetics in vitro: dosimetry considerations for in vitro nanoparticle toxicity assessments. *Toxicological Sciences.* 2007;95(2):300-312.

113. Wittmaack K. Excessive Delivery of Nanostructured Matter to Submersed Cells Caused by Rapid Gravitational Settling. *Acs Nano.* 2011;5(5):3766-3778.

114. ISO B. 10993-5: Biological evaluation of medical devices. *Tests for in vitro cytotoxicity*. 1999.

115. Wallin RF, Arscott E. A practical guide to ISO 10993-5: Cytotoxicity. *Medical Device and Diagnostic Industry*. 1998;20:96-98.

116. Mahto SK, Park C, Yoon TH, Rhee SW. Assessment of cytocompatibility of surface-modified CdSe/ZnSe quantum dots for BALB/3T3 fibroblast cells. *Toxicology in vitro.* 2010;24(4):1070-1077.

117. Ponti J, Sabbioni E, Munaro B, et al. Genotoxicity and morphological transformation induced by cobalt nanoparticles and cobalt chloride: an in vitro study in Balb/3T3 mouse fibroblasts. *Mutagenesis.* 2009;24(5):439-445.

118. Zucker R, Massaro E, Sanders K, Degn L, Boyes W. Detection of TiO2 nanoparticles in cells by flow cytometry. *Cytometry Part A.* 2010;77(7):677-685.

119. Suzuki H, Toyooka T, Ibuki Y. Simple and easy method to evaluate uptake potential of nanoparticles in mammalian cells using a flow cytometric light scatter analysis. *Environmental science & technology.* 2007;41(8):3018-3024.

120. Choi M-R, Stanton-Maxey KJ, Stanley JK, et al. A cellular Trojan Horse for delivery of therapeutic nanoparticles into tumors. *Nano letters.* 2007;7(12):3759-3765.

121. Edwards D, Wataha J, Hanks C. Uptake and reversibility of uptake of nickel by human macrophages. *Journal of oral rehabilitation.* 1998;25:2-7.

122. Caballero-Díaz E, Pfeiffer C, Kastl L, et al. The toxicity of silver nanoparticles depends on their uptake by cells and thus on their surface chemistry. *Particle & Particle Systems Characterization.* 2013;30(12):1079-1085.

123. Chithrani BD, Chan WC. Elucidating the mechanism of cellular uptake and removal of protein-coated gold nanoparticles of different sizes and shapes. *Nano letters.* 2007;7(6):1542-1550.

124. Chithrani BD, Ghazani AA, Chan WC. Determining the size and shape dependence of gold nanoparticle uptake into mammalian cells. *Nano letters.* 2006;6(4):662-668.

125. Huang X, Teng X, Chen D, Tang F, He J. The effect of the shape of mesoporous silica nanoparticles on cellular uptake and cell function. *Biomaterials.* 2010;31(3):438-448.

126. Limbach LK, Li Y, Grass RN, et al. Oxide Nanoparticle Uptake in Human Lung Fibroblasts: Effects of Particle Size, Agglomeration, and Diffusion at Low Concentrations. *Environmental Science & Technology.* 2005;39(23):9370-9376.

127. Lu F, Wu SH, Hung Y, Mou CY. Size Effect on Cell Uptake in Well-Suspended, Uniform Mesoporous Silica Nanoparticles. *Small.* 2009;5(12):1408-1413.

128. Zhu M, Nie G, Meng H, Xia T, Nel A, Zhao Y. Physicochemical Properties Determine Nanomaterial Cellular Uptake, Transport, and Fate. *Accounts of Chemical Research.* 2013;46(3):622-631.

129. Lundqvist M, Stigler J, Elia G, Lynch I, Cedervall T, Dawson KA. Nanoparticle size and surface properties determine the protein corona with possible implications for biological impacts. *Proceedings of the National Academy of Sciences.* 2008;105(38):14265-14270.

130. Bird RB, Stewart WE, Lightfoot EN. Transport Phenomena John Wiley & Sons. *New York.* 1960:413.

131. Renkin EM. Filtration, diffusion, and molecular sieving through porous cellulose membranes. *The Journal of general physiology.* 1954;38(2):225-243.

132. Takahashi R, Sato S, Sodesawa T, Nishida H. Effect of pore size on the liquid-phase pore diffusion of nickel nitrate. *Physical Chemistry Chemical Physics.* 2002;4(15):3800-3805.

133. Nel A, Xia T, Madler L, Li N. Toxic potential of materials at the nanolevel. *Science.* 2006;311(5761):622-627.

134. Oberdorster G, Oberdorster E, Oberdorster J. Nanotoxicology: An emerging discipline evolving from studies of ultrafine particles. *Environmental Health Perspectives.* 2005;113(7):823-839.

135. Jiang W, Kim BYS, Rutka JT, Chan WCW. Nanoparticle-mediated cellular response is size-dependent. *Nat Nanotechnol.* 2008;3(3):145-150.

136. Uzio D, Berhault G. Factors Governing the Catalytic Reactivity of Metallic Nanoparticles. *Catal Rev - Sci Eng.* 2010;52(1):106-131.

137. Shang Y, Zhu T, Li Y, Zhao J. Size-dependent hydroxyl radicals generation induced by SiO2 ultra-fine particles: The role of surface iron. *Science in China Series B: Chemistry.* 2009;52(7):1033-1041.

138. Napierska D, Rabolli V, Thomassen LC, et al. Oxidative stress induced by pure and iron-doped amorphous silica nanoparticles in subtoxic conditions. *Chemical Research in Toxicology.* 2012;25(4):828-837.

139. Nel A, Xia T, Meng H, et al. Nanomaterial Toxicity Testing in the 21st Century: Use of a Predictive Toxicological Approach and High-Throughput Screening. *Acc Chem Res.* 2012;46(3):607-621.

140. Bai W, Zhang Z, Tian W, et al. Toxicity of zinc oxide nanoparticles to zebrafish embryo: a physicochemical study of toxicity mechanism. *Journal of Nanoparticle Research.* 2010;12(5):1645-1654.

141. Hill AJ, Teraoka H, Heideman W, Peterson RE. Zebrafish as a model vertebrate for investigating chemical toxicity. *Toxicological sciences.* 2005;86(1):6-19.

142. Nusslein-Volhard C, Dahm R. *Zebrafish.* Oxford University Press; 2002.

143. Brannen KC, Panzica-Kelly JM, Danberry TL, Augustine-Rauch KA. Development of a zebrafish embryo teratogenicity assay and quantitative prediction model. *Birth Defects Research Part B: Developmental and Reproductive Toxicology.* 2010;89(1):66-77.

144. Kimmel CB, Ballard WW, Kimmel SR, Ullmann B, Schilling TF. Stages of embryonic development of the zebrafish. *Developmental dynamics.* 1995;203(3):253-310.

145. Peterson RE, Theobald HM, Kimmel GL. Developmental and reproductive toxicity of dioxins and related compounds: cross-species comparisons. *CRC Critical Reviews in Toxicology.* 1993;23(3):283-335.

146. Selderslaghs IW, Van Rompay AR, De Coen W, Witters HE. Development of a screening assay to identify teratogenic and embryotoxic chemicals using the zebrafish embryo. *Reproductive Toxicology.* 2009;28(3):308-320.

147. Zon LI, Peterson RT. In vivo drug discovery in the zebrafish. *Nature reviews Drug discovery.* 2005;4(1):35-44.

148. Levin ED, Swain HA, Donerly S, Linney E. Developmental chlorpyrifos effects on hatchling zebrafish swimming behavior. *Neurotoxicology and teratology.* 2004;26(6):719-723.

149. Thomas JK, Janz DM. In ovo exposure to selenomethionine via maternal transfer increases developmental toxicities and impairs swim performance in F1 generation zebrafish (Danio rerio). *Aquatic Toxicology.* 2014;152:20-29.

150. Padilla S, Corum D, Padnos B, et al. Zebrafish developmental screening of the ToxCast™ Phase I chemical library. *Reproductive Toxicology.* 2012;33(2):174-187.

151. Borm P, Klaessig FC, Landry TD, et al. Research strategies for safety evaluation of nanomaterials, part V: role of dissolution in biological fate and effects of nanoscale particles. *Toxicological Sciences.* 2006;90(1):23-32.

152. Dave G, Xiu R. Toxicity of mercury, copper, nickel, lead, and cobalt to embryos and larvae of zebrafish, Brachydanio rerio. *Archives of Environmental Contamination and Toxicology.* 1991;21(1):126-134.

153. Scheil V, Köhler H-R. Influence of nickel chloride, chlorpyrifos, and imidacloprid in combination with different temperatures on the embryogenesis of the zebrafish Danio rerio. *Archives of environmental contamination and toxicology.* 2009;56(2):238-243.

154. Duan J, Yu Y, Li Y, et al. Developmental toxicity of CdTe QDs in zebrafish embryos and larvae. *Journal of Nanoparticle Research.* 2013;15(7):1-11.

155. George S, Xia T, Rallo R, et al. Use of a High-Throughput Screening Approach Coupled with In Vivo Zebrafish Embryo Screening To Develop Hazard Ranking for Engineered Nanomaterials. *Acs Nano.* 2011;5(3):1805-1817.

156. Kienle C, Köhler H-R, Gerhardt A. Behavioural and developmental toxicity of chlorpyrifos and nickel chloride to zebrafish (Danio rerio) embryos and larvae. *Ecotoxicology and Environmental Safety.* 2009;72(6):1740-1747.

157. Lin S, Zhao Y, Nel AE, Lin S. Zebrafish: An In Vivo Model for Nano EHS Studies. *Small (Weinheim an der Bergstrasse, Germany).* 2013;9(9-10):1608-1618.

158. Lin S, Zhao Y, Xia T, et al. High Content Screening in Zebrafish Speeds up Hazard Ranking of Transition Metal Oxide Nanoparticles. *Acs Nano.* 2011;5(9):7284-7295.

159. Yang SP, Bar-Ilan O, Peterson RE, Heideman W, Hamers RJ, Pedersen JA. Influence of humic Acid on titanium dioxide nanoparticle toxicity to developing zebrafish. *Environmental science & technology.* 2013;47(9):4718-4725.

160. Lee KJ, Nallathamby PD, Browning LM, Osgood CJ, Xu X-HN. In vivo imaging of transport and biocompatibility of single silver nanoparticles in early development of zebrafish embryos. *ACS nano.* 2007;1(2):133-143.

161. Scheil V, Zürn A, Köhler HR, Triebskorn R. Embryo development, stress protein (Hsp70) responses, and histopathology in zebrafish (Danio rerio) following exposure to nickel chloride, chlorpyrifos, and binary mixtures of them. *Environmental toxicology.* 2010;25(1):83-93.

162. Duan J, Yu Y, Li Y, Yu Y, Sun Z. Cardiovascular toxicity evaluation of silica nanoparticles in endothelial cells and zebrafish model. *Biomaterials.* 2013;34(23):5853-5862.

163. Duan J, Yu Y, Shi H, et al. Toxic Effects of Silica Nanoparticles on Zebrafish Embryos and Larvae. *PloS one.* 2013;8(9):e74606.

164. Powers CM, Yen J, Linney EA, Seidler FJ, Slotkin TA. Silver exposure in developing zebrafish (Danio rerio): Persistent effects on larval behavior and survival. *Neurotoxicology and teratology.* 2010;32(3):391-397.

165. Lieschke GJ, Currie PD. Animal models of human disease: zebrafish swim into view. *Nature Reviews Genetics.* 2007;8(5):353-367.

166. Brunner TJ, Wick P, Manser P, et al. In vitro cytotoxicity of oxide nanoparticles: comparison to asbestos, silica, and the effect of particle solubility. *Environmental science & technology.* 2006;40(14):4374-4381.

167. Napierska D, Thomassen LC, Rabolli V, et al. Size-Dependent Cytotoxicity of Monodisperse Silica Nanoparticles in Human Endothelial Cells. *Small.* 2009;5(7):846-853.

168. ASTM. *D859-00 Standard Test Method for Silica in Water.* West Conshohocken, PA2000.

169. Streisinger G, Walker C, Dower N, Knauber D, Singer F. Production of clones of homozygous diploid zebra fish (Brachydanio rerio). *Nature.* 1981;291(5813):293-296.

170. Cario CL, Farrell TC, Milanese C, Burton EA. Automated measurement of zebrafish larval movement. *The Journal of Physiology.* 2011;589(15):3703-3708.

171. Zhou Y, Cattley RT, Cario CL, Bai Q, Burton EA. Quantification of larval zebrafish motor function in multiwell plates using open-source MATLAB applications. *Nature protocols.* 2014;9(7):1533-1548.

172. Farrell TC, Cario CL, Milanese C, Vogt A, Jeong J-H, Burton EA. Evaluation of spontaneous propulsive movement as a screening tool to detect rescue of Parkinsonism phenotypes in zebrafish models. *Neurobiology of disease.* 2011;44(1):9-18.

173. Borgmann U, Neron R, Norwood W. Quantification of bioavailable nickel in sediments and toxic thresholds to Hyalella azteca. *Environmental Pollution.* 2001;111(2):189-198.

174. Limbach LK, Wick P, Manser P, Grass RN, Bruinink A, Stark WJ. Exposure of engineered nanoparticles to human lung epithelial cells: influence of chemical composition and catalytic activity on oxidative stress. *Environmental Science & Technology.* 2007;41(11):4158-4163.

175. Alexander GB, Heston W, Iler RK. The solubility of amorphous silica in water. *The Journal of Physical Chemistry.* 1954;58(6):453-455.

176. Semisch A, Ohle J, Witt B, Hartwig A. Cytotoxicity and genotoxicity of nano-and microparticulate copper oxide: role of solubility and intracellular bioavailability. *Part Fibre Toxicol.* 2014;11(10).

177. Johnson A, Carew E, Sloman K. The effects of copper on the morphological and functional development of zebrafish embryos. *Aquatic Toxicology.* 2007;84(4):431-438.

178. Bar-Ilan O, Louis KM, Yang SP, et al. Titanium dioxide nanoparticles produce phototoxicity in the developing zebrafish. *Nanotoxicology.* 2012;6(6):670-679.

179. Westerfield M. *The zebrafish book.* University of Oregon press; 2000.

180. Das K, Das S, Dhundasi S. Nickel, its adverse health effects & oxidative stress. *Indian Journal of Medical Research.* 2008;128(4):412.

181. Xu SC, He MD, Lu YH, et al. Nickel exposure induces oxidative damage to mitochondrial DNA in Neuro2a cells: the neuroprotective roles of melatonin. *Journal of pineal research.* 2011;51(4):426-433.

182. Slotkin TA, Seidler FJ. Developmental neurotoxicants target neurodifferentiation into the serotonin phenotype: chlorpyrifos, diazinon, dieldrin and divalent nickel. *Toxicology and applied pharmacology.* 2008;233(2):211-219.

183. Orger MB, Gahtan E, Muto A, Page-McCaw P, Smear MC, Baier H. Behavioral screening assays in zebrafish. *Essential Zebrafish Methods: Genetics and Genomics: Genetics and Genomics.* 2009:113.

184. Baganz D, Staaks G, Steinberg C. Impact of the cyanobacteria toxin, microcystin-lr on behaviour of zebrafish, danio rerio. *Water research.* 1998;32(3):948-952.

185. Gerlai R, Lahav M, Guo S, Rosenthal A. Drinks like a fish: zebra fish (Danio rerio) as a behavior genetic model to study alcohol effects. *Pharmacology biochemistry and behavior.* 2000;67(4):773-782.

186. Alsop D, Lall SP, Wood CM. Reproductive impacts and physiological adaptations of zebrafish to elevated dietary nickel. *Comparative Biochemistry and Physiology Part C: Toxicology & Pharmacology.* 2014.

187. Couto GG, Klein JJ, Schreiner WH, Mosca DH, de Oliveira AJ, Zarbin AJ. Nickel nanoparticles obtained by a modified polyol process: synthesis, characterization, and magnetic properties. *Journal of colloid and Interface science.* 2007;311(2):461-468.

188. Metin O, Mazumder V, Ozkar S, Sun S. Monodisperse nickel nanoparticles and their catalysis in hydrolytic dehydrogenation of ammonia borane. *Journal of the American Chemical Society.* 2010;132(5):1468-1469.

189. Park J, Kang E, Son SU, et al. Monodisperse nanoparticles of Ni and NiO: synthesis, characterization, self-assembled superlattices, and catalytic applications in the Suzuki coupling reaction. 2005.

190. Jiang W, Kim BY, Rutka JT, Chan WC. Nanoparticle-mediated cellular response is size-dependent. *Nature Nanotechnology.* 2008;3(3):145-150.

191. Uzio D, Berhault G. Factors governing the catalytic reactivity of metallic nanoparticles. *Catalysis Reviews.* 2010;52(1):106-131.

192. Lin S, Zhao Y, Ji Z, et al. Zebrafish High-Throughput Screening to Study the Impact of Dissolvable Metal Oxide Nanoparticles on the Hatching Enzyme, ZHE1. *Small.* 2013;9(9-10):1776-1785.

193. Ong KJ, Zhao X, Thistle ME, et al. Mechanistic insights into the effect of nanoparticles on zebrafish hatch. *Nanotoxicology.* 2014;8(3):295-304.

194. Asharani P, Wu YL, Gong Z, Valiyaveettil S. Toxicity of silver nanoparticles in zebrafish models. *Nanotechnology.* 2008;19(25):255102.

195. Bai W, Tian W, Zhang Z, et al. Effects of copper nanoparticles on the development of zebrafish embryos. *Journal of nanoscience and nanotechnology.* 2010;10(12):8670-8676.

196. Kovrižnych JA, Sotníková R, Zeljenková D, Rollerová E, Szabová E, Wimmerová S. Acute toxicity of 31 different nanoparticles to zebrafish (Danio rerio) tested in adulthood and in early life stages–comparative study. *Interdisciplinary toxicology.* 2013;6(2):67-73.

197. Schulte C, Nagel R. Testing acute toxicity in the embryo of zebrafish, Brachydanio rerio, as an alternative to the acute fish test: preliminary results. *Alternatives to laboratory animals: ATLA.* 1994.

198. Henschel K-P, Wenzel A, Diedrich M, Fliedner A. Environmental hazard assessment of pharmaceuticals. *Regulatory Toxicology and Pharmacology.* 1997;25(3):220-225.

199. Hutchinson TH, Barrett S, Buzby M, et al. A strategy to reduce the numbers of fish used in acute ecotoxicity testing of pharmaceuticals. *Environmental toxicology and chemistry.* 2003;22(12):3031-3036.

200. Lammer E, Carr G, Wendler K, Rawlings J, Belanger S, Braunbeck T. Is the fish embryo toxicity test (FET) with the zebrafish (Danio rerio) a potential alternative for the fish acute toxicity test? *Comparative Biochemistry and Physiology Part C: Toxicology & Pharmacology.* 2009;149(2):196-209.

201. Verdouw H, Van Echteld C, Dekkers E. Ammonia determination based on indophenol formation with sodium salicylate. *Water Research.* 1978;12(6):399-402.

202. Onofri F, Barbosa S, Touré O, Woźniak M, Grisolia C. Sizing highly-ordered buckyball-shaped aggregates of colloidal nanoparticles by light extinction spectroscopy. *Journal of Quantitative Spectroscopy and Radiative Transfer.* 2013;126:160-168.

203. Braun MH, Steele SL, Ekker M, Perry SF. Nitrogen excretion in developing zebrafish (Danio rerio): a role for Rh proteins and urea transporters. *American Journal of Physiology-Renal Physiology.* 2009;296(5):F994-F1005.

204. Wood C, Evans D. Ammonia and urea metabolism and excretion [in fish]. *CRC Marine science series 379Á426.* 1993.

205. Ip Y, Chew S, Randall D. Ammonia toxicity, tolerance, and excretion. *Fish physiology.* 2001;20:109-148.

206. Farhadi S, Roostaei-Zaniyani Z. Simple and low-temperature synthesis of NiO nanoparticles through solid-state thermal decomposition of the hexa (ammine) Ni (II) nitrate,[Ni (NH 3) 6](NO 3) 2, complex. *Polyhedron.* 2011;30(7):1244-1249.

207. Trapp C, Shyr CI. Paramagnetic Resonance in Transition-Metal Hexammine Complexes. I The Ni (II)(NH3) 6 Complex Ion. *The Journal of Chemical Physics.* 1971;54(1):196-203.

208. Okuda M, Iwahori K, Yamashita I, Yoshimura H. Fabrication of nickel and chromium nanoparticles using the protein cage of apoferritin. *Biotechnology and bioengineering.* 2003;84(2):187-194.

209. Bonneviot L, Legendre O, Kermarec M, Olivier D, Che M. Characterization by UV-vis-NIR reflectance spectroscopy of the exchange sites of nickel on silica. *Journal of colloid and interface science.* 1990;134(2):534-547.

210. Ertl G, Rüstig J. Decomposition of NH3 on nickel: Absence of a magneto-catalytic effect. *Surface Science.* 1982;119(1):L314-L318.

211. Grunze M, Golze M, Driscoll R, Dowben P. Ammonia adsorption and decomposition on a Ni (110) surface. *Journal of Vacuum Science & Technology.* 1981;18(2):611-615.

212. Ip AY, Chew SF. Ammonia production, excretion, toxicity, and defense in fish: a review. *Frontiers in physiology.* 2010;1:134.

213. Ebrahimnia-Bajestan E, Niazmand H, Duangthongsuk W, Wongwises S. Numerical investigation of effective parameters in convective heat transfer of nanofluids flowing under a laminar flow regime. *International journal of heat and mass transfer.* 2011;54(19):4376-4388.

214. Cioffi N, Ditaranto N, Torsi L, et al. Analytical characterization of bioactive fluoropolymer ultra-thin coatings modified by copper nanoparticles. *Analytical and bioanalytical chemistry.* 2005;381(3):607-616.

215. Carnes CL, Klabunde KJ. The catalytic methanol synthesis over nanoparticle metal oxide catalysts. *Journal of Molecular Catalysis A: Chemical.* 2003;194(1):227-236.

216. Batchelor-McAuley C, Du Y, Wildgoose GG, Compton RG. The use of copper (II) oxide nanorod bundles for the non-enzymatic voltammetric sensing of carbohydrates and hydrogen peroxide. *Sensors and Actuators B: Chemical.* 2008;135(1):230-235.

217. Guo Z, Ng HW, Yee GL, Hahn HT. Differential scanning calorimetry investigation on vinyl ester resin curing process for polymer nanocomposite fabrication. *Journal of nanoscience and nanotechnology.* 2009;9(5):3278-3285.

218. Kahru A, Savolainen K. Potential hazard of nanoparticles: from properties to biological and environmental effects. *Toxicology.* 2010;269(2):89-91.

219. Liu G, Li X, Qin B, Xing D, Guo Y, Fan R. Investigation of the mending effect and mechanism of copper nano-particles on a tribologically stressed surface. *Tribology Letters.* 2004;17(4):961-966.

220. Lipshutz BH, Taft BR. Heterogeneous Copper-in-Charcoal-Catalyzed Click Chemistry. *Angewandte Chemie.* 2006;118(48):8415-8418.

221. Doudi M, Setorki M. Acute effect of nano-copper on liver tissue and function in rat. *Nanomedicine Journal.* 2014;1(5):331-338.

222. Griffitt RJ, Weil R, Hyndman KA, et al. Exposure to copper nanoparticles causes gill injury and acute lethality in zebrafish (Danio rerio). *Environmental Science & Technology.* 2007;41(23):8178-8186.

223. Hua J, Vijver MG, Ahmad F, Richardson MK, Peijnenburg WJ. Toxicity of different sized copper nano-and sub-micron particles and their shed copper ions to zebrafish embryos. *Environmental Toxicology and Chemistry.* 2014.

224. Lei R, Wu C, Yang B, et al. Integrated metabolomic analysis of the nano-sized copper particle-induced hepatotoxicity and nephrotoxicity in rats: A rapid invivo screening method for nanotoxicity. *Toxicology and applied pharmacology.* 2008;232(2):292-301.

225. Steele CW. Effects of sublethal exposure to copper on diel activity of sea catfish, Arius felis. *Hydrobiologia.* 1989;178(2):135-141.

226. Studer AM, Limbach LK, Van Duc L, et al. Nanoparticle cytotoxicity depends on intracellular solubility: comparison of stabilized copper metal and degradable copper oxide nanoparticles. *Toxicology letters.* 2010;197(3):169-174.

227. Karlsson HL, Cronholm P, Gustafsson J, Moller L. Copper oxide nanoparticles are highly toxic: a comparison between metal oxide nanoparticles and carbon nanotubes. *Chemical research in toxicology.* 2008;21(9):1726-1732.

228. Cronholm P, Karlsson HL, Hedberg J, et al. Intracellular uptake and toxicity of Ag and CuO nanoparticles: a comparison between nanoparticles and their corresponding metal ions. *Small.* 2013;9(7):970-982.

229. Ingle AP, Duran N, Rai M. Bioactivity, mechanism of action, and cytotoxicity of copper-based nanoparticles: a review. *Applied microbiology and biotechnology.* 2014;98(3):1001-1009.

230. Huang Z, Cui F, Kang H, Chen J, Zhang X, Xia C. Highly dispersed silica-supported copper nanoparticles prepared by precipitation− gel method: a simple but efficient and stable catalyst for glycerol hydrogenolysis. *Chemistry of Materials.* 2008;20(15):5090-5099.

231. Liu H, Huang Z, Han Z, et al. Efficient production of methanol and diols via the hydrogenation of cyclic carbonates using copper–silica nanocomposite catalysts. *Green Chemistry.* 2015;17(8):4281-4290.

232. Scotti N, Monticelli D, Zaccheria F. Dispersed copper oxide: A multifaceted tool in catalysis. *Inorganica Chimica Acta.* 2012;380:194-200.

233. Bush AI, Masters CL, Tanzi RE. Copper, β-amyloid, and Alzheimer's disease: tapping a sensitive connection. *Proceedings of the National Academy of Sciences.* 2003;100(20):11193-11194.

234. Rasia RM, Bertoncini CW, Marsh D, et al. Structural characterization of copper (II) binding to α-synuclein: Insights into the bioinorganic chemistry of Parkinson's disease. *Proceedings of the National Academy of Sciences of the United States of America.* 2005;102(12):4294-4299.

235. Mahoney S, Najera M, Bai Q, Burton EA, Veser G. The Developmental Toxicity of Complex Silica-Embedded Nickel Nanoparticles Is Determined by Their Physicochemical Properties. *PLOS ONE.* 2016;11(3):e0152010.

236. Irons T, MacPhail R, Hunter D, Padilla S. Acute neuroactive drug exposures alter locomotor activity in larval zebrafish. *Neurotoxicology and teratology.* 2010;32(1):84-90.

237. EPA. Technical Overview of Ecological Risk Assessment - Analysis Phase: Ecological Effects Characterization. 2016, 2016.

238. Control CfD, Prevention. *NIOSH pocket guide to chemical hazards.* 1997.

239. ACGIH CO. TLVs and BEIs Based on the Documentation of the Threshold Limit Values for Chemical Substances and Physical Agents, and Biological Exposure Indices. Paper presented at: American Conference of Governmental Industrial Hygienists Cincinnati2008.

240. Rendall R, Phillips J, Renton K. Death following exposure to fine particulate nickel from a metal arc process. *Annals of Occupational Hygiene.* 1994;38(6):921-930.

241. Sunderman FW, Dingle B, Hopfer SM, Swift T. Acute nickel toxicity in electroplating workers who accidently ingested a solution of nickel sulfate and nickel chloride. *American journal of industrial medicine.* 1988;14(3):257-266.

242. Fahmy B, Cormier SA. Copper oxide nanoparticles induce oxidative stress and cytotoxicity in airway epithelial cells. *Toxicology In Vitro.* 2009;23(7):1365-1371.

243. Pereira S, Tettamanti M. Testing Times in Toxicology–In Vitro vs In Vivo Testing.

244. Auffan M, Bottero J, Chaneac C, Rose J. Inorganic manufactured nanoparticles: how their physicochemical properties influence their biological effects in aqueous environments. *Nanomedicine.* 2010;5(6):999-1007.

245. Marambio-Jones C, Hoek EM. A review of the antibacterial effects of silver nanomaterials and potential implications for human health and the environment. *Journal of Nanoparticle Research.* 2010;12(5):1531-1551.

246. Whaley L. *Synthesis and evaluation of metal-silica core-shell nanomaterials for catalysis*: Chemical Engineering, University of Pittsburgh; 2012.

247. Cioffi N, Torsi L, Ditaranto N, et al. Copper nanoparticle/polymer composites with antifungal and bacteriostatic properties. *Chemistry of Materials.* 2005;17(21):5255-5262.

248. Cioffi N, Torsi L, Ditaranto N, et al. Antifungal activity of polymer-based copper nanocomposite coatings. *Applied physics letters.* 2004;85(12):2417-2419.

249. Anyaogu KC, Fedorov AV, Neckers DC. Synthesis, characterization, and antifouling potential of functionalized copper nanoparticles. *Langmuir.* 2008;24(8):4340-4346.

250. Raffi M, Mehrwan S, Bhatti TM, et al. Investigations into the antibacterial behavior of copper nanoparticles against Escherichia coli. *Annals of Microbiology.* 2010;60(1):75-80.

251. More A, Bhavsar S, Veser G. Iron–Nickel Alloys for Carbon Dioxide Activation by Chemical Looping Dry Reforming of Methane. *Energy Technology.* 2016.

252. Zhen L, Gong Y, Jiang J, Shao W. Electromagnetic properties of FeNi alloy nanoparticles prepared by hydrogen-thermal reduction method. *Journal of Applied Physics.* 2008;104(3):034312.

253. Zheng X, Deng J, Wang N, et al. Podlike N-Doped Carbon Nanotubes Encapsulating FeNi Alloy Nanoparticles: High-Performance Counter Electrode Materials for Dye-Sensitized Solar Cells. *Angewandte Chemie International Edition.* 2014;53(27):7023-7027.

254. Kim M-Y, Park J-H, Shin C-H, Han S-W, Seo G. Dispersion improvement of platinum catalysts supported on silica, silica-alumina and alumina by titania incorporation and pH adjustment. *Catalysis letters.* 2009;133(3-4):288-297.

255. Jiang T, Mowbray D, Dobrin S, et al. Trends in CO oxidation rates for metal nanoparticles and close-packed, stepped, and kinked surfaces. *The Journal of Physical Chemistry C.* 2009;113(24):10548-10553.

256. Li L, Larsen AH, Romero NA, et al. Investigation of catalytic finite-size-effects of platinum metal clusters. *The journal of physical chemistry letters.* 2012;4(1):222-226.

257. Nørskov JK, Bligaard T, Rossmeisl J, Christensen CH. Towards the computational design of solid catalysts. *Nature chemistry.* 2009;1(1):37-46.

258. Galeano C, Güttel R, Paul M, Arnal P, Lu AH, Schüth F. Yolk-Shell Gold Nanoparticles as Model Materials for Support-Effect Studies in Heterogeneous Catalysis: Au,@ C and Au,@ ZrO2 for CO Oxidation as an Example. *Chemistry–A European Journal.* 2011;17(30):8434-8439.

259. Arnal PM, Comotti M, Schüth F. High-Temperature-Stable Catalysts by Hollow Sphere Encapsulation
Angewandte Chemie Volume 118, Issue 48. *Angewandte Chemie.* 2006;118(48):8404-8407.

260. Comotti M, Li W-C, Spliethoff B, Schüth F. Support effect in high activity gold catalysts for CO oxidation. *Journal of the American Chemical Society.* 2006;128(3):917-924.

261. Campbell CT, Parker SC, Starr DE. The effect of size-dependent nanoparticle energetics on catalyst sintering. *Science.* 2002;298(5594):811-814.

262. Shinjoh H, Hatanaka M, Nagai Y, et al. Suppression of noble metal sintering based on the support anchoring effect and its application in automotive three-way catalysis. *Topics in Catalysis.* 2009;52(13-20):1967-1971.

263. Nagai Y, Hirabayashi T, Dohmae K, et al. Sintering inhibition mechanism of platinum supported on ceria-based oxide and Pt-oxide–support interaction. *Journal of Catalysis.* 2006;242(1):103-109.

264. Ferreira AdP, Zanchet D, Araújo J, et al. The effects of CeO 2 on the activity and stability of Pt supported catalysts for methane reforming, as addressed by in situ

temperature resolved XAFS and TEM analysis. *Journal of Catalysis.* 2009;263(2):335-344.

265. Bhavsar S, Tackett B, Veser G. Evaluation of iron-and manganese-based mono-and mixed-metallic oxygen carriers for chemical looping combustion. *Fuel.* 2014;136:268-279.

266. Estevez AY, Erlichman JS. The potential of cerium oxide nanoparticles (nanoceria) for neurodegenerative disease therapy. *Nanomedicine.* 2014;9(10):1437-1440.

267. Celardo I, Traversa E, Ghibelli L. Cerium oxide nanoparticles: a promise for applications in therapy. *Journal of Experimental Therapeutics & Oncology.* 2011;9(1):47-51.

268. Gao YY. Cerium oxide nanoparticles in cancer. *OncoTargets and therapy.* 2014;7:835.

269. Schubert D, Dargusch R, Raitano J, Chan S-W. Cerium and yttrium oxide nanoparticles are neuroprotective. *Biochemical and biophysical research communications.* 2006;342(1):86-91.

270. Pagliari F, Mandoli C, Forte G, et al. Cerium oxide nanoparticles protect cardiac progenitor cells from oxidative stress. *ACS nano.* 2012;6(5):3767-3775.

271. Xia T, Kovochich M, Liong M, et al. Comparison of the mechanism of toxicity of zinc oxide and cerium oxide nanoparticles based on dissolution and oxidative stress properties. *ACS nano.* 2008;2(10):2121-2134.

272. Tarnuzzer RW, Colon J, Patil S, Seal S. Vacancy engineered ceria nanostructures for protection from radiation-induced cellular damage. *Nano letters.* 2005;5(12):2573-2577.

273. Asati A, Santra S, Kaittanis C, Perez JM. Surface-charge-dependent cell localization and cytotoxicity of cerium oxide nanoparticles. *ACS nano.* 2010;4(9):5321-5331.

274. Ahamed M, Akhtar MJ, Siddiqui MA, et al. Oxidative stress mediated apoptosis induced by nickel ferrite nanoparticles in cultured A549 cells. *Toxicology.* 2011;283(2):101-108.

275. Siddiqui MA, Ahamed M, Ahmad J, et al. Nickel oxide nanoparticles induce cytotoxicity, oxidative stress and apoptosis in cultured human cells that is abrogated by the dietary antioxidant curcumin. *Food and Chemical Toxicology.* 2012;50(3):641-647.

276. Yang H, Liu C, Yang D, Zhang H, Xi Z. Comparative study of cytotoxicity, oxidative stress and genotoxicity induced by four typical nanomaterials: the role of particle size, shape and composition. *Journal of applied Toxicology.* 2009;29(1):69-78.

277. Pujalté I, Passagne I, Brouillaud B, et al. Cytotoxicity and oxidative stress induced by different metallic nanoparticles on human kidney cells. *Particle and Fibre Toxicology.* 2011;8(1):1.

278. Gojova A, Guo B, Kota RS, Rutledge JC, Kennedy IM, Barakat AI. Induction of inflammation in vascular endothelial cells by metal oxide nanoparticles: effect of particle composition. *Environmental health perspectives.* 2007:403-409.